

ANOMALIES IN THE SUPERCONDUCTING LEAD-LEAD OXIDE-
LEAD TUNNELING JUNCTION INDUCED BY AGING:
INCLUDING SUBHARMONIC STRUCTURE AND
OXIDE MODIFICATION

By

KENNETH DEAN DUERKSEN

Bachelor of Science
Southwestern Oklahoma State University
Weatherford, Oklahoma
1966

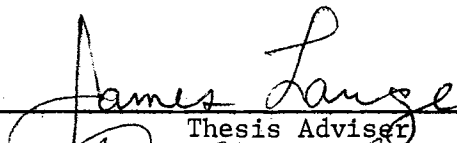
Master of Science
Oklahoma State University
Stillwater, Oklahoma
1972

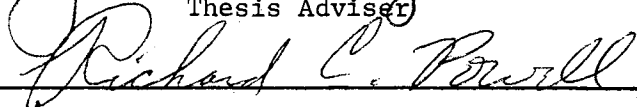
Submitted to the Faculty of the Graduate College
of the Oklahoma State University
in partial fulfillment of the requirements
for the Degree of
DOCTOR OF PHILOSOPHY
December, 1974

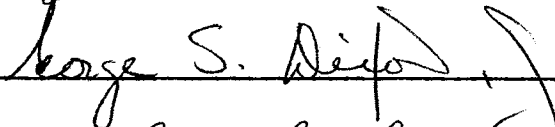
MAY 11 1976

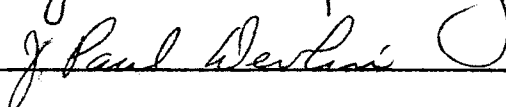
ANOMALIES IN THE SUPERCONDUCTING LEAD-LEAD OXIDE-
LEAD TUNNELING JUNCTION INDUCED BY AGING:
INCLUDING SUBHARMONIC STRUCTURE AND
OXIDE MODIFICATION


Thesis Approved:



Thesis Adviser








Dean of the Graduate College

938618

ACKNOWLEDGEMENTS

The author wishes to express his deep gratitude to Dr. James Lange who gave direction and encouragement throughout the course of this work. Heinz Hall, Floyd Vulgamore, Richard Gruhlkey and Dennis Singer of the Chemistry-Physics Machine Shop were very helpful with the design and fabrication of the apparatus. The System Control Unit was designed by Joe Guess who also aided in its construction. Wayne Adkins was invaluable for the research in doing the glass work on the vacuum system, the gas system and the various dewars. A note of thanks is given to Mrs. Janet Sallee for excellence in typing the manuscript. The author also enjoyed and benefited from the many informal conversations about this work with Professors Larry Halliburton and Joel Martin.

Finally special appreciation is expressed to my wife, Ila, and my son, Kent, for their many sacrifices, infinite patience, and constant encouragement.

TABLE OF CONTENTS

Chapter	Page
I. INTRODUCTION.	1
A. Scope of Study	1
B. Fabrication of Tunneling Devices	2
C. Discussion of the Tunneling Process.	2
II. EXPERIMENTAL PROCEDURES	12
A. Substrate Preparation.	12
B. Film Fabrication System.	14
C. Vacuum and Gas Handling System	17
D. Oxide-Forming System	17
E. Film Thickness Measurement Apparatus	19
F. Dry Box Procedure.	21
G. Electrical Characteristic Measurement Apparatus.	21
H. Power Supply	27
I. Low Temperature Technique.	27
III. RESULTS AND DISCUSSION.	32
A. Determination of Oxide Parameters.	32
1. Resistance Measurement.	33
2. Implied Oxide Thickness	35
3. Calculated Oxide Thickness.	36
4. Oxide Characteristics	43
5. Summary and Discussion.	44
B. Results of I-V and dV/dI Measurements of Unaltered Junctions.	46
C. Results of Junction Aging.	50
1. Aging of Junction Geometry A in the "Neck" Region.	52
2. Aging of Junction Geometry B in the "Neck" Region.	56
3. Aging of Junctions in a Helium Atmosphere	59
4. Fiske Modes	61
5. Discussion of Aging	69
D. Subharmonic Structure.	70

TABLE OF CONTENTS (Continued)

Chapter	Page
1. Introduction.	70
2. The Creation of Subharmonic Structure . . .	72
3. Investigations of the Detail of Subharmonic Structure	76
4. Review of Some Models of Subharmonic Struc- ture.	83
5. Conclusions on Subharmonic Structure. . . .	84
E. The Filaments Formed	85
1. Introduction.	85
2. Nature of the Filament.	86
3. Measurement of Filament Size.	99
4. Critical Current Density for Lead Filaments	103
5. Summary	106
IV. SUMMARY AND SUGGESTIONS FOR FUTURE STUDY.	107
BIBLIOGRAPHY.	110
APPENDIX.	113

LIST OF TABLES

Table	Page
I. Lead Deposition Rate.	16
II. Resistance Change of A Typical Film (584)	22
III. Comparison of 4 Probe ΔR Measurements	34
IV. Effect of Oxidation Parameters.	37
V. Oxide Resistivity and Thickness	42
VI. Change in Junction Parameters Due to Aging.	55
VII. Values of Zero Bias Current	73
VIII. Ratio of Peak Height to Average Minimum	77
IX. Comparison of Conductance Minimum of Two Junctions.	78
X. Original Resistance for Sample 551.	93
XI. Critical Current Density of Filaments	102
XII. Critical Current Density of Films	104

LIST OF FIGURES

Figure	Page
1. Current Versus Voltage for Junctions With Two Different Current Patterns	4
2. Semiconductor Model of Tunneling	5
3. The Derivative Versus Voltage of a Normal Tunneling Junction	7
4. A Typical Room Temperature Resistance as a Function of Time	8
5. A Typical Subharmonic Pattern.	10
6. Typical Tunneling Junction Sample.	13
7. Film Evaporation Chamber	15
8. Diagram of Vacuum and Gas Handling System.	18
9. Schematic Diagram of Film Thickness Measurement Circuit.	20
10. Diagram of Dry Box System.	23
11. Block Diagram of Tunneling Measurement Circuit	25
12. Schematic Diagram of Tunneling Measurement Circuit	26
13. Schematic Diagram of D.C. Power Supply of Tunneling Measurement Circuit.	28
14. Diagram of Helium Storage Dewar Showing Sample Heights During Aging	29
15. Glass Helium Dewar System With Temperature Measurement Sample Cover	31
16. Diagram of Lead Film Before and After Oxidation.	38
17. Diagram of Junction Showing Oxide.	41
18. I-V Curve for a Typical Superconducting Tunneling Junction	47

LIST OF FIGURES (Continued)

Figure	Page
19. dV/dI Curve for a Typical Superconducting Tunneling Junction	49
20. I-V Curve for Two Junctions of Different Q	53
21. Diagram of Two Junction Geometries	54
22. Resistance Versus Time for Aging of Sample 534	57
23. Resistance Versus Time for Aging of Sample 537	58
24. Resistance Versus Time for Aging of Sample 545	60
25. Block Diagram of Aging System for Sample 547	62
26. Resistance Versus Time for Aging of Sample 547	63
27. Semi Log Plot of Resistance Versus Time for Sample 547	64
28. Resistance Versus Time for Sample 539.	66
29. Fiske Mode Pattern in an Aged Junction	68
30. Subharmonic Structure in a Sample Without Zero Bias Current	71
31. Subharmonic Structure in a Sample With Zero Bias Current	75
32. Conductance Versus Voltage for a Junction Before and After Aging.	79
33. Subharmonic Peak Maxima Versus N	81
34. Divergence From Pure Subharmonic Series for Maxima and Minima	82
35. Zero Bias Current in I-V Curve	87
36. Diagram of Filament Region	90
37. Cross Sectional View of Junction Showing Overlay	91
38. Resistance Versus Time for Sample 549.	92
39. Resistance Versus Time for Sample 551J1.	94
40. Resistance Versus Time for Sample 551J2.	95
41. Resistance Versus Time for Sample 551J3.	96

LIST OF FIGURES (Continued)

Figure	Page
42. The Temperature Dependence of the Critical Current in a Filament	100

CHAPTER I

INTRODUCTION

A. Scope of Study

The quantum mechanical tunneling between two superconductors separated by an insulating barrier, reported by Giaever (1,2), was a landmark experiment because it offered a definitive method for measuring the energy gap in a superconductor. Since that time many experiments have been reported on various aspects of the tunneling phenomenon. However, little work has been done on determining the characteristics of the insulating barrier. It was the scope of this study to determine some of these characteristics and to study the effect of a barrier modification on the superconducting tunneling properties. The barrier characteristics were studied by two methods. One method was to vary the parameters of the system used to make the insulator, and the other method was to measure its thickness. The barrier was modified by aging the tunneling junctions at room temperature in various atmospheres and by completely destroying the insulator in small regions by a transient electrical discharge. It was found that when the barrier was modified by these methods, subharmonic structure appeared in some cases and in other cases relatively large superconducting filaments formed across the insulating region. An explanation of the origin of the subharmonic structure was sought, and a study of the critical current in the filaments was made. A method for increasing the room temperature lifetime of the tunneling

junctions has been developed.

B. Fabrication of Tunneling Devices

The tunneling sample consists of two lead films being separated by an oxide layer. The fabrication process is as follows: A lead film is evaporated onto a glass substrate; the oxide layer is formed by a plasma glow discharge; and a second metal is evaporated onto the oxide barrier. The current which flows through an insulating barrier between two metal plates depends exponentially on the barrier thickness. In order to obtain an easily measured current level, the barrier thickness should be on the order of 100\AA or less (3). In this study, as well as past studies (4-6), the oxide barrier formed yields the desired results.

Other investigators (5) have formed the oxide by exposing the metal film to the atmosphere, or to air at some reduced pressure. The plasma glow discharge (6) is a more desirable method due to the better control of the parameters. Furthermore, with this method one can use gases other than air. By using other gases such as Nitrogen and Argon, it was found that an oxide barrier must be present to form a tunneling junction in the lead film system.

C. Discussion of the Tunneling Process

One of the salient features of the BCS Theory (7) is the theoretical prediction of the energy gap in a superconductor (8). Giaever (1,2) first reported the experimental evidence for the energy gap as measured by tunneling.

When two normal metals are separated by an insulating barrier, a tunneling current appears simultaneously with the application of an emf.

However, when one or both metals are a superconductor, the current is very small until the applied emf reaches a potential which is related to Δ , the BCS energy gap. This phenomenon is illustrated in curve A of Figure 1. Note that the current-voltage characteristic is not linear. This is due to the rapidly varying density of single particle electronic states (s) in a superconductor. The single particle states of an electron in a solid are called quasiparticle states due to the polarization induced by the coulombic interaction (8). The density of states is the number of electron states per unit energy, similar to the electron states in the Fermi Gas model (8). Figure 2 is a schematic representation of the semiconductor model of superconducting tunneling. The density of electron pair states is plotted on the horizontal scale as a function of energy on the vertical scale with the shaded region being the filled states. Superconducting tunneling can be partially explained using this model. When the applied emf is less than 2Δ , a quasiparticle cannot tunnel across the barrier due to the absence of an empty state on the other side. When the applied potential is $\geq 2\Delta$, tunneling can occur since at this potential enough energy is supplied to break up BCS electron pairs thus forming quasiparticles which can tunnel.

The tunneling phenomenon also yields a measure of the density of states (3). The tunneling current is given by

$$I = \frac{1}{eR_{NN}} \int_{-\infty}^{\infty} \rho(E) \rho(E + eV) [f(E) - f(E + eV)] dE \quad (I-1)$$

where $f(E)$ is the Fermi function with $E_F = 0$,

$$f(E) = 1/[1 + \exp(-E/kT)], \quad (I-2)$$

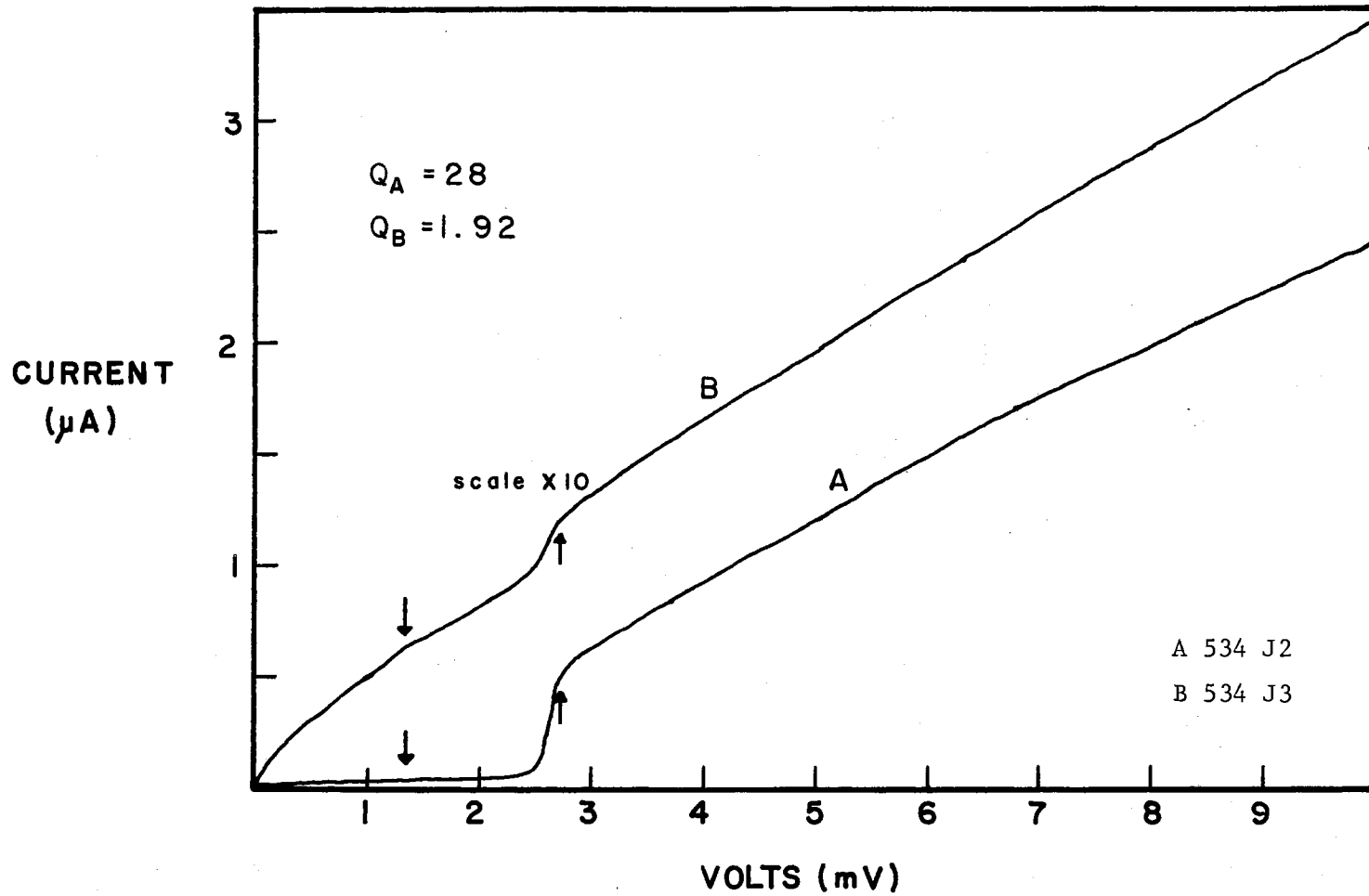


Figure 1. Current Versus Voltage for Junctions With Two Different Current Patterns

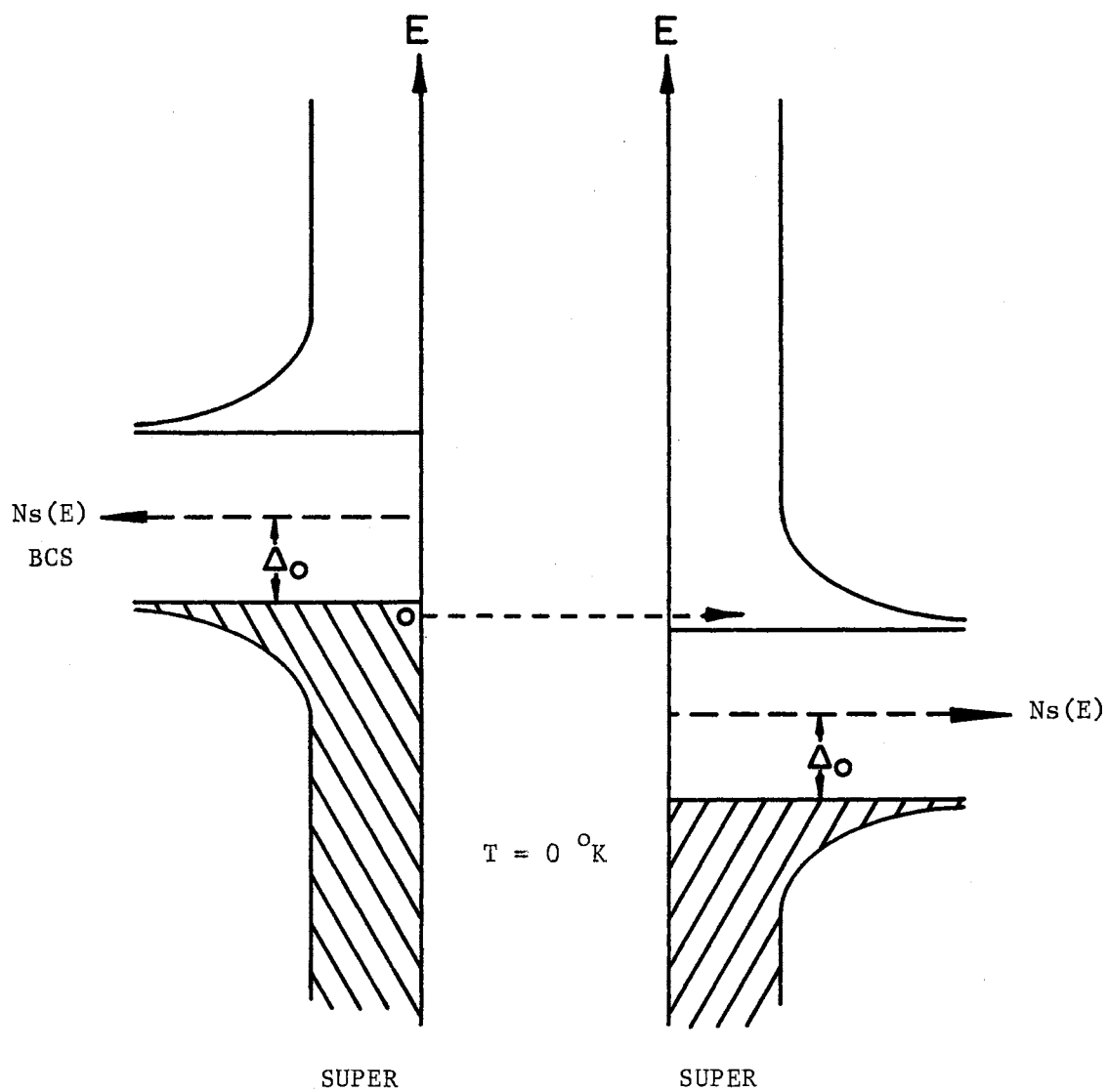


Figure 2. Semiconductor Model of Tunneling

and ρ is the ratio between the superconducting and normal density of states given by (3)

$$\rho(E) = |E|/[E^2 - \Delta^2]^{1/2}, \quad (\text{I-3})$$

and R_{NN} is the normal resistance of the junction, e is the electron charge, E is the electron energy, V is the applied voltage and 2Δ is the energy gap from BCS theory. Assuming one could solve Equation (I-1) for dI/dV , one could calculate the density of states from a dI/dV measurement. Giaever (9) has solved Equation (I-1) for a normal metal-insulator-superconductor system. His result at absolute zero temperature is

$$\begin{aligned} \frac{d I_{\text{NS}}}{dV} &= C_{\text{NN}} \frac{eV}{[(eV)^2 - \Delta^2]^{1/2}} \quad eV > \Delta \\ &= 0 \quad eV < \Delta \end{aligned} \quad (\text{I-4})$$

where C_{NN} is the conductance when both metals are normal. Because the 2Δ transition in the I-V curves is smeared out rather than sharp, the derivative measurement gives a better value for 2Δ than does the I-V measurement. Thus a measurement of the derivative yields the density of states. Figure 3 is an example of a dV/dI versus V curve, dV/dI being measured because of the experimental difficulty of measuring dI/dV .

When the barrier has been modified as discussed in Section I, the room temperature resistance of the junction changes. Figure 4 displays the room temperature resistance versus the time the junction is out of the cryogenic system. The sharp decrease in R at 1.75 hours seems to indicate a breakdown in the barrier in a small region at the edge of the junction. This breakdown is due to a filament which has formed between

$\frac{dV}{dI}$
(ARB)
UNITS

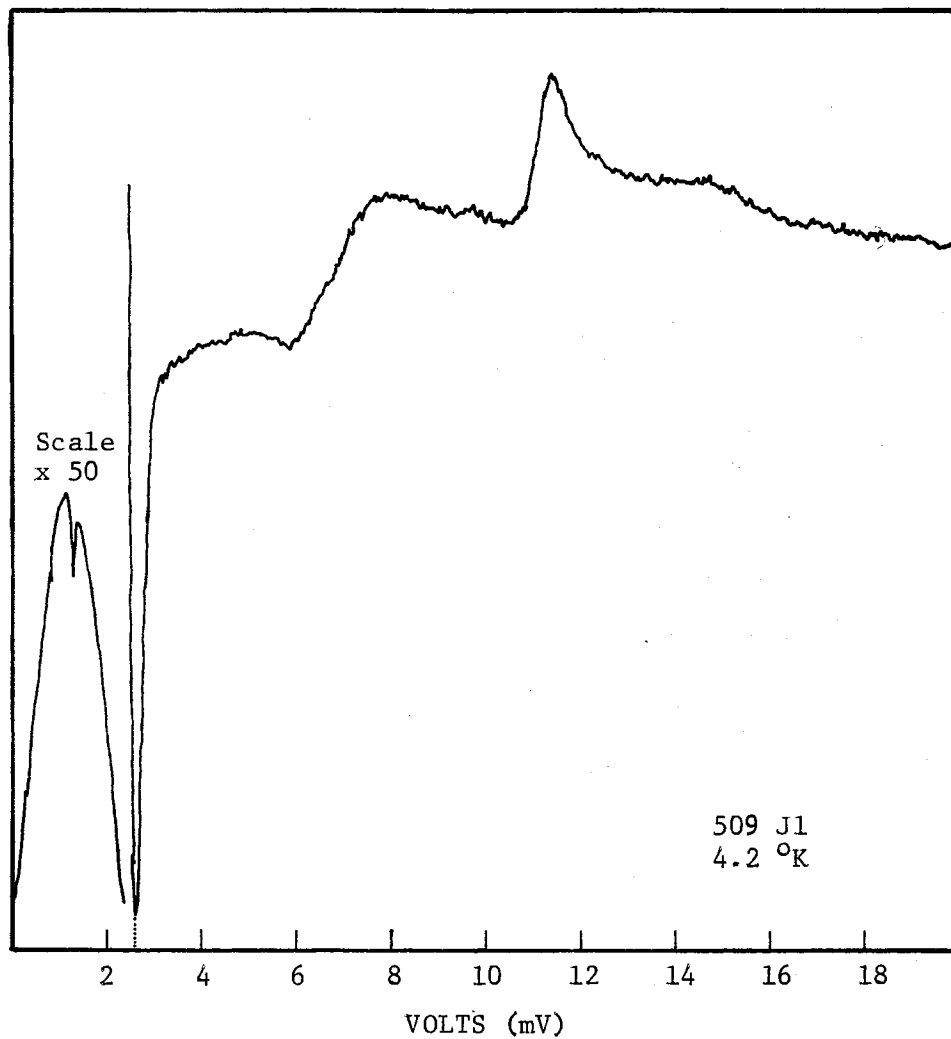


Figure 3. The Derivative Versus Voltage of a Normal Tunneling Junction

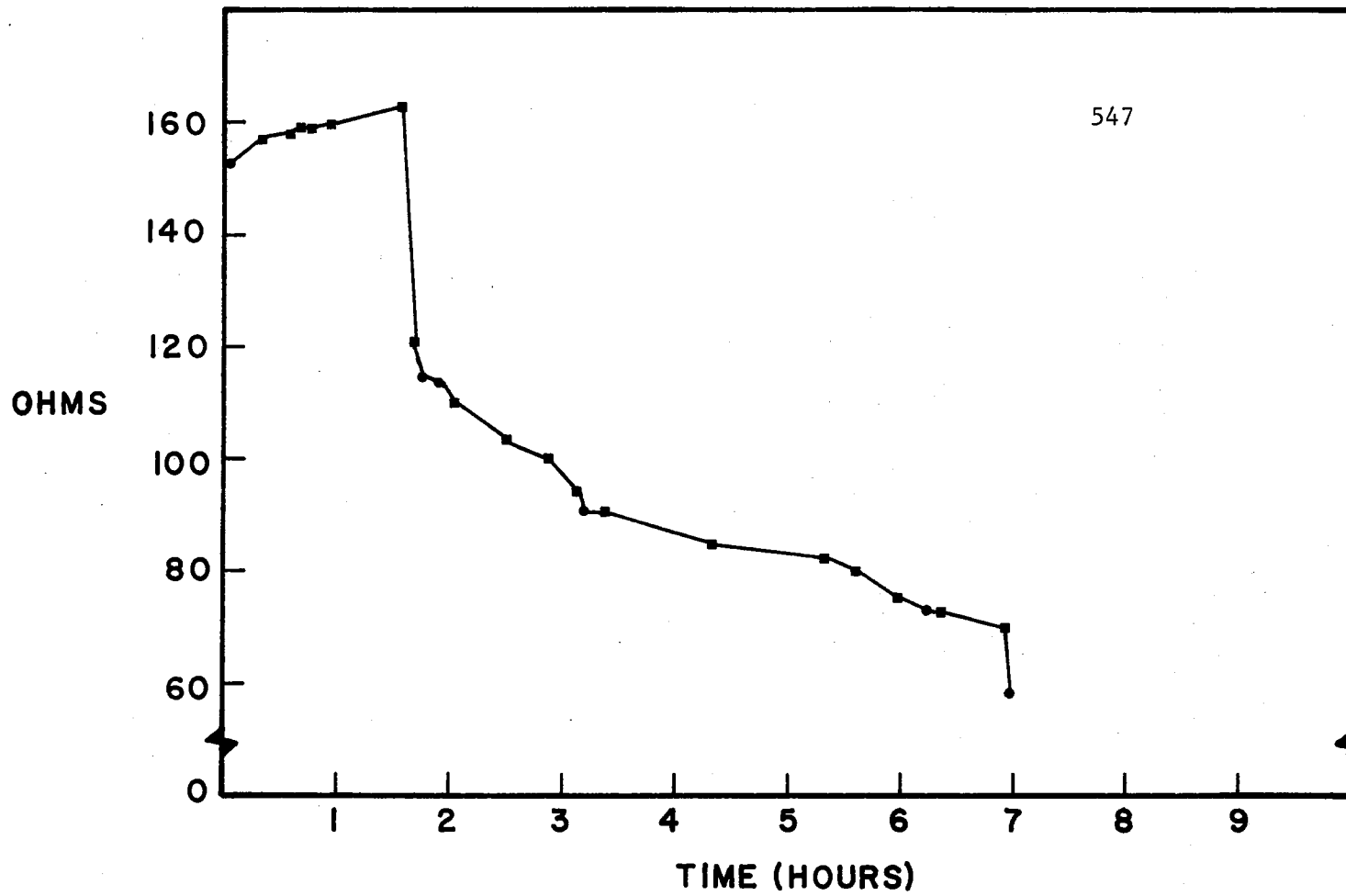


Figure 4. A Typical Room Temperature Resistance as a Function of Time

the two plates. The 4.2°K I-V characteristics of this effect are displayed by curve B in Figure 1 where there is considerable current at V less than 2Δ . The filament in Figure 1 is not a superconductor, although in many cases the filaments are superconductors.

Prior to this study and that of Giaever and Zeller (10), the excess current phenomenon was considered a nuisance to the study of the tunneling phenomena. The excess currents arose in junctions in a random way due to some unusual circumstance either in the fabrication, measurement system, or handling of the junctions (11).

One of the dominant features of junctions with excess current (i.e., curve B, Figure 1) is the appearance of subharmonic structure as seen in Figure 5. The peaks occur at $\approx 2\Delta/N$ where N is an integer hence the term subharmonic structure. This study indicates that a filament, although not necessarily a superconducting filament, can cause the appearance of SHS (Subharmonic Structure), but the $2\Delta/N$ structure does not depend in any apparent way on the method used to generate the filament.

An explanation for the SHS, presented in a number of references (10,11,12) has for its foundation the a.c. Josephson current (3), which exists in a tunneling junction giving rise to a radiation of frequency

$$\nu = \frac{2eV}{h} \quad (I-5)$$

There exist higher harmonics of ν such that

$$N\nu = \frac{N2eV}{h} \quad \text{or} \quad hN\nu = N2eV \quad (I-6)$$

Hence, when the applied voltage is varied such that $N2eV = 2\Delta$, pairs can be broken allowing quasiparticles to tunnel at a voltage less than

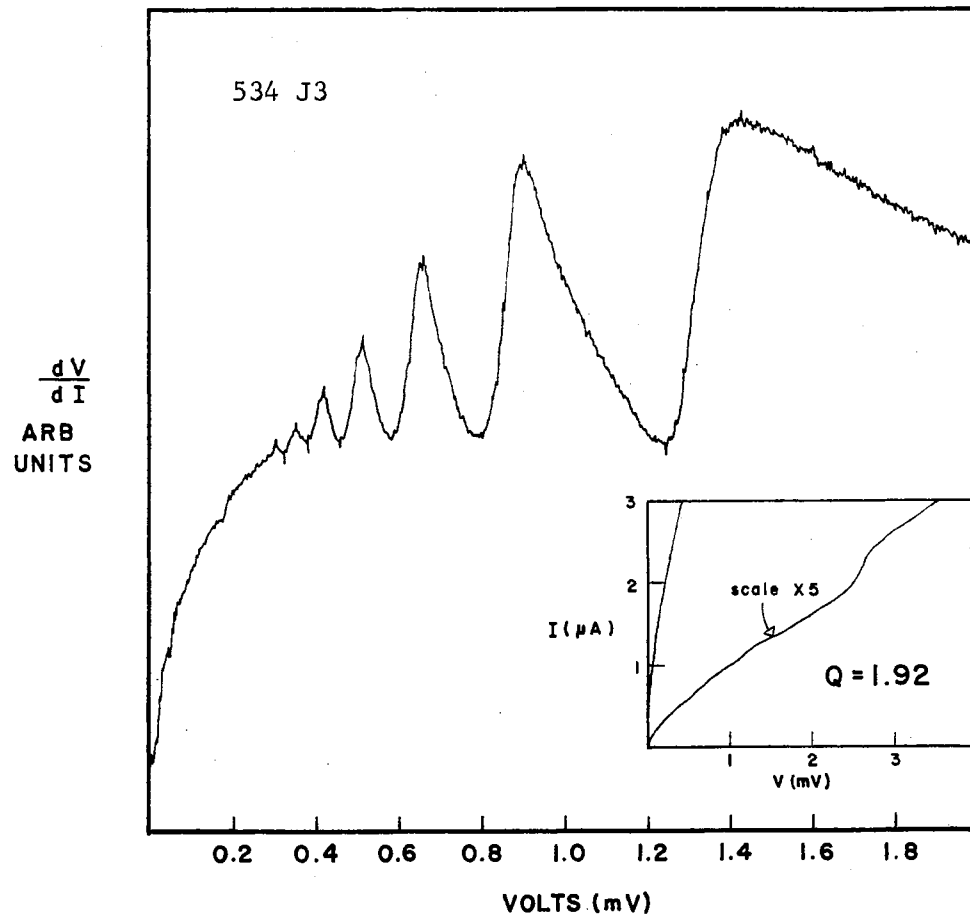


Figure 5. A Typical Subharmonic Pattern

2Δ. The problem arises that

$$eV = \frac{2\Delta}{2N} \quad (\text{I-7})$$

yields only the even subharmonic series. The odd series is explained by an interaction of the Josephson radiation with the single particle tunneling current. The objection to this explanation of SHS is that two separate mechanisms are used to explain a single phenomenon which is independent of the method used to generate it.

Finally, the critical current densities of the filaments, mentioned in Section A, have been investigated. The results indicate that the superconducting filaments are lead as opposed to some alloy or mixed material and that the critical current densities are orders of magnitude greater than those of the thin film plates. Further evidence indicates that the non-superconducting filaments exhibit semiconducting characteristics with the filament becoming more metallic as the aging process progresses.

CHAPTER II

EXPERIMENTAL PROCEDURES

This chapter describes all of the experimental apparatus, its use as it pertains to this study, and some of the various experimental procedures applied in the course of this study. When a procedure was unique to a particular sample, it will be described along with the data for that sample in Chapter III. Unless a specific manufacturer is mentioned, the apparatus was constructed specifically for this and one other previous study (13).

A. Substrate Preparation

The sample, illustrated in Figure 6, consists of two lead films evaporated onto a glass substrate and separated by an oxide layer. The substrate was cut from standard 1 mm thick microscope slides and then was washed in alcohol. The contacts were formed by painting Bright Gold, an Englehard product, onto the substrate which was then fired at 550°C for 2 hours. The substrates were then scrubbed in hot tap water and Alconox and were placed with the number end down in a cleaning holder. The holder with the samples was then immediately placed in a beaker of distilled water. Next the holder was alternately rotated in a beaker of hot Alconox solution and rinsed with hot tap water for 2 or 3 cycles and then was rinsed 3 times in distilled water and once in ethyl alcohol. The final step was an isopropyl alcohol degrease. The degreasing appa-

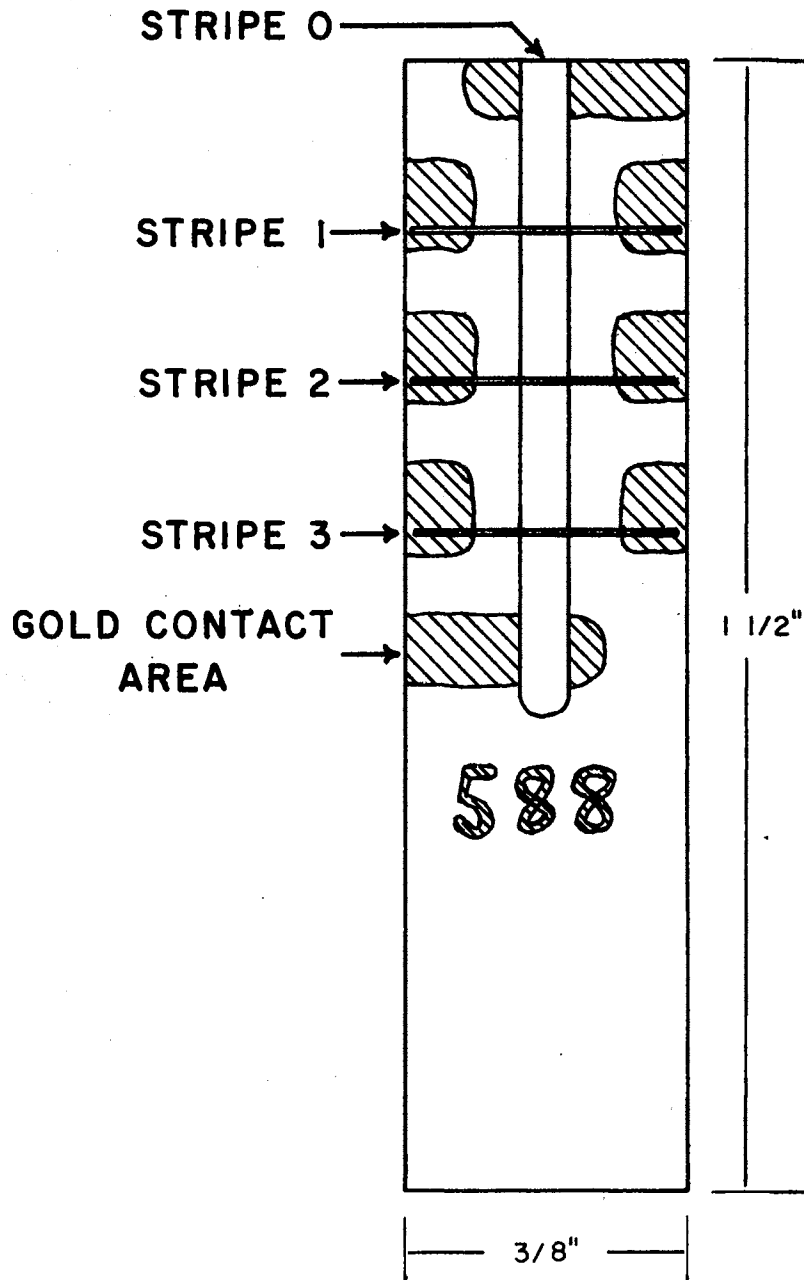


Figure 6. Typical Tunneling Junction Sample

ratus consisted of a 3000 ml beaker with a copper water circulating coil inserted near the top and about 500 ml of isopropyl alcohol boiling in the bottom. After the cleaning procedure, the prepared substrates were placed in vials for storage.

B. Film Fabrication System

The entire sample fabricating vacuum chamber is illustrated in Figure 7. The lead films were formed by vaporizing a lead charge with ≈ 70 amps passing through a R. D. Mathis Company S8A005W tungsten boat. The current was supplied by a Todd Electric #36100B high current transformer and was varied with a Powerstat Variac. The lead was degased for about 40 secs during which time the shutter was closed; then, by use of a magnet from the outside, the shutter was opened for 10 to 20 sec and lead was deposited on the substrate at a rate varying from 26 to $80 \text{ \AA}^{\circ}/\text{sec}$ as illustrated in Table I. The rate varied as the amount of lead in the boat decreased.

The charge was Marz grade lead from Materials Research Corporation prepared by severely etching in equal parts hydrogen peroxide and glacial acetic acid. After etching, the lead was rinsed in distilled water containing a small amount of acetic acid to prevent scale build up on the surface during evaporation. The Variac was set at 20% (22 VAC on the primary of transformer) for both degas and deposition procedures. The lead stripe size was determined by 2 molybdenum masks attached to the mask platform and positioned by the mask platform feedthrough. One mask had a .092 cm opening forming Stripe 0, and the other had three .012 cm openings forming Stripes 1, 2, and 3 thus making the junction area $1.10 \times 10^{-3} \text{ cm}^2$.

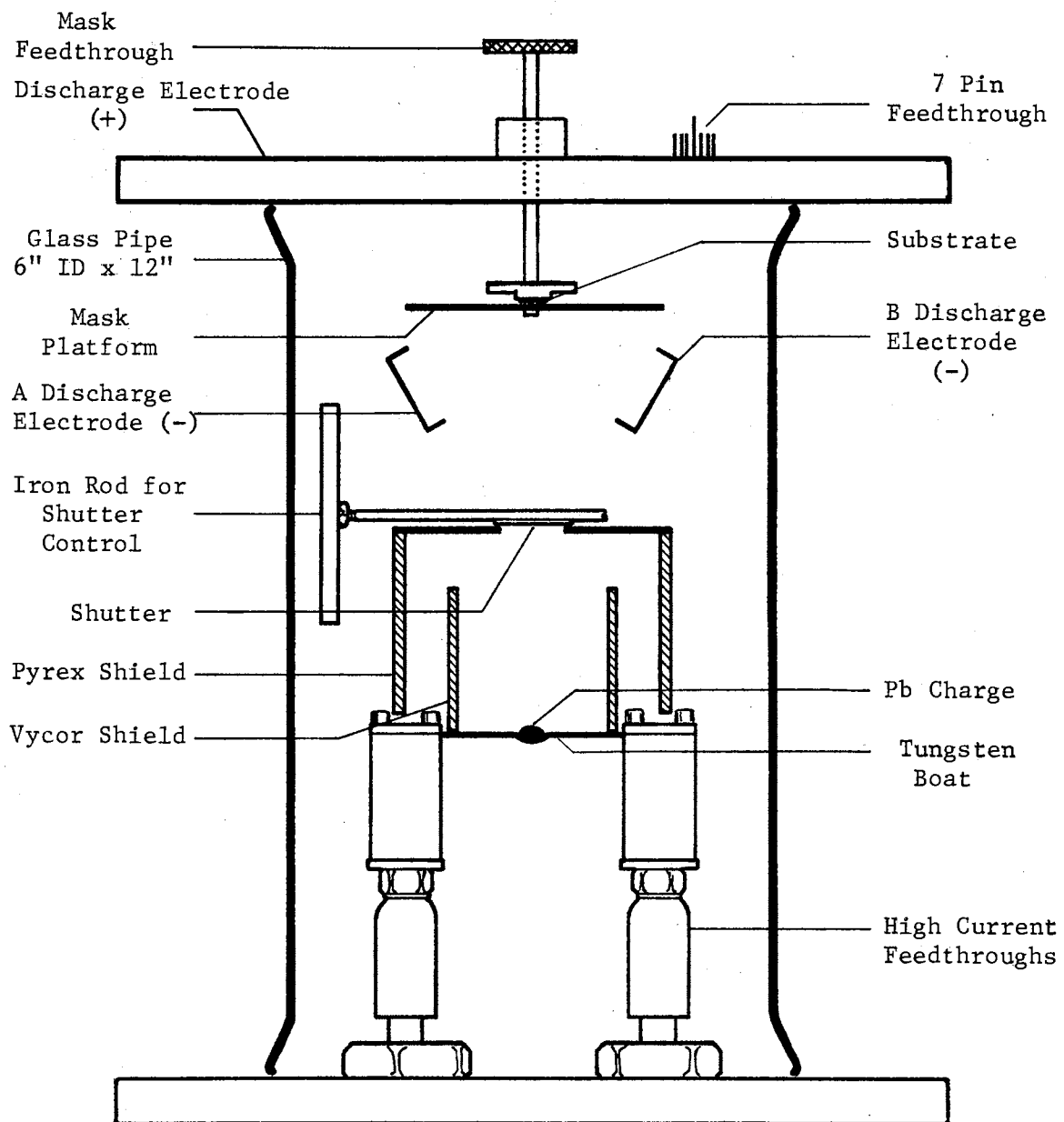


Figure 7. Film Evaporation Chamber

TABLE I
LEAD DEPOSITION RATE

Sample Number	Degas Time Sec	Deposition Time Sec	Transformer Primary Current Amps	$\frac{\text{O}}{\text{A/Sec}}$
568	40	20	2.98	69
569	30	15	2.95	57
571	30	15	≈ 3	69
572	30	15	2.9	69
573	30	15	2.85	69
574	30	15	2.85	75
575	30	15	2.8	75
576	30	15	2.8	89
578	30	15	2.75	83
New Lead Charge Added to Boat				
579	50	10	3.05	26
580	40	15	3.05	25
581	40	20	3.0	36
582	40	20	3.0	36
583	40	20	3.0	45
584	40	20	3.0	46
585	40	20	2.98	46
586	40	15	3.0	55

C. Vacuum and Gas Handling System

The vacuum system, illustrated in Figure 8, was capable of evacuating the evaporation chamber to a pressure of $\approx 6 \times 10^{-7}$ torr which was measured with a Veeco RG 75P Ion Gauge controlled by a Veeco Type RG-31A controller. The thermocouple gauge, which was also controlled by the RG-31A, was a Veeco DV-1M. The lead films were deposited with a pressure which was $< 2.0 \times 10^{-6}$ torr prior to evaporation and which went to $\approx 4 \times 10^{-6}$ torr during evaporation.

The glass diffusion pump was similar to the CVC GF-26 which had a pumping speed of 26 liters per second. The system was cycled to room pressure by closing gate valve V3 and bleeding up to atmosphere with dry oxygen through valves V1, V2 and V6. The number V1 and V2 valves were also used to let oxygen into the system for the plasma glow discharge which formed the oxide barrier. The capillary had an approximate volume of 70 mm^3 , with this volume at 25 PSI above atmospheric pressure raising the pressure in the system to ≈ 100 microns. The oxygen from the supply bottle was passed through a "U" tube in a dewar of dry ice and acetone thus trapping impurities with a condensation temperature above -56.6°C . The vacuum system used was similar to that used in a previous work (13).

D. Oxide-Forming System

A plasma glow discharge was used for forming the oxide barrier as well as cleaning the substrate prior to evaporation of the lead films. This technique has been used by other investigators (14) to form the insulating barrier. After the O_2 gas was bled into the system as described in the previous section, the two discharge electrodes A and B in Figure 7 were biased negatively with respect to the top plate of the

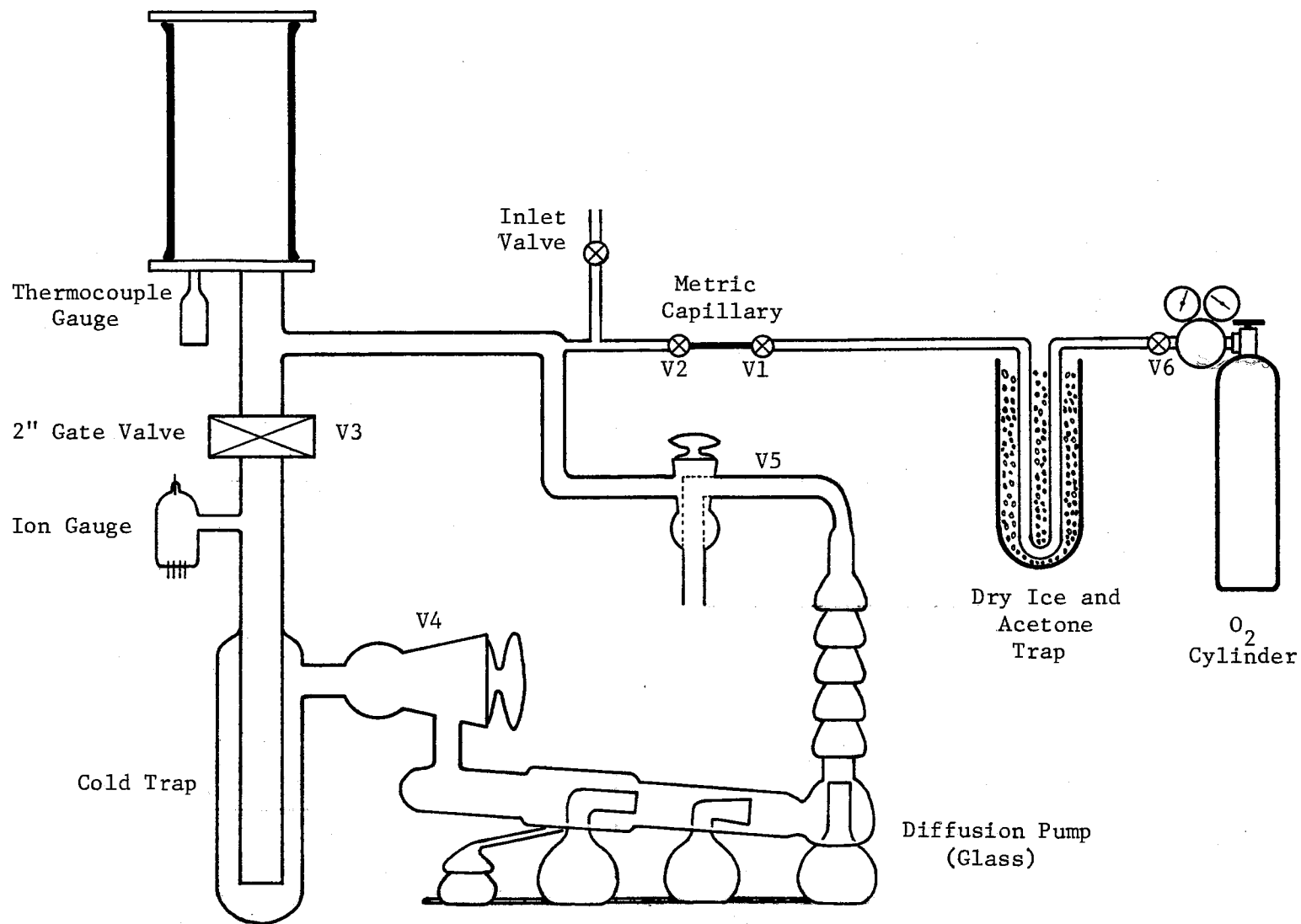


Figure 8. Diagram of Vacuum and Gas Handling System

vacuum system and hence the mask platform. When the high voltage primary Variac was set at 100%, the position for substrate cleaning, a 1675 volt potential was developed between the negative electrodes and positive mask platform and when the Variac was set at 32%, the position for oxide formation, a 480 volt potential was developed. It was found that tilting the negative electrodes ≈ 15 degrees from the vertical improved the oxide. The glow discharge was maintained for ≈ 200 seconds during cleaning and from 10 to 15 sec during oxide formation. The junction resistance as a function of oxidation time will be discussed in the results section.

E. Film Thickness Measurement Apparatus

The film thickness was determined by measuring the film resistance both before and after oxidation by the 4 probe technique and the bridge technique. The measurement circuit is illustrated in Figure 9. In the 4 probe technique the current was determined by measuring the voltage across a 100 ohm $\pm 1\%$ resistor, and the voltage drop across the film was measured directly. A reversing switch was used to determine the effect of any rectification in the contacts. For comparison, the resistance was measured directly with a Leeds and Northrup 4760 Bridge on both pair of leads A, B and C, D. The 6V supply and Keithley Voltmeters were out of the circuit when the bridge was used, and the bridge was out of the circuit when the 4 probe technique was used.

The electrical contact to the film was made with AWG #24 stranded copper wire connected to a stainless steel sleeve which was connected to the top feedthrough in Figure 7. On the inside of the vacuum system connection was made from stainless steel sleeves to phosphor bronze spring clips by AWG #30 magnet wire. The phosphor bronze spring clips

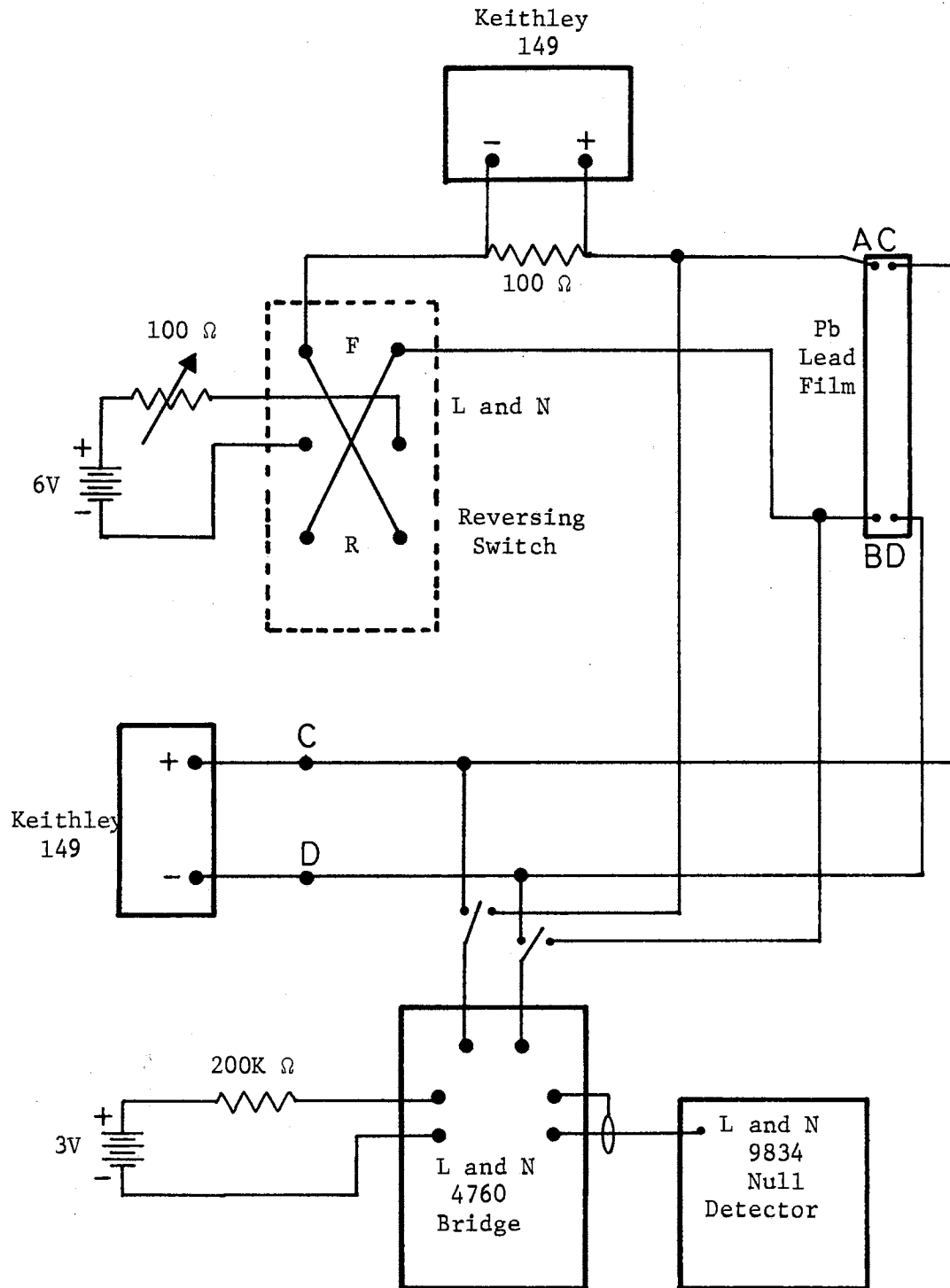


Figure 9. Schematic Diagram of Film Thickness Measurement Circuit

made contact with the gold or the lead which was evaporated onto the gold.

The resistance changes of all the measurements were averaged to give a ΔR which was used in the calculation of the oxide thickness. Table II is a sample of data from the #584 film. The columns are the voltage readings across the 100 ohm resistor and the film, respectively, and the two bridge measurements are appropriately labeled. A discussion of the accuracy of these measurements will be presented in Chapter III along with the results of the thickness measurement.

F. Dry Box Procedure

It was found in the course of this work that the junctions were extremely sensitive to the humidity of the ambient conditions surrounding the samples. Hence, a mechanism was devised to keep the samples as dry as possible while transferring from the vacuum system to the electrical characteristics sample holder. A block diagram of this mechanism is illustrated in Figure 10. Air was passed through CaSO_4 and then silica gel and on into a dry box. The humidity in the dry box was typically on the order of 20% when the sample was changed. The vacuum system was bled up to atmosphere with the oxygen from the glow discharge supply after which the sample was quickly transferred to the dry box.

G. Electrical Characteristic

Measurement Apparatus

The sample holder which makes the electrical connection between the measurement devices and the junction sample was described and illustrated in a previous work (13). This holder was so designed that it can be used

TABLE II
RESISTANCE CHANGE OF A TYPICAL FILM (584)

Before Oxidation			
Volts 100 Ω Resistor	Volts Film	Switch Position	Resistance Ohms
N .2 μ V		F	
N- 4 μ V		R	
	N- .6 μ V	F	
	N-2.5 μ V	R	
.900 mV	.342 mV	F	38.00 F
-.900 mV	-.350 mV	R	38.89 R
.900 mV	.342 mV	F	38.00 F
-.900 mV	-.350 mV	R	38.89 R
.600 mV	.227 mV	F	37.83 F
-.605 mV	-.240 mV	R	39.67 R
.600 mV	.228 mV	F	38.00 F
-.605 mV	-.240 mV	R	39.67 R
			Average = 38.62
			Ave. R = 39.28
Bridge Measurements AB 39.68 CD 39.83			Ave. F = 37.96
After Oxidation			
N-1.4 μ V		F	
N-2.7 μ V		R	
	N-1.1 μ V	F	
	N-1.8 μ V	R	
.900 mV	.355 mV	F	39.44 F
-.900 mV	-.360 mV	R	40.00 R
.900 mV	.355 mV	F	39.44 F
-.900 mV	-.360 mV	R	40.00 R
.600 mV	.233 mV	F	38.83 F
-.600 mV	-.247 mV	R	41.17 R
.600 mV	.232 mV	F	38.67 F
-.600 mV	-.246 mV	R	41.00 R
Bridge Measurements AB 41.14 CD 41.48			
Δ RF = 1.14			
Δ RR = 1.26			
Δ RT = 1.20			Average = 39.82
Δ R AB = 1.46			Ave. R = 40.54
Δ RCD = 1.65			Ave. F = 39.10
Ave. Δ R = 1.38			

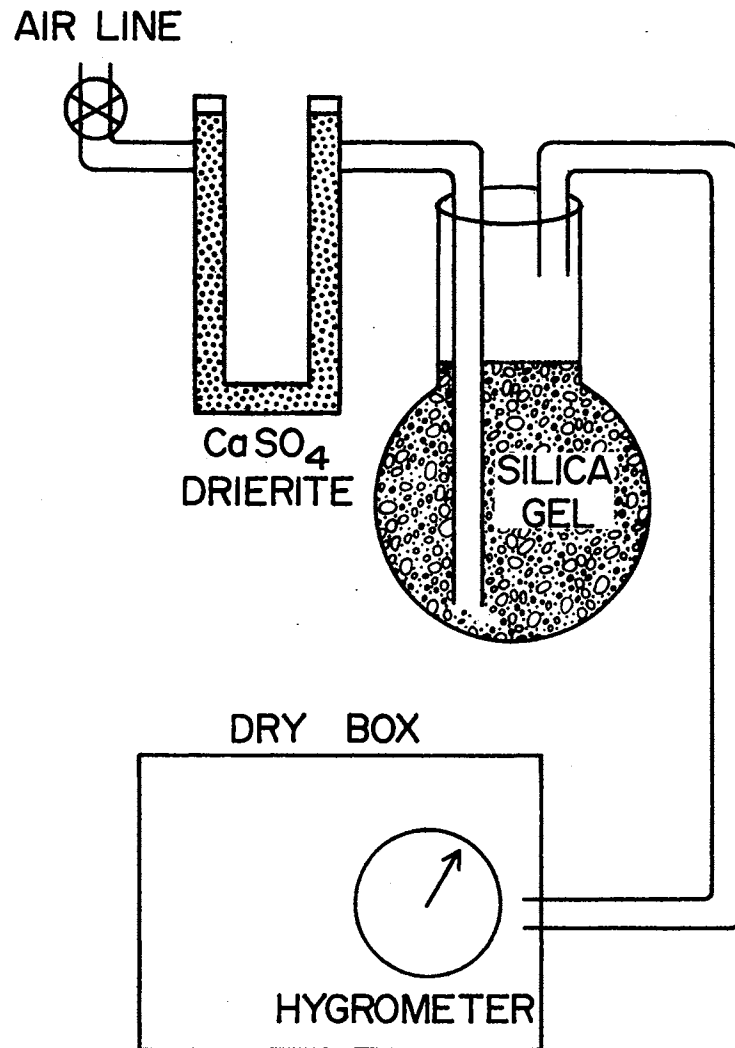


Figure 10. Diagram of Dry Box System

to immerse the sample directly into the liquid helium storage dewar or a vacuum-tight glass dewar system, both of which will be described in the next section.

The electrical system, Figure 11, was capable of measuring the current voltage characteristics of the junction, the derivative dV/dI and the second derivative d^2V/dI^2 . The schematic diagram of the System Control Unit, Figure 12, makes the interaction of the components in Figure 11 more clear. The d.c. power supply will be discussed in detail below in this section.

The current-voltage characteristics were measured by the four probe technique as follows. The main function selector switch, S2 in the schematic was in position 1. The coils and transformers were then out of the circuit and a current from the constant current d.c. source could flow through the current shunts, selected by S3, and the junction. The current was monitored by measuring the voltage drop across the appropriate shunt and was displayed on the Y axis of the recorder with full scale being 10 mV in each current range. The voltage drop across the junction was measured directly by the recorder and was displayed on the X axis. The four probe technique was established by connecting the current leads directly to one end of Stripe S0 and Stripe S1, 2 or 3 depending on which junction was being investigated. The voltage leads were then connected to the other end of Stripe S0 and S1, 2 or 3. The recorder, a Leeds and Northrup XL 680, had a 4 megohm input impedance.

The derivative measured was a change in voltage with respect to the change in current as a function of voltage. A 2000 Hz signal from a General Radio 1161A Coherent Decade Frequency Synthesizer was connected to the reference of the PAR Model HR-8 Lock-In Amplifier and to the

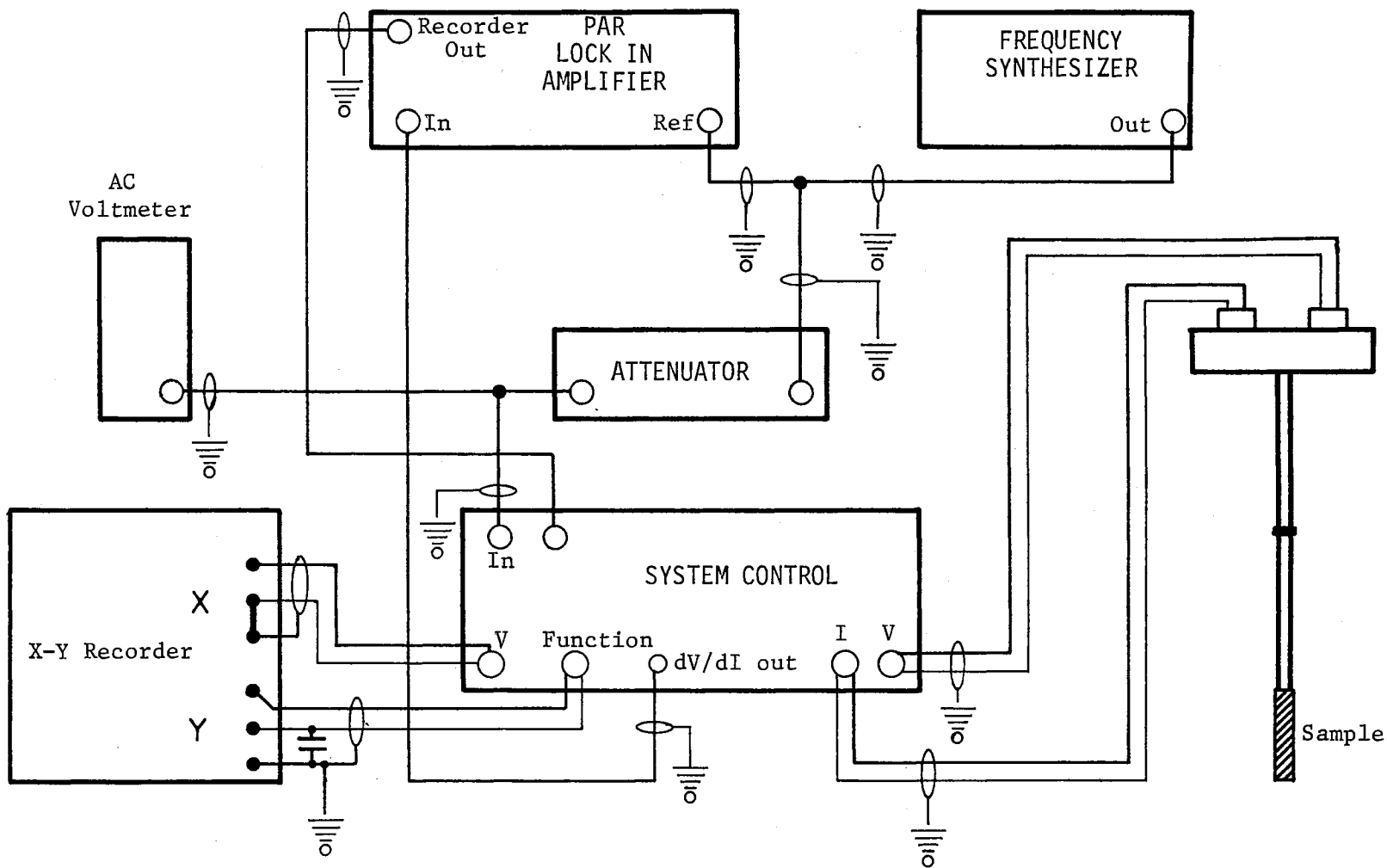


Figure 11. Block Diagram of Tunneling Measurement Circuit

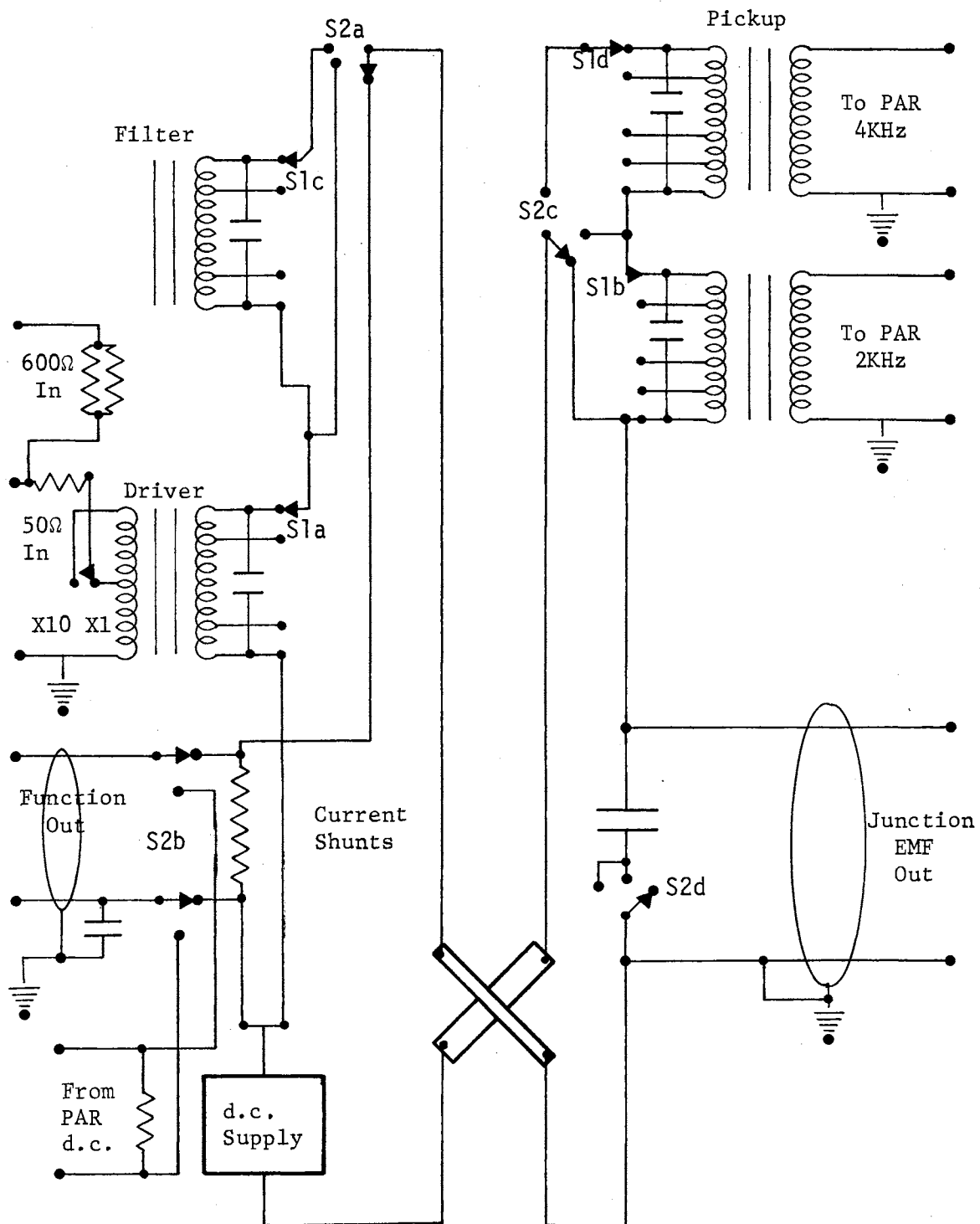


Figure 12. Schematic Diagram of Tunneling Measurement Circuit

input of a calibrated attenuator. The output of the attenuator was then connected to the 600 ohm input of the Driver transformer and to a Hewlett Packard 400D a.c. voltmeter. When the selector switch, S2, was in the number 2 position, the system was in the dV/dI mode of operation. A 2000 Hz a.c. current was added to the d.c. current by the Driver transformer. The resultant a.c. voltage was detected by the dV/dI Pickup transformer whose output was put into the input of the Lock-In Amplifier. This signal was compared with the reference signal thus eliminating noise of frequency other than 2000 Hz. The transformers, coils, and filters in the System Control Unit were wound on Magnetics Incorporated #55252 Permalloy Cores.

H. Power Supply

The schematic diagram of the d.c. Power Supply in the System Control Unit is illustrated in Figure 13. The resistors R_1 were chosen such that the output voltage ranged from 0.05 mv to 5000 mv in 11 ranges. On each range the output voltage was varied from 0 to V_{max} for that range by a 10 turn 2.9 ohms Amphenol 205 potentiometer. To maintain a constant current source, the power is supplied by 2 alkaline 1.5 volt D cells connected in parallel. To supply the 1500 and 5000 mV ranges, the Power Supply is switched into the amplifier mode. The 1.5 volts is then amplified up to 5 volts by a General Electric D12A8 Differential Amplifier. The other components are shown in Figure 13.

I. Low Temperature Technique

Most of the measurements were made at 4.2°K by immersing the sample into a liquid helium storage dewar which is illustrated in Figure 14. A

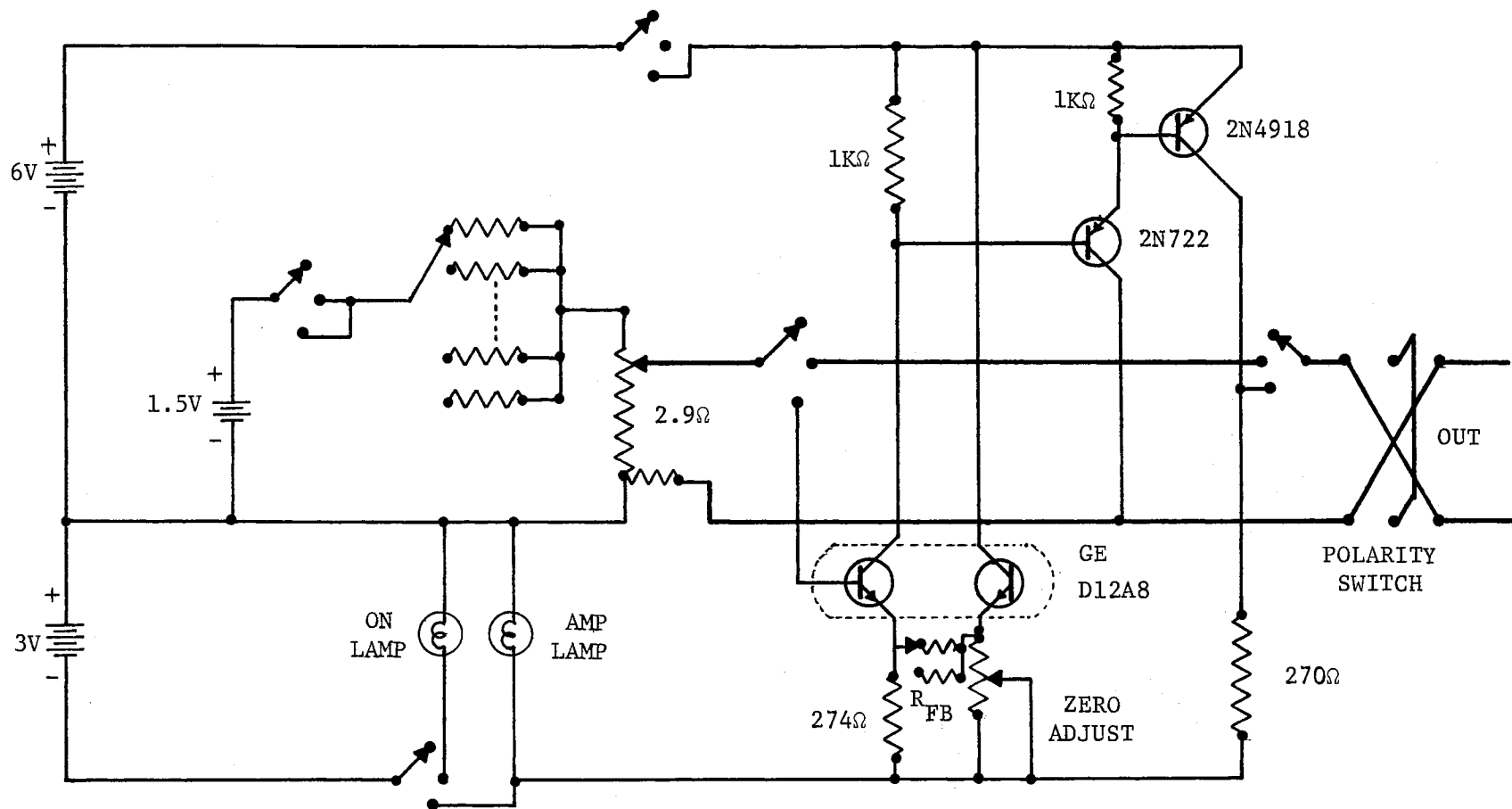


Figure 13. Schematic Diagram of D.C. Power Supply of Tunneling Measurement Circuit

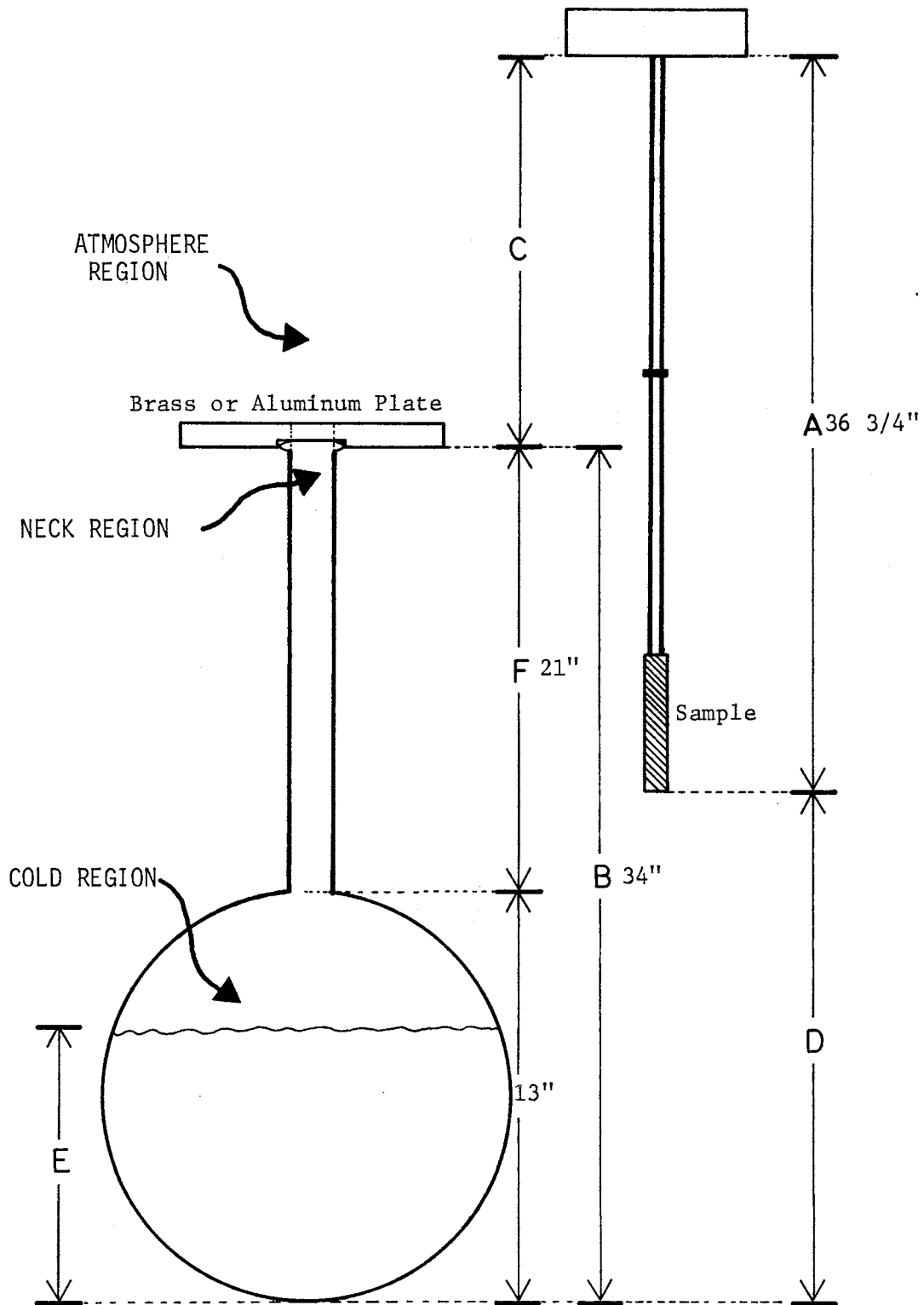


Figure 14. Diagram of Helium Storage Dewar Showing Sample Heights During Aging

is the length between the top of the sample holder and the bottom of the stainless tube which covered the samples, B is the distance from the top plate to the bottom of the dewar, C is the height measured when withdrawing or inserting the sample holder, and D is the height of the sample cover above the bottom of the dewar. Thus

$$D = C - 2.75''$$

and

$$H = D - E .$$

H, the height of the sample above the helium is equal to $D - E$ where E, the height of the helium liquid, is measured before insertion of the sample holder. F is the length of the neck of the dewar. The length C determined the type of aging experiment which was performed. For example, if $30.75'' < C < 36.75''$ the aging procedure was said to be a "neck" aging meaning that the helium boil off gas constitutes the ambient of the samples.

The measurements with the sample temperature $T > 4.2^{\circ}\text{K}$ were made in a glass dewar system illustrated in Figure 15. The sample cover was copper and was covered with $\sim 0.075''$ of teflon tape. Attached to the bottom of the can were a number of copper wires 3", 2" and 1" in length. The sample was lowered into the liquid helium until $\sim 1/2$ of the cover was immersed. As the liquid helium level fell below the bottom of the cover, the heat in the sample was conducted away by the wires. As the level dropped, fewer wires were immersed thus conducting less heat and raising the temperature of the sample. The temperature of the sample was measured by utilizing its superconducting nature in a way which will be discussed in Chapter III.

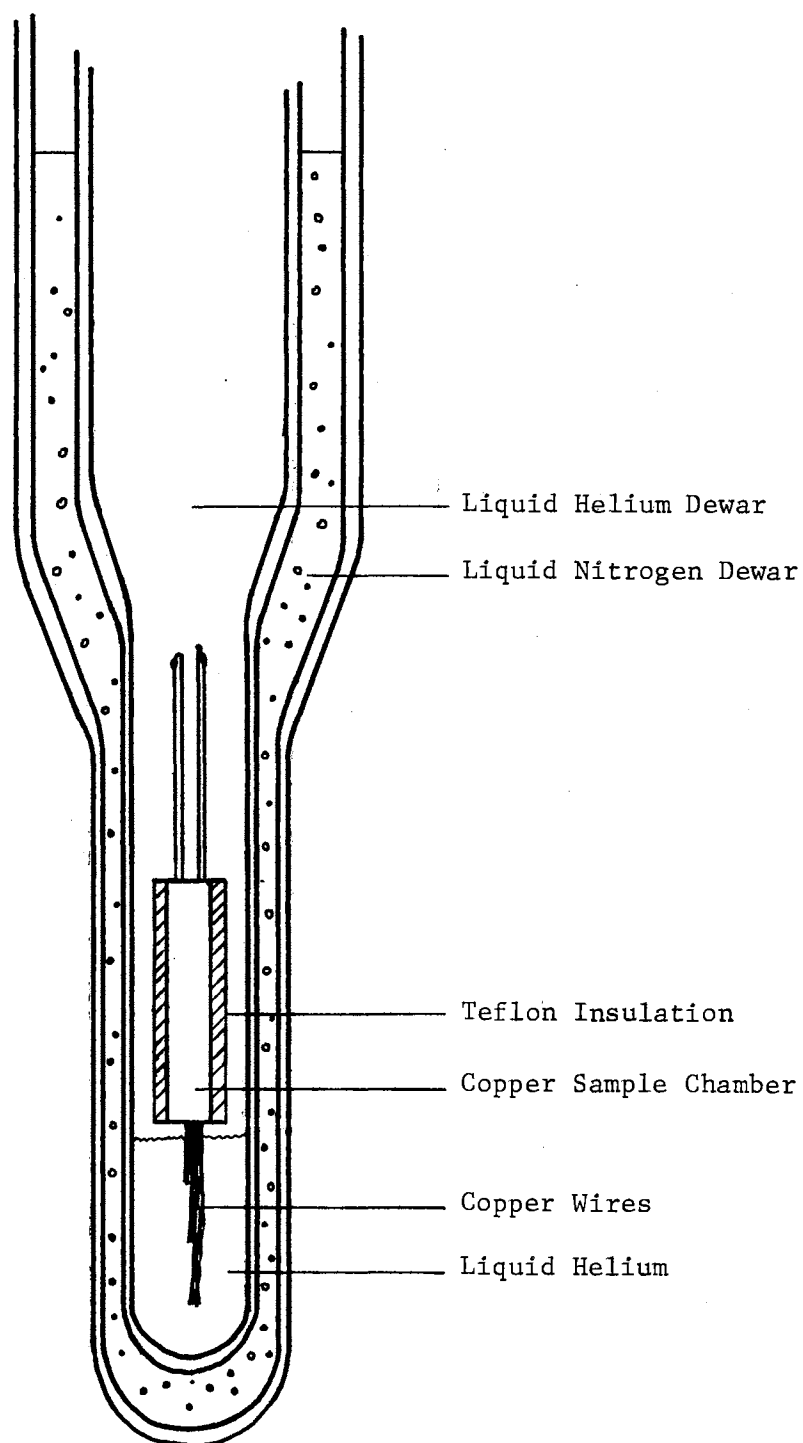


Figure 15. Glass Helium Dewar System With Temperature Measurement Sample Cover

CHAPTER III

RESULTS AND DISCUSSION

This chapter is divided into five major sections, each one of which is subdivided. The first section deals with the determination of the insulating barrier parameters including the thickness, and the nature of the oxide. The second section merely describes the I-V and dV/dI data for normal unaltered junctions. Section III goes into the detailed aspects of the aging procedure and the results obtained. Rather than make a general discussion of this section, selected aging data are presented in the form of examples. The fourth section gives a detailed analysis of the subharmonic structure and discusses the mechanism in the junction which leads to its appearance. The final section is a discussion of the nature of the filaments which are formed including their semiconducting and superconducting behavior.

A. Determination of Oxide Parameters

One of the fundamental and important problems in the study of superconducting tunneling phenomena is the determination of the various parameters of the tunneling barrier. The problem is difficult because the thickness of the barrier is on the order of 50\AA ⁰ which is a few molecular layers. The methods of determining the thickness have ranged from ellipsometry (15) to Fowler-Nordheim plots (16) to capacitance measurements (16). These methods are cumbersome, require elaborate apparatus,

and require assumptions which may be incorrect. In the case of ellipsometry the complex refractive index $[n_{pb}^* = n_{pb} (1 - i\kappa_{pb})]$ of the unoxidized lead can vary with the average oxide thickness (15). Here n_{pb} is the real part of the refractive index and κ_{pb} is the extinction coefficient. In the capacitance measurements the dielectric constant of bulk material is usually assumed.

1. Resistance Measurement

In this work the oxide thickness was determined by measuring the change in resistance (ΔR) of the lead film both before and after oxidation. This ΔR , when coupled with the room temperature junction resistance, yielded the resistivity and thickness of the oxide. As was pointed out in Chapter II, Section E, the ΔR from the forward direction, the reverse direction, and the bridge measurements were averaged to yield a mean ΔR . Table III presents the results of the 0 stripe resistance change measurements for a number of samples. The columns present the following information: the first is the sample number, the second is the resistance change in the forward direction, the third is the resistance change in the reverse direction, the fourth is the average of the resistance change of the forward and reverse directions, the fifth is the percent change of the forward and reverse ΔR compared to the average ΔR , and the sixth is the ΔR used in the calculation of the thickness. This last ΔR includes the measurements made with the bridge. The bridge measurement was the only one used in Sample Number 583 as the 4 probe measurements were deemed unacceptable. With the possible exception of numbers 569, 583, and 586 the agreement of the measurements is on the average, about 6% which is greater than the accuracy of the measurement.

TABLE III
COMPARISON OF 4 PROBE ΔR MEASUREMENTS

Sample Number	ΔRF	ΔRR	Ave. ΔRT	$\frac{\Delta RF - \Delta RT}{\Delta RT}$	Used ΔR
				%	
569	1.04	.34	.69	51%	1.1
571	1.21	1.52	1.37	12%	1.2
572	2.18	2.23	2.21	1.4%	2.2
573	.87	1.03	.95	84%	.9
579	19.1	19.0	19.1	0.5%	19
580	9.76	9.39	9.58	1.9%	9.4
581	1.85	2.04	1.95	5.1%	1.98
582	2.16	2.88	2.52	14%	2.42
583 { Bridge Only	.46	1.91	1.19	61%	1.32
584	1.14	1.26	1.2	5%	1.38
585	1.18	1.16	1.17	0.85%	1.27
586	1.45	.71	1.08	34%	1.5

To illustrate this fact the following analysis is presented. Assuming that the ability to read the meter scale is $\pm .003$ mV on the 1 mV full scale reading, the error in the measurement of .9 mV on the Keithley 149 is $\pm .33\%$. Since the current $I = V/R$ where R is the 100 ohm resistor and V is the voltage drop across the resistor,

$$I = I \text{ measured} \pm .33\%$$

The voltage measured across the film is on the order of

$$.342 \text{ mV} \pm .003 \text{ mV},$$

$$\text{or, } .342 \text{ mV} \pm .88\%$$

Hence, the accuracy in measuring the resistance is

$$R = \frac{V}{I} = \frac{V_{\text{Film}}}{V_{\text{Resistor}}} R \pm (.33\% + .88\%),$$

$$\text{thus, } R = R \text{ measured} \pm 1.21\%$$

One can notice in Table III that the agreement between R_{FORWARD} and R_{REVERSE} is better in some cases than the accuracy of the measurement.

2. Implied Oxide Thickness

The oxide thickness can be implied directly from the resistance measurements by using the definition of resistivity,

$$R = \frac{\rho L}{tW}, \quad t = \frac{\rho L}{RW}, \quad (\text{III-1})$$

where R is the measured resistance of the film, ρ is assumed to be the resistivity of bulk lead, L is the length of the film, and W is the

width of the film. For all of the samples measured $L = 1.65$ cm, $W = .092$ cm, and $\rho = 19.8 \times 10^{-6}$ ohm-cm. Thus, Equation (III-1) becomes

$$t = \frac{3.551 \times 10^{-4} \text{ cm}}{R}, \quad (\text{III-2})$$

which was used for all samples measured. The thickness of the oxide is Δt in Equation (III-3),

$$\Delta t = t_B - t_A$$

where (III-3)

$$t_A = \frac{R_B}{R_A} t_B,$$

and the B represents measurements before oxidation and A represents measurements made after oxidation. R_B is determined by using the average forward value of the resistance as determined by the 4 probe technique. Calculating the thickness in this manner one assumes that the resistivity of the oxide is infinite. Hence, in Table IV the column listing the oxide thickness is an Implied Oxide Thickness. The other columns in the table will be discussed below. Figure 16 depicts the lead film before oxidation and the film and oxide layer after oxidation. In this figure t_T is the total thickness of the lead before oxidation with the oxide thickness being t_o and the after oxidation lead being t_{pb} .

3. Calculated Oxide Thickness

To avoid the problem of assuming the resistivity of the oxide is infinite, one can solve a set of equations for the ρ_{oxide} using measured parameters. Assuming that the film after oxidation is a pair of resis-

TABLE IV
EFFECT OF OXIDATION PARAMETERS

Sample Number	Gas	Pressure (X 10 ⁻³ mm)	Oxidation Time (Sec)	Implied Oxide Thickness (Å)	Junction Resistance (Ohms at 300°K)		
					1	2	3
578	Nitrogen	320	150	9	0	0	0
576	Nitrogen	155	12	10	0	0	0
575	Argon	95	100	7	0	0	0
574	Argon	95	11	0	0	0	0
572	Oxygen	50	100	62	0	0	0
571	Oxygen	50	10	22	0	0	0
569	Oxygen	50	30	33	0	0	0
581	Oxygen	97	12	27	34	48	19
582	Oxygen	105	12	33	.5	.1	.1
583	Oxygen	150	12	29	1.56K	2.04K	5.35
584	Oxygen	150	11	31	392	313	149
585	Oxygen	150	12	29	1.98K	1.90K	1.88
573	Oxygen	155	11	26	1.37K	1.82K	253
579	Oxygen	325	12	32	1.67	1.63	1.72
580	Oxygen	350	12	34	504	16	27

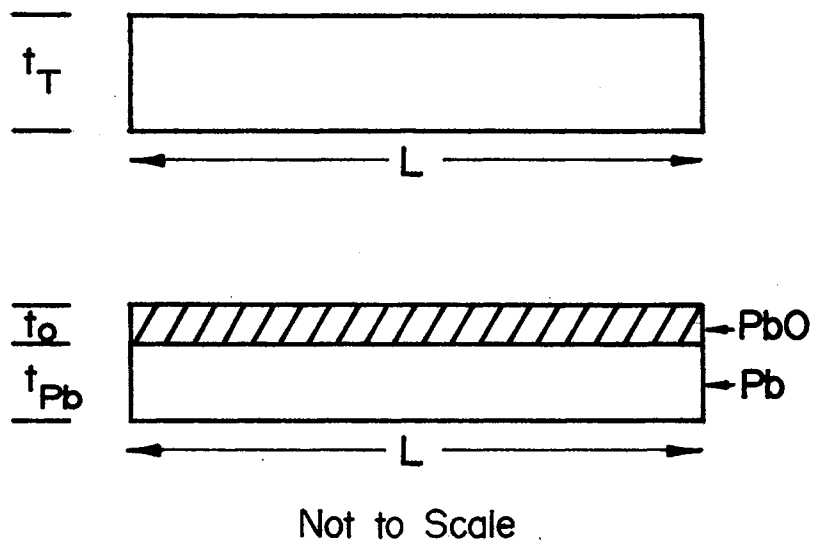


Figure 16. Diagram of Lead Film Before and After Oxidation

tors in parallel,

$$\frac{1}{R_T} = \frac{1}{R_o} + \frac{1}{R_{Pb}} \quad (\text{III-4})$$

where R_T is the total resistance, R_o is the oxide resistance, and R_{Pb} is the lead film resistance. Now,

$$R = \frac{\rho L}{tW} = \frac{\rho K}{t} \quad (\text{III-5})$$

where K is the length divided by the width of the film, this quantity being a constant. Then

$$\frac{1}{R_T} = \frac{1}{\rho_o K} + \frac{1}{\rho_{Pb} K} \cdot \frac{1}{t_o} \quad (\text{III-6})$$

From Figure 16 one can assume that

$$t_T - t_o = t_{Pb} \cdot \quad (\text{III-7})$$

Replacing t_{Pb} in Equation (III-6) by Equation (III-7), $1/R_T$ becomes

$$\frac{1}{R_T} = \frac{t_o}{\rho_o K} + \frac{t_T}{\rho_{Pb} K} - \frac{t_o}{\rho_{Pb} K} \cdot \quad (\text{III-8})$$

The quantity of interest is the thickness of the oxide, t_o . Solving Equation (III-8) for this quantity one obtains Equation (III-9), which is

$$\left(\frac{K}{R_T} - \frac{t_T}{\rho_{Pb}} \right) \left(\frac{\rho_o \rho_{Pb}}{\rho_{Pb} - \rho_o} \right) = t_o \cdot \quad (\text{III-9})$$

Equation (III-9) contains the measured quantities K , R_T and t_T , the resistivity of the lead film, ρ_{Pb} , which is assumed to have the bulk value of lead, and two unknowns, the resistivity of the oxide, ρ_o , and the oxide thickness.

The thickness of the oxide can also be obtained from the room temperature junction resistance. From Figure 17 one can see

$$R_J = \frac{\rho_o t_o}{C'} \quad \text{or} \quad \frac{R_J C'}{\rho_o} = t_o, \quad (\text{III-10})$$

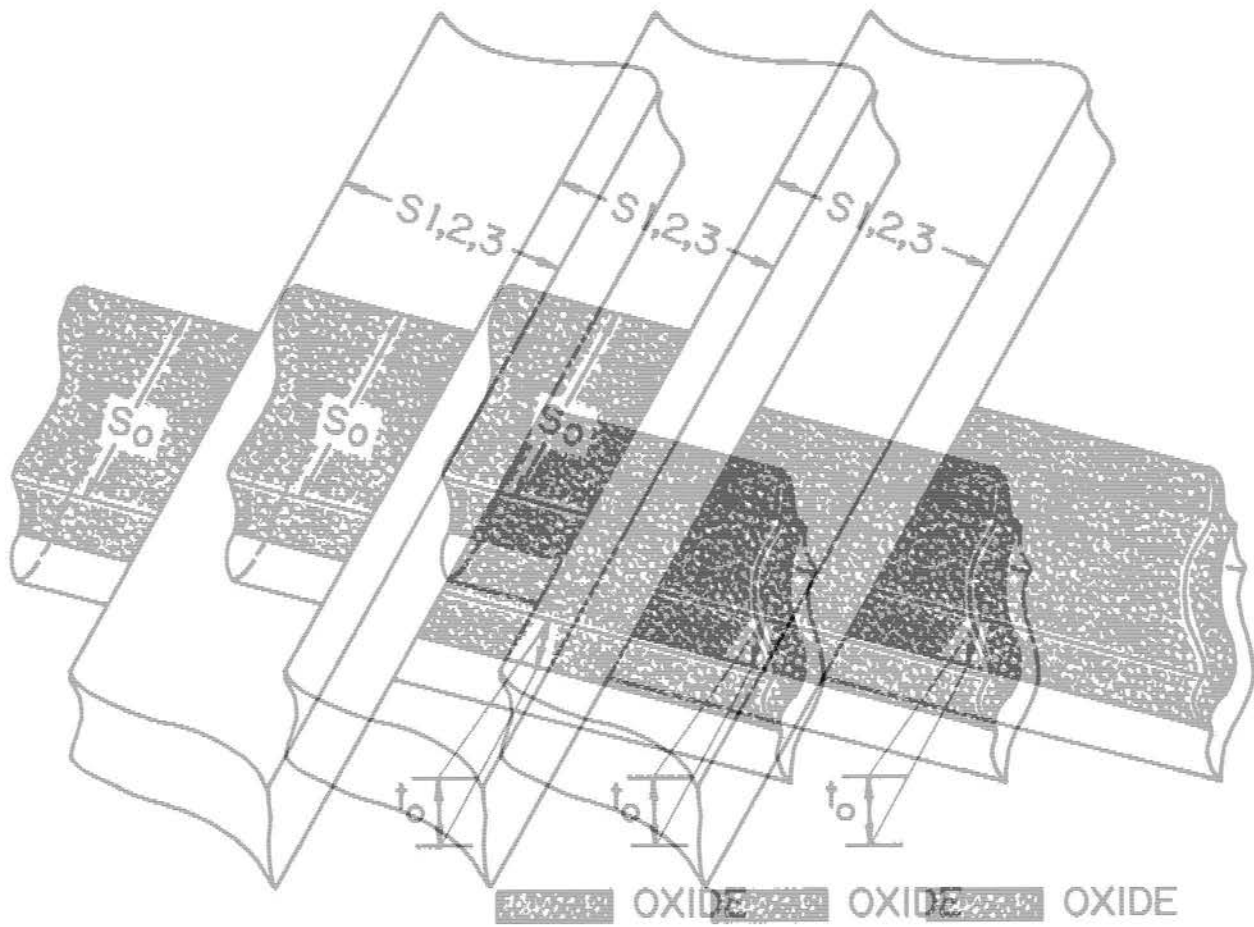
where R_J is the junction resistance, ρ_o is the oxide resistivity, t_o is the oxide thickness, and C' is the area of the junction. Simultaneously solving (III-9) and (III-10) for ρ_o one gets the quadratic equation

$$\frac{1}{\rho_o^2} - \frac{1}{\rho_o \rho_{Pb}} + \left[\left(\frac{t_T}{\rho_{Pb}} - \frac{K}{R_T} \right) \frac{1}{R_J C'} \right] = 0, \quad (\text{III-11})$$

which has the solution

$$\rho_o = \frac{1}{\rho_{Pb} \left[\left(\frac{t_T}{\rho_{Pb}} - \frac{K}{R_T} \right) \frac{1}{R_J C'} \right]}. \quad (\text{III-12})$$

The development of this solution is presented in the Appendix. Replacing ρ_o in Equation (III-10) by Equation (III-12), one has an expression for t_o in terms of measured quantities with the only assumption being that $\rho_{Pb} = \rho_{Pb}$ for bulk lead. The results of this analysis are displayed in Table V. In comparing the values for oxide thickness with the results in Table IV one sees quite good agreement. The significant point to note about the results in Tables IV and V is that the oxide



Not to Scale Not to Scale Not to Scale

Figure 17. Diagram of Junctions Showing Oxide Showing Oxide Showing Oxide

TABLE V
OXIDE RESISTIVITY AND THICKNESS

Sample Number	Junction Resistance (Ohms at 300°K)	Calculated Oxide Thickness (Å)	Resistivity (Ohm-Cm) Room Temperature
585-1	1.98K	28	7.86×10^6
585-2	1.90K	28	7.54×10^6
583-1	1.56K	28	6.19×10^6
583-2	2.04K	28	8.09×10^6
584-1	392	30	1.45×10^6
584-2	313	30	1.16×10^6
584-3	48.5	30	1.80×10^5
581-1	33.8	26	1.44×10^5
581-2	48.0	26	2.05×10^5
581-3	18.7	26	7.99×10^4
580-1	504	32	1.76×10^6
579-1	1.67	32	5.80×10^3
579-2	1.63	32	5.66×10^3

thickness is the same for all junctions independent of the parameters used in the oxidation process. The immediate conclusion one draws from this result is that the three orders of magnitude difference in the tunneling junction resistances must be due to some other mechanism than a change in barrier thickness. This mechanism, discussed below, is to model the oxide as a semiconductor which during formation reaches a cut-off thickness after which it is doped by adding additional oxygen. The physical chemistry of the process is unknown, but it is feasible to picture the PbO changing to PbO_2 or Pb_3O_4 as oxygen is added. Further reference to the constant oxide thickness will be made in the sections discussing subharmonic structure, and the creation of filaments. The barrier thickness is a fundamental parameter which must be known in order to discuss many aspects of the tunneling phenomenon.

4. Oxide Characteristics

The fact that the oxide thickness is approximately constant and yet the room temperature junction resistance varies with both time of oxidation and oxygen pressure, gave impetus to the investigation of the nature of the insulating layer. It was noted that after long periods of inactivity of the system, the resistance of the junctions was larger than in times of normal use, all of the controllable parameters being the same. To determine if the barrier was being formed by impurities being sputtered off of the surfaces in the vacuum system onto the film, an inert gas of Argon was used in the glow discharge. The results, displayed in Table IV, show that no barrier was formed with the Argon glow discharge. The $7\overset{\circ}{A}$ thickness recorded for #575 could be due to part of the lead surface being sputtered off or partially due to inaccuracies in

measurement on this order of thickness. To determine if a nitride barrier could be formed, nitrogen gas was used in the glow discharge. Again the results, displayed in Table IV, show that no barrier was formed. This leads one to the conclusion that impurities alone were not generating a tunneling barrier and that oxygen must have been present in the glow discharge to have tunneling. This is not to imply that tunneling can only occur with an oxide barrier. This investigator has formed junction barriers by pumping on a chamber containing the lead film and a small amount of polymerized methyl methacrylate. Other investigators (17) have formed tunneling junctions using a plastic material for the insulating barrier.

The effect of the glow discharge parameters on the oxide characteristics was investigated by changing both the time of oxidation and the oxygen pressure. Again the results can be seen in Table IV. Generally the junctions were formed with a pressure of 150×10^{-3} torr for 10-12 secs. It is interesting to note that for pressures less than 100 microns, an oxide was formed but the barrier was not insulating as is evidenced by the junction resistance. Also, for pressures greater than 300 microns the junction resistance was lower, for equal oxidation times, than for pressures on the order of 150 microns.

5. Summary and Discussion

A number of points regarding the oxide barrier can be made in light of the results presented. First, the results indicate that the oxide thickness is constant over the time range and pressure range used in this work. Basavaiah et al. (15) suggest that the oxide layer grows exponentially with time, the rate being dependent on the substrate material

and temperature, with film thickness ranging from 15-30 $\overset{\circ}{\text{A}}$ at room temperature. It should be pointed out that the lead films in their work were evaporated on mica and sapphire substrates and the oxide barriers were formed in situ. Other investigators (18) state that the growth rate changes from a linear to a logarithmic time dependence when the oxide thickness reaches a certain value. Eldridge and Dong (19) made extensive studies of the growth rate using ellipsometry and tunneling to characterize the PbO grown in situ. They report that the tunneling current is highly dependent on oxide thickness with 3 orders of magnitude change for less than a 10 $\overset{\circ}{\text{A}}$ change in oxide thickness. However, this work shows that the junction resistance depends on oxide conductivity rather than on oxide thickness, a fact which is in agreement with other investigators (20,21).

The model for the oxide character is as follows. For the pressure, time, and glow discharge voltage used in this work, the oxide thickness is constant with a small increase in the time of oxidation or an increase or decrease in the pressure of oxidation changing the stoichiometry of the oxide similar to the doping of a semiconductor. This work substantiates Schwidtal and Finegan's (20) suggestion that the additional oxygen discharge dopes the existing layer of oxide and Heijne's (21) point that the conductivity of PbO is highly dependent on the oxygen pressure and stoichiometry. The conclusion is that the constant thickness oxide behaves like a semiconductor changing conductivity with the addition of more oxygen. Knowledge of the oxide characteristics contributes to an understanding of the aging phenomenon discussed below.

B. Results of I-V and dV/dI Measurements of Unaltered Junctions

The most prominent feature of the BCS theory (see Chapter I) is the concept of an energy gap, 2Δ , in a superconducting material. This 2Δ , the energy required to break a quasiparticle pair in a superconductor, is easily measured using the tunneling phenomenon, a point which will be discussed below. If in a tunneling junction there is a weak coupling between quasiparticles through the barrier region, the pairs can tunnel giving rise to a current, called the d.c. Josephson current (43), with zero voltage drop across the junction. This should, and will be, differentiated from a current due to a shorted superconducting region. The reason the pairs can behave in this manner is that their electron wavefunctions are coupled in phase. If a potential difference, V , is established between the two superconductors, the relative difference in energy between pairs (called Cooper pairs) in each superconductor is $2eV$. This gives rise to a voltage dependent phase relationship which varies like $2eV/\hbar$, which is observed as an a.c. Josephson current with $\nu = 2eV/h$. Up to this point it has been thought that the two currents depended mainly on barrier thickness, however, the previous section has shown that the conductivity is the main determination of the tunneling properties.

In the current versus voltage measurement the 2Δ of the superconductor can easily be observed. One sees 2Δ since the gap is Δ wide on either side of the Fermi energy (see Figure 3). In Figure 18 the I-V characteristics for a typical Pb/PbO/Pb tunneling junction are displayed. The 4.2°K resistance, measured from the point of intersection with 10 mV extrapolated to zero, is 59.2 ohms, and the room temperature re-

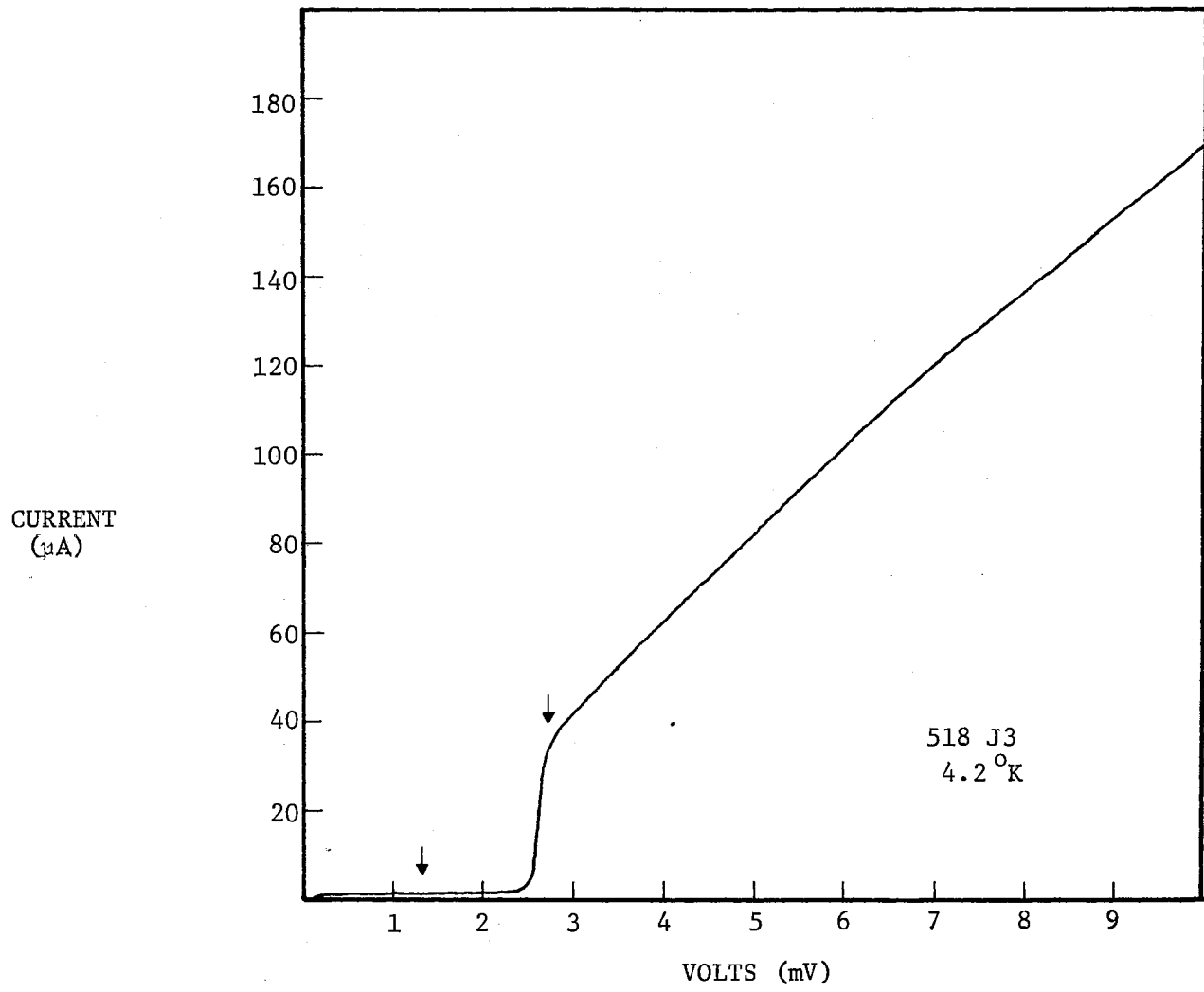


Figure 18. I-V Curve for a Typical Superconducting Tunneling Junction

sistance is 28 ohms. As the junctions in this study were changed (see later sections), the current value in the $V < 2.7$ mV region changed. To characterize these junctions during the modification, a quality factor, Q , is defined as the current at 2.7 mV divided by the current at 1.3 mV. Typically, "good" junctions, i.e., those with low excess current below 2.7 mV, have a Q factor of ≈ 30 . The sharp rise in current at 2.6 mV corresponds to 2Δ , the energy gap of lead. The small amount of current below 2Δ is due to the fact that some electrons will have energies higher than the Fermi energy due to the thermal motion of the ions (3). It has been shown (13) that when the temperature of the sample is reduced the level of this current is reduced. The salient feature is that when the Q factor is high (≈ 30) essentially no current flows until $V = 2\Delta$, and the junction is a good tunneling junction. At $V = 2\Delta$ the quasi-particles then tunnel from one superconductor through the barrier to the other superconductor.

A more sensitive measurement of the tunneling properties is the derivative measurement (dV/dI) or density of states measurement (see Chapter I). The derivative of the curve in Figure 18 is seen in Figure 19. Note the difference in the two voltage scales and the vertical scale for $V < 2.6$ mV. The dV/dI measurement is the resistance of the junction as a function of the emf developed across the junction. The large resistance can be seen for $V < 2.6$ mV, and the sharp decrease in resistance at $V = 2.61$ mV is another means of measuring 2Δ and in later sections will be referred to as 2Δ (density of states).

In "good" junction density of states (derivative) curves little information is displayed in the region $V < 2.7$ mV, however, as the junctions are changed (aged) it is this region which becomes significant.

$\frac{dV}{dI}$
(ARB)
UNITS

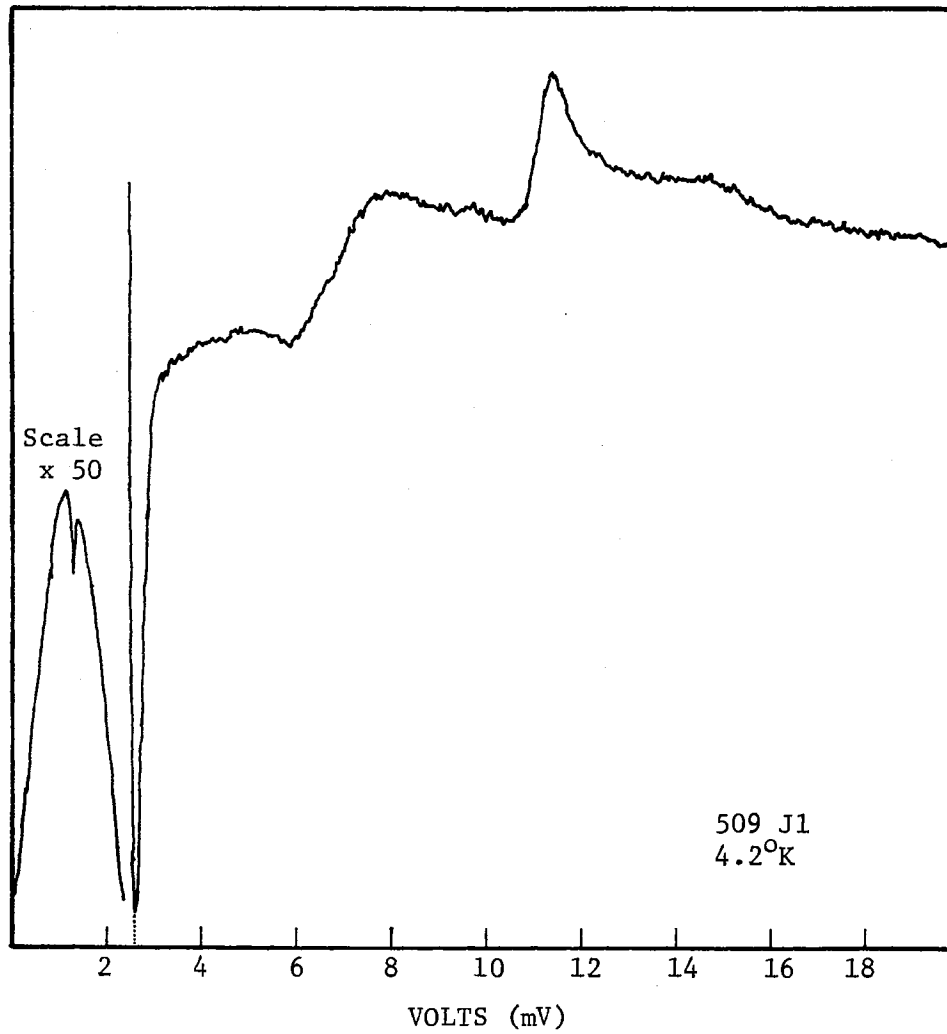


Figure 19. dV/dI Curve for a Typical Superconducting Tunneling Junction

The subharmonic structure discussed below appears in the 0 to 2 mV region.

The density of states measurement is also useful in measuring the phonon density of states. Before tunneling, the investigation of the lattice dynamics of metals, in particular the phonon density of states, was done by using the technique of neutron scattering (22). However, most of these measurements were made with limited resolution along symmetry directions. One can use tunneling to measure the phonon densities by realizing that the effect of phonons occurs at energy $\omega_p + 2\Delta$. The transverse phonons have a large density of states at $\omega_T = 4.5$ mV and the longitudinal phonons have a large density of states at $\omega_L = 8.5$ mV (23). Since $2\Delta \approx 2.6$ mV the changes in the derivative curve should occur at 7.1 mV and at 11.1 mV which is what can be seen in Figure 19. The increase in resistance at these energies reflects a decrease in electron density of states due to emission of phonons (24). These measurements are beyond the scope of this study; more detail on this procedure can be found in the literature (13,22,23,24).

In summary, this section indicates some of the tunneling properties which are observed for good quality superconducting junctions. It was the scope of this study to determine the effect of a barrier modification on the tunneling properties. Hence, in future sections measurements will be compared with the measurements of "good" junctions presented in this section.

C. Results of Junction Aging

Thus far it has been established that the oxide barrier thickness is the same for all junctions. This fact along with the junction resis-

tance led to the conclusion that the oxide barrier behaves much like a semiconductor. In order to further determine the nature of the barrier, the junctions were aged in different atmospheres. For instance over a finite period of time, does this semiconducting oxide diffuse into the lead causing the junctions to become shorted, does it remain constant, or does it increase in resistivity causing the junction resistance to increase? The answers to these questions, will lead to a better understanding of the barrier which ultimately will lead to a better understanding of the tunneling phenomenon.

The aging study was also made to better determine the stability of the junctions at room temperatures. It was discovered that when the samples were left in the room atmosphere for any length of time, they were shorted with the effect being more noticeable on some days than on others. This observation was finally associated with the relative humidity of the room. Combining these two motives the ensuing study was made.

This section discusses the most difficult part of the experiment in that the humidity of the ambient for the most part could not be controlled and the amount of room air leaking into the neck (see Chapter I, Section I) of the dewar could not be controlled. Hence, the exact method of aging varied from sample to sample but, with the exception of time for the event, the results were the same. Thus, a sample of the results will be displayed here but the conclusions drawn are applicable to all the data. The position of the sample during aging will be referred to by the various sections of Figure 14, Chapter II. The "cold" region means the sample was in the liquid helium or helium vapor near 4.2°K , the "neck" region is near the top of the dewar where the sample is in

the helium boil off gas at or near room temperature, and the "atmosphere" region is out in the room. With the exceptions which are noted, the relative humidity stated in any result is the humidity of the room.

The conclusions drawn from the results to be presented are 1) the failure of a "good" junction, i.e., high Q, is enhanced by the presence of water vapor, and 2) the junction Q is reduced by the formation of a shorted region on the edge of the junction area. The effects of point 2 will be presented in this and the remaining sections of this work.

The term aging as used in this work will be defined in each of the succeeding examples. To illustrate the terms low Q and high Q the I-V curves for a sample are displayed in Figure 20. Curve A is a typical I-V curve of a junction at 4.2°K which has not been aged. After aging the Q goes from 30.9 to 2.79.

The amount of junction edge exposed to the humidity was changed by putting down the narrow cross stripes first, performing the oxidation, and then evaporating the wide lead stripe on top of the oxide. Thus, there are two possible junction geometries as illustrated in Figure 21. These will be referred to by letter. Configuration A has 2 edges exposed each one being .092 cm long and configuration B has 2 edges exposed each one being .012 cm long. Table VI summarizes the conditions of a sample of junctions during aging. The junction geometry column refers to Figure 21 with the other columns being discussed below for each particular sample.

1. Aging of Junction Geometry A in the
"Neck" Region

The initial conditions of this sample (#534) are illustrated in

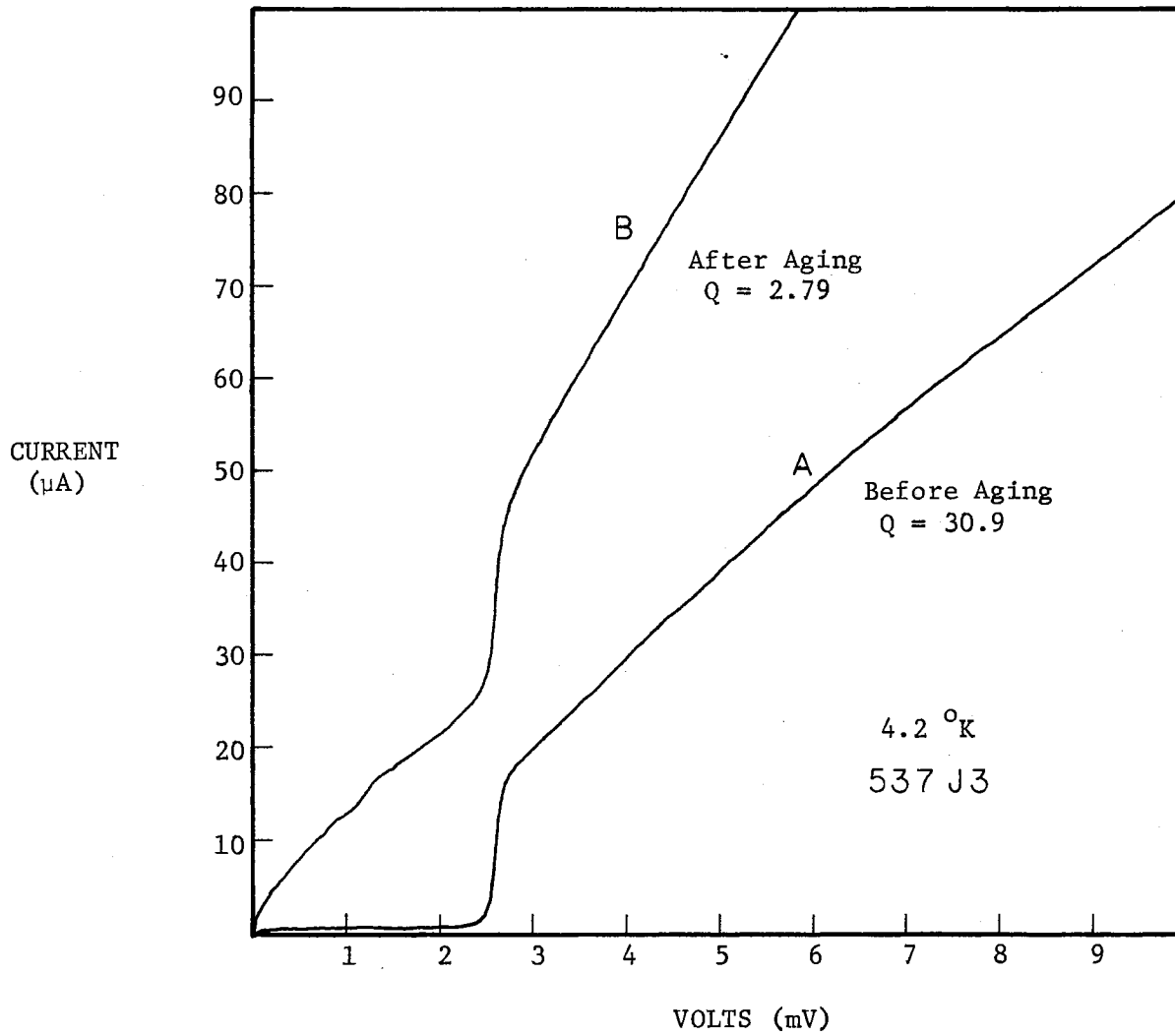


Figure 20. I-V Curve for Two Junctions of Different Q

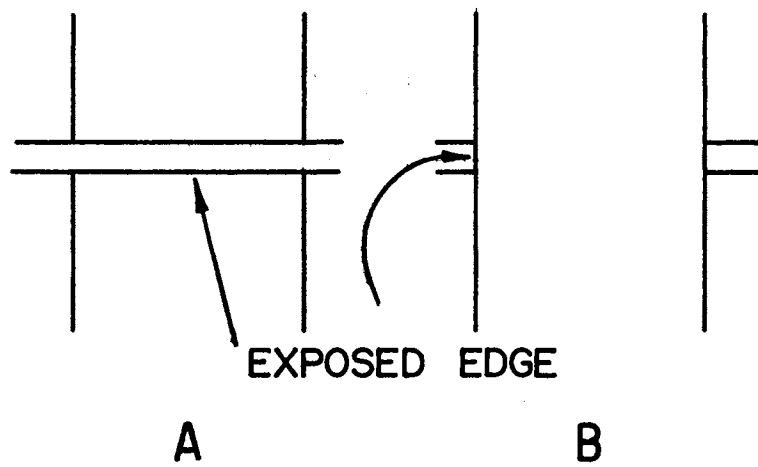


Figure 21. Diagram of Two Junction Geometries

TABLE VI
CHANGE IN JUNCTION PARAMETERS DUE TO AGING

Sample Number	Junction Geometry	Before Aging									Relative Humidity at Start of Aging	Temp. at Start of Aging °F	After Aging									Comments	
		Room Temp. Resistance Ohms			4.2°K Resistance Ohms			Q					Room Temp. Resistance Ohms			4.2°K Resistance Ohms			Q				
		J1	J2	J3	J1	J2	J3	J1	J2	J3			J1	J2	J3	J1	J2	J3	J1	J2	J3		
534	A	5.33K	2.94K	610	10K	5.63K	1.36K	21.4	27.2	30.7	Room 54%	71	6.2K	2.53K	353	11.4K	4.08K	290	30	28	1.92	Neck aging at C = 33" using brass plate	
536	B	17.5K	27.0K	6.7K	25K	41.7K	10.3K	14.5	11.3	23.7	Room 69%	≈72	160	388	308	85	247	187	1.76	1.78	1.8	Aged at C = 35" using brass plate with brass tube - 1.6 hours age time No I _c	
537	B	118	131	63.5	233	250	125	30.2	30.2	30.9	Room 60%	72	130	62.5	51.5	227	58.8	58.5	≈30	2.11	2.79	Neck aging C = 32" using aluminum plate - Ice in lower neck	
539	A	15.2	14.9	---	25.6	26.9	---	30.9	31.6	---	Room 57%	74	Short	20.4	---	Short	35.1	---	---	30.5	---	Two agings on Junction 2. Test made while R was increasing	
545	A	82.3	71.5	29	---	---	---	---	---	---	Chamber 12%	73	23.9	12.8	6.08	---	---	---	---	---	---	Junctions in chamber with helium gas flowing through	
546	A	13.3	37.4	17.7	No 4.2°K Data Before Aging	---	---	---	---	---	---	Chamber Unknown	≈72	7.3	12.6	9.3	1.28	12.2	10.9	1.4	1.9	2.1	Junctions in chamber with helium gas flowing through trap then chamber
547	A	202	147	47.8	---	---	---	---	---	---	Chamber Unknown	75	250	58.5	4.03	448	32.8	.32	≈30	1.67	1.1	Junctions in chamber with helium gas flowing through trap then chamber	
583	A	1.56K	2.04K	5.35	2.44K	3.60K	.308	≈30	≈30	1.33	Glass Dewar Unknown	≈72	15.8	3.68K	---	---	5.71K	---	≈1	≈30	≈1	Age J1 by passing ≈160 μA through junction	
588	A	725	345	336	No 4.2°K Data Before Aging	---	---	---	---	---	---	Glass Dewar Unknown	≈72	7	---	40	0.6	37.4	2.6	≈1	1.79	≈1	Age J1 and J3 by passing ≈160 μA through junctions
589	A	1.75K	1.63K	540	4.17K	3.33K	1.09K	≈30	≈30	≈30	Glass Dewar Unknown	≈72	2.5K	5.58	610	5.5K	---	1.27K	≈30	1.53	≈30	Aged all three junctions at room temperature in glass dewar system	

Table VI. After the initial measurements were made the sample was stored overnight in the cold region with no change in the derivative measurements. The sample was then removed from the helium to the neck region. The resistance of this sample was monitored as a function of time by making an I-V measurement, the results of which are displayed in Figure 22. The initial drop in resistance is due to the junction temperature rising from 4.2°K to room temperature after which the resistance begins to increase, a fact which was observed in all of the samples. The dip at 2.2 hours can be explained by a filament growing from both lead films, then breaking contact. This type of behavior is not observed in all junctions. The prominent feature of this curve which is common to all junctions aged in this manner is the sudden decrease in resistance at 3 hours signifying the formation of a filament between the lead films. In later curves more data will be displayed indicating the speed with which this decrease occurs. Another interesting point to note is that the aging affected only one of the three junctions. From Table VI it can be noted that J1 was still increasing in resistance after the 6 hours age time and J2 was only slightly reduced in resistance. Again, the sudden decrease in the resistance corresponds to a filament being formed.

2. Aging of Junction Geometry B in the * "Neck" Region

An aging study was made on a number of samples of geometry B, i.e., junctions which had less edge exposed to the atmosphere. The results for a particular sample (#537) are displayed in Figure 23. Nothing conclusive about the geometric dependence of the aging can be said but all of the other tunneling properties were identical to geometry A. The

RESISTANCE
(OHMS)

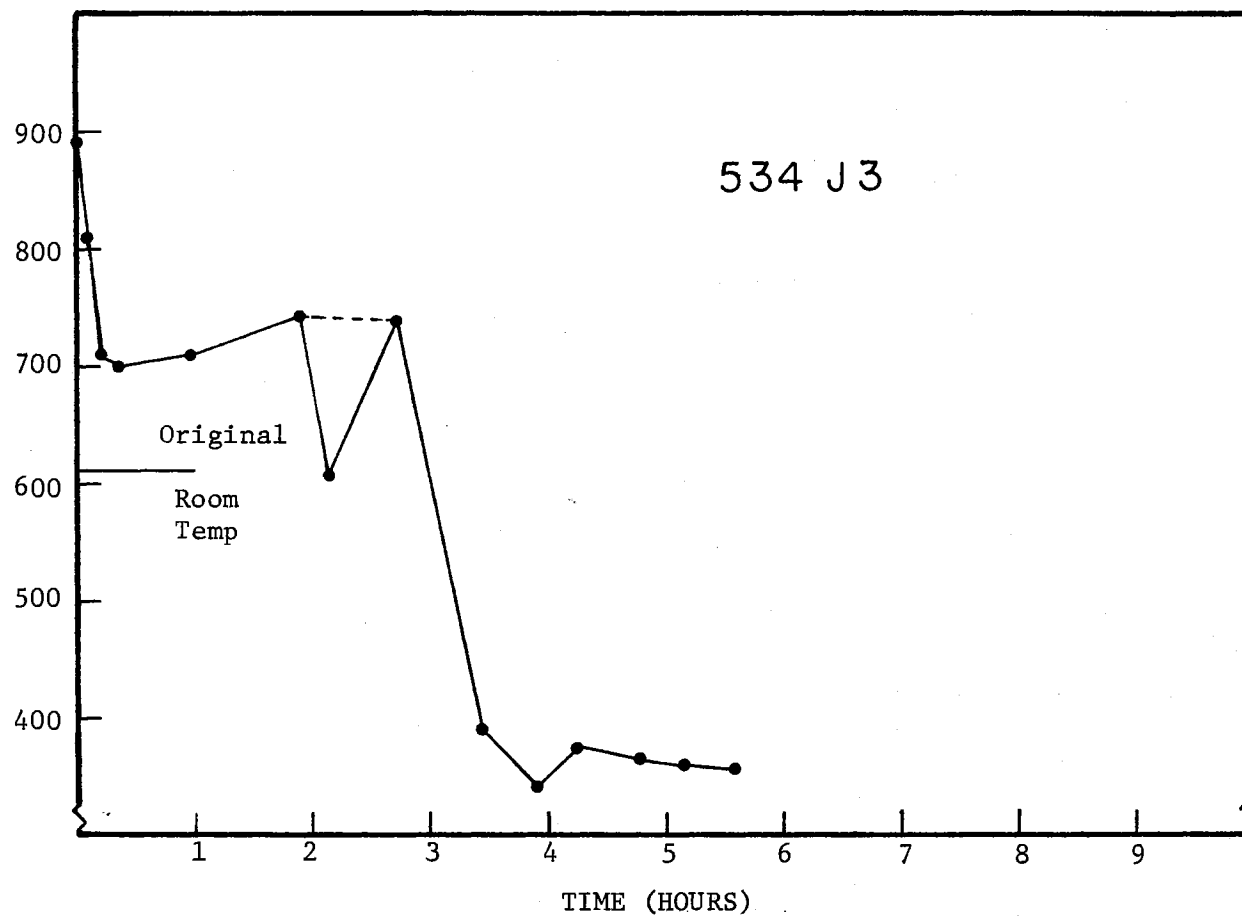


Figure 22. Resistance Versus Time for Aging of Sample 534

RESISTANCE
(OHMS)
J1, J2

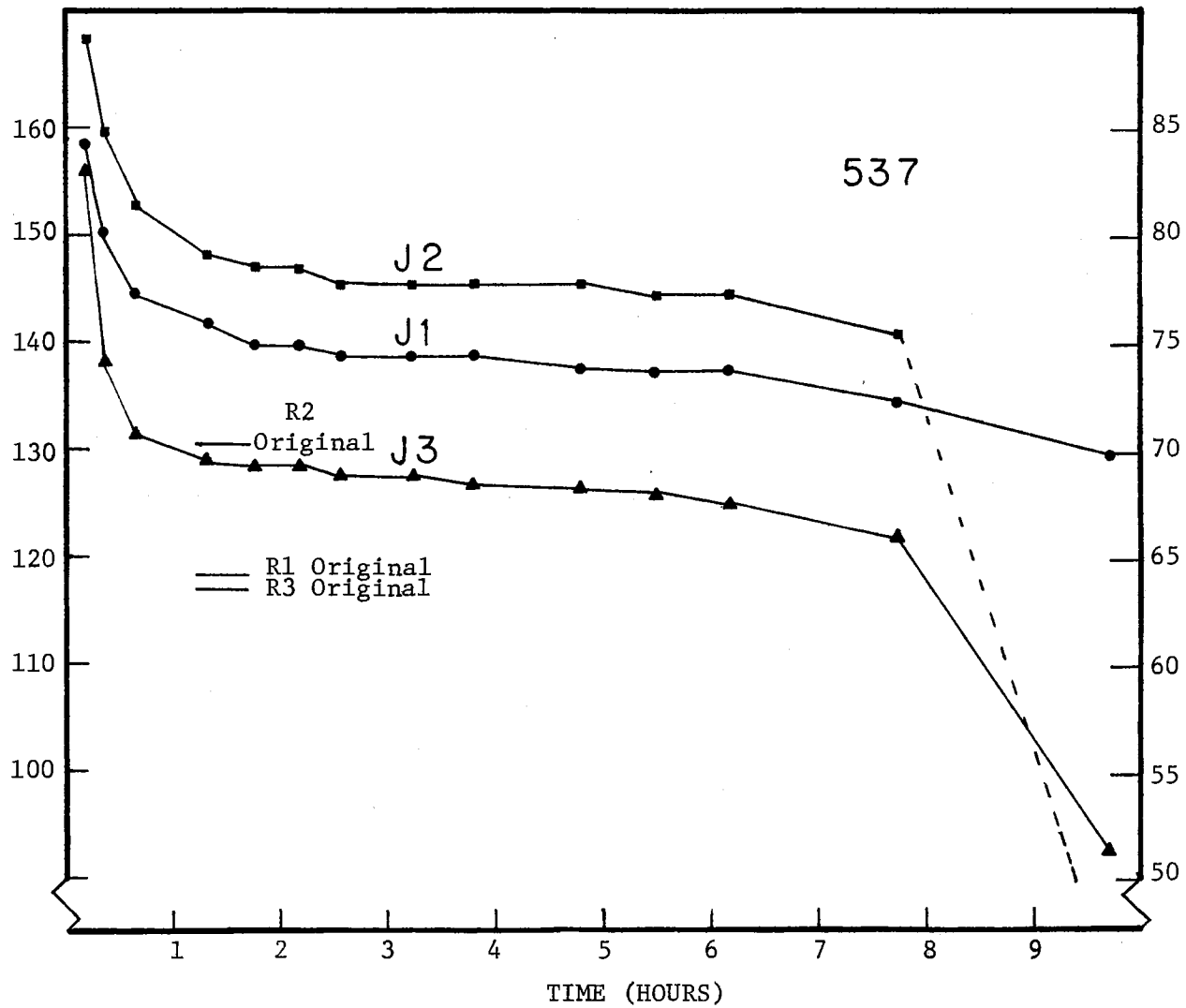


Figure 23. Resistance Versus Time for Aging of Sample 537

subharmonic structure, filamentary behavior, and general tunneling properties were identical to all other samples independent of the junction geometry.

3. Aging of Junctions in a Helium Atmosphere

As was mentioned in the previous aging discussion, a question as to the true water vapor content in the gas surrounding the sample arises. It was found in this study that if the sample was aged in the "atmosphere" region, i.e., out in the room, it became shorted in a very short period of time, depending on the relative humidity of the room. Thus, an attempt was made to age the junctions in a controlled atmosphere by placing the samples in a chamber through which "dry" helium gas was flowing. To get continuous data points the resistance was monitored with the derivative measuring device. The results for a typical sample (#545) are displayed in Figure 24.

In this curve junction 1 was biased with 0.5 mV and the a.c. drive was 3.3×10^{-8} amps. As the junction aged, the current through the junction increased from 6 μ A to 21 μ A. The sample was immersed in a container with a hygrometer, and the gas was passed through silica gel into this chamber. The relative humidity in the chamber dropped from 19% at the start of the experiment to 12% at the end. Again, note the sudden drop in resistance at 3.75 hours. It is felt that the fast flow of gas contributed to the aging of the samples even though the humidity was relatively low. Also, the humidity recorded in the other samples was the humidity of the room and was not an indication of the actual water vapor content of the gas around the junctions.

A determined effort was made to "dry" the helium gas by passing it

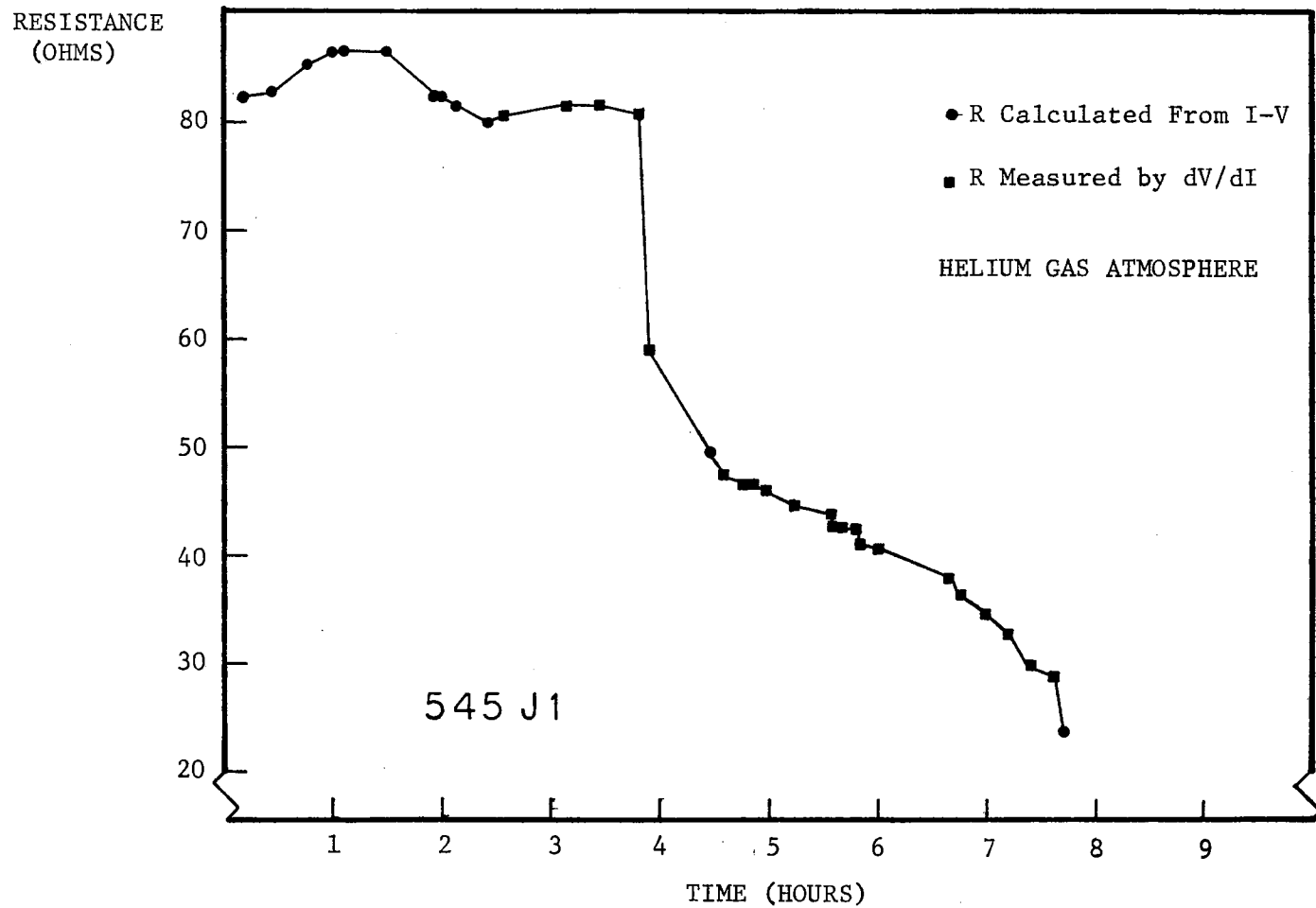


Figure 24. Resistance Versus Time for Aging of Sample 545

through the system illustrated in Figure 25. The gas passed through a silica gel chamber, then through a coil immersed in liquid nitrogen, through a coil immersed in room temperature water, into the sample chamber, through a second liquid nitrogen trap, through an oil trap and out into the room. The purpose of the first liquid nitrogen trap was to remove any water vapor in the gas. The gas was then warmed to room temperature before flowing through the sample chamber. The second trap was a test to see if any water vapor was getting through and the results were positive. The resistance of this sample (547 J2) was monitored in the same manner as in the previous sample. The results illustrated in Figure 26 show a dramatic rapid decrease in resistance after only 1.75 hours. Again the forced flow of an inert gas containing water vapor enhanced the decay of the junctions. After the sudden decrease in resistance, the decay has regions in which the resistance changes exponentially with time. This effect can be seen in Figure 27. The logarithmic resistance change in aging time is in agreement with Yanson and Albegova (25) although they do not report any sudden decrease in resistance which is humidity related. The exponential behavior is an annealing process which is probably associated with the diffusion of the oxide into the lead.

4. Fiske Modes

The best evidence for the existence of the a.c. Josephson current is the appearance of Fiske Modes (26). Recalling that the a.c. current has a frequency $\nu = 2eV/h$, the modes appear at regular intervals in the density of states curve as the voltage reaches a value such that the electromagnetic wave is in resonance with the cavity, i.e., oxide region

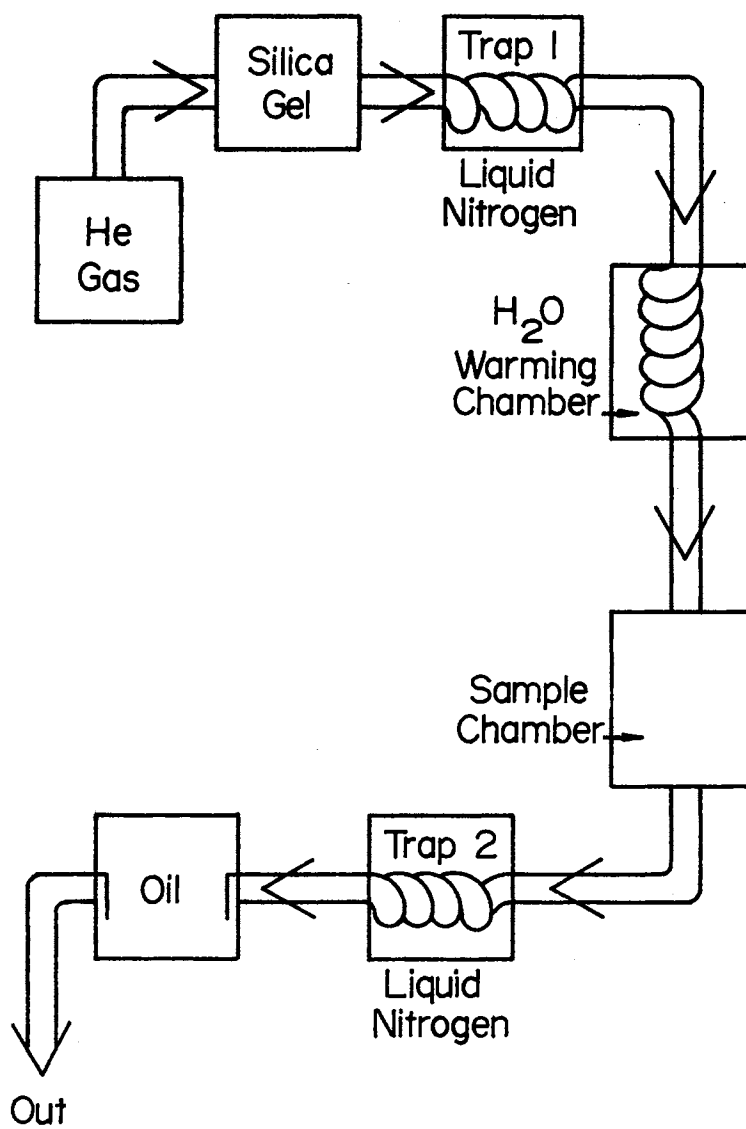


Figure 25. Block Diagram of Aging System for Sample 547

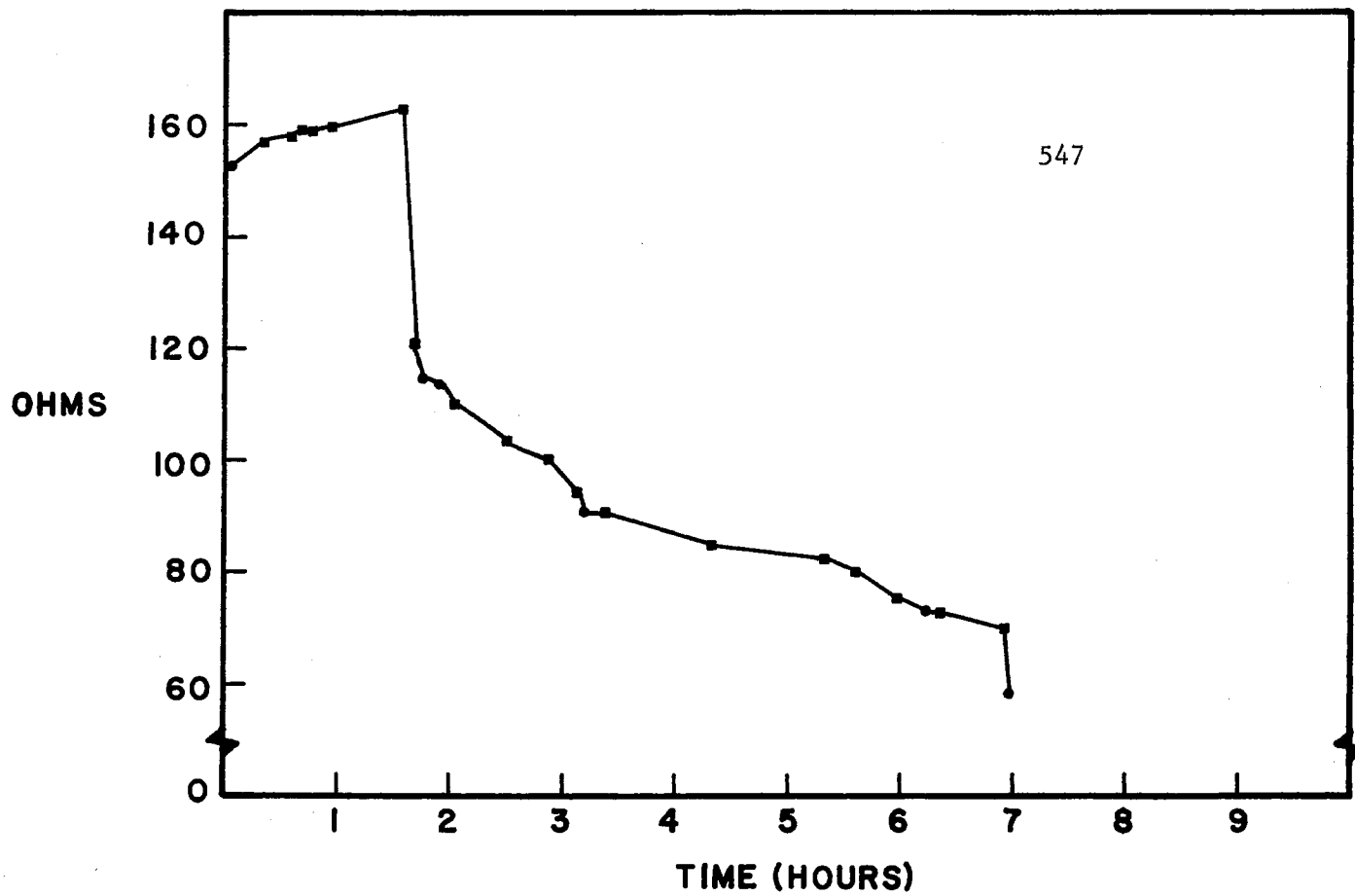


Figure 26. Resistance Versus Time for Aging of Sample 547

RESISTANCE
(OHMS)

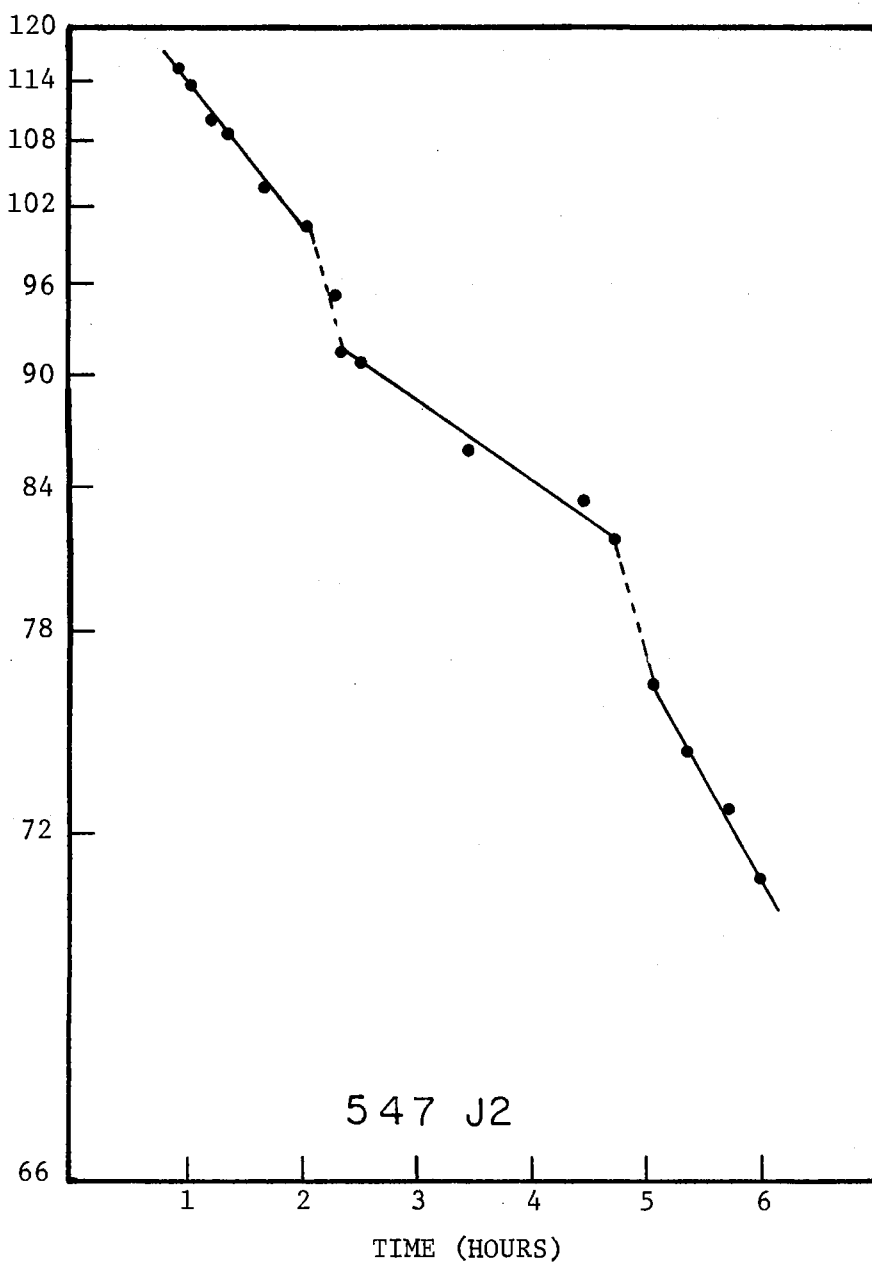


Figure 27. Semi Log Plot of Resistance Versus Time for Sample 547

in the junction. Thus, if the barrier geometry is changed, the Fiske Modes would be changed. The aging of one particular sample (#539) caused a dramatic change in the Fiske Mode pattern. As a matter of explanation J3 was shorted from the beginning and was not used in this study. J1 was decayed with a current of approximately 0.5 ma flowing through the junction continuously with the sample in the neck region for 1.41 hours. J2 was being aged at the same time with a room atmosphere of 57% relative humidity and a temperature of 74^oF. After the aging period the samples were immersed in liquid helium and tested, a process during which J1 was shorted. It was found that J2 had a new 4.2^oK resistance of 27 ohms and a Q of 32.1. The sample was then removed from the helium to the neck region and was allowed to age again. The results of this second age are displayed in Figure 28. Note the decrease in resistance while the sample is warming up to room temperature followed by an increase. The sample aging was stopped during this increase and tested at 4.2^oK. The new 4.2^oK resistance of J2 was 35.1 ohms with a Q of 30.5. It should be noted that all of the aging experiments show an increase in resistance before a decrease. The model for this increase is as follows.

As the glow discharge proceeds, the lower layer of lead is oxidized to a constant thickness of $\approx 35\text{\AA}$ during some initial time period. As the glow discharge continues the oxide layer is doped with additional oxygen atoms thus forming an oxygen rich region in the oxide as has been proposed by Schwidtal and Finnegan (20). After the oxidation procedure, the second layer of lead is evaporated over this oxygen rich region. Thus during the initial phase of the room temperature decay, oxygen atoms from this oxygen rich oxide are diffusing into or reacting with the lead

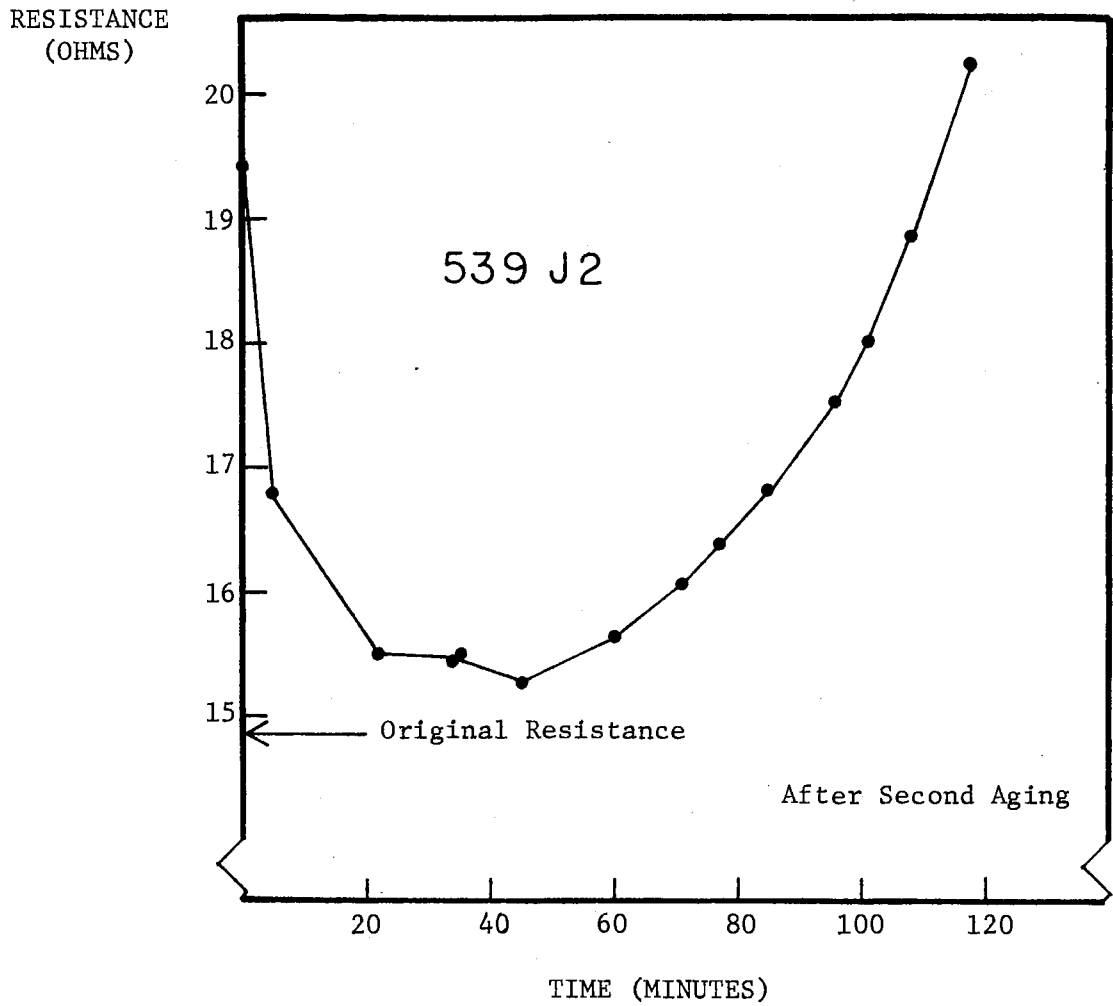


Figure 28. Resistance Versus Time for Sample 539

evaporated into this region resulting in a stoichiometry change which in turn increases the resistance slightly. This small subtle change affects the dimensions of the barrier region. If one wants to look at the junction area as though it were a cavity filled with oxide dielectric, the junction behaves as an open ended resonator. One of the dramatic features of the tunneling phenomena discussed previously is the existence of the a.c. Josephson effect (26). This current oscillates in the open-ended resonator with modes which correspond to the Josephson frequency $\nu = 2eV/h$. In Figure 29 these steps, called Fiske Modes, can be seen with a separation of .04 mV which corresponds to a Josephson frequency of $\nu = 9.67 \times 10^9$ cycles/sec. Coon and Fiske (26) believe that the velocity of the electromagnetic wave in the junction is

$$\frac{v}{c} = (\ell/\epsilon (2\lambda + \ell))^{\frac{1}{2}} \quad (\text{III-13})$$

where ℓ is the junction thickness, ϵ is the oxide dielectric constant, and λ is the London penetration depth. Assuming some values for ℓ , ϵ , and λ they have determined that their Josephson frequency has a half-wavelength which is equal to one dimension of their junction. Applying their theory to this work by assuming $\ell = 30\text{\AA}$, $\lambda = 500\text{\AA}$, and $\epsilon = 26$, the CRC (27) value for lead monoxide,

$$\frac{v}{c} = .0335, \quad \nu = 1 \times 10^9 \text{ cm/sec} .$$

Letting $\nu d = \nu$,

$$d = .103 \text{ cm, and}$$

$$\frac{1}{2}d = .052 \text{ cm.}$$

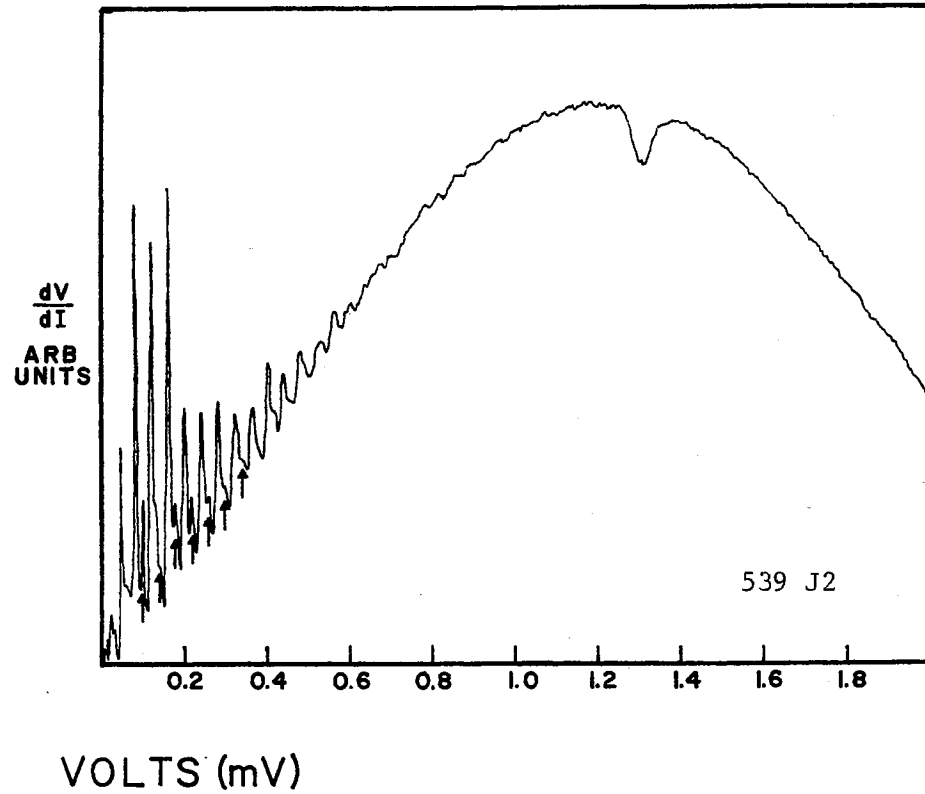
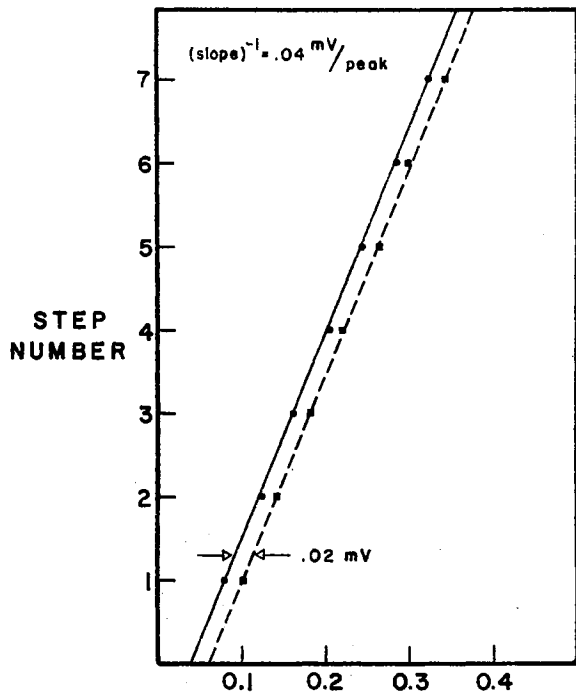


Figure 29. Fiske Mode Pattern in an Aged Junction

Thus, for this work the half wavelength is equal to a value which is ≈ 4 times the junction dimension. This is fairly good agreement considering what is known about ϵ and λ for thin oxides and films. Fiske, too, must assume an ϵ and λ to get the proper agreement. The point to be made is that the a.c. Josephson effect is dramatically displayed in the data. The very salient feature of Figure 29 is the appearance of the second set of modes denoted by the arrows. This set was not apparent in the data prior to aging the junction. The plot of step number versus volts shows the displacement of the second set from the first. The frequency of the two sets are the same but the modes of vibration of the second set has changed. All of this indicates that the early stages of the aging process change the dimensions of the cavity, i.e., the oxide. Thus, the conclusion can be drawn that either l or ϵ or both in Equation (III-13) are changed during this annealing process. Using Equation (III-13) and assuming $\lambda = 500\text{\AA}$, ϵ was calculated for a number of samples in the 4.2°K resistance range 17 - 67 ohms. Over this range ϵ was the same for all samples. When the resistance is greater than 100 ohms, Fiske Modes could not be observed indicating that ϵ must be changing with resistivity since the oxide thickness (l) remains constant over different resistance ranges.

5. Discussion of Aging

From the results that have been presented, and many results which have not been presented here, one can draw a number of conclusions. These are that 1) during the aging process the resistance initially increases due to the diffusion of the lead oxide into the "top" lead film thus effectively changing the oxide stoichiometry. 2) After a period of

aging there occurs a rapid decrease in the resistance which is due to the formation of a conducting filament across the edge of the junction. This filament may be a complete lead filament but is not always a pure lead filament. When the filament is lead, a zero bias current appears in the I-V plot. The speed with which the sudden decrease in resistance occurs is evidence that the filament is forming at the edge. Another evidence for a filament formulation, either superconducting or nonsuperconducting, is after aging the 4.2°K resistance is less than the room temperature resistance. Finally, the change in the Fiske mode pattern indicates a small change in the geometry of the oxide barrier during the initial phases of aging. The onset of subharmonic structure is a dramatic result of the filament formation which will be discussed below. The measurement of the sizes of the filaments formed and the critical current densities of superconducting filaments will also be discussed in later sections.

D. Subharmonic Structure

1. Introduction

One of the outstanding features of the measurements which are made on low Q junctions is the presence of subharmonic structure, the main characteristic of which is an oscillatory behavior with maximas occurring at $\approx 2\Delta/n$ where n is an integer. An example of this behavior is displayed in Figure 30 with the inset displaying the I-V measurements for this same sample. Some important points to be made are: 1) that the subharmonic structure (henceforth referred to as SHS) appears after the formation of a filament, either superconducting or nonsuperconducting (the I-V data in Figure 30 indicate that the filament which is formed is

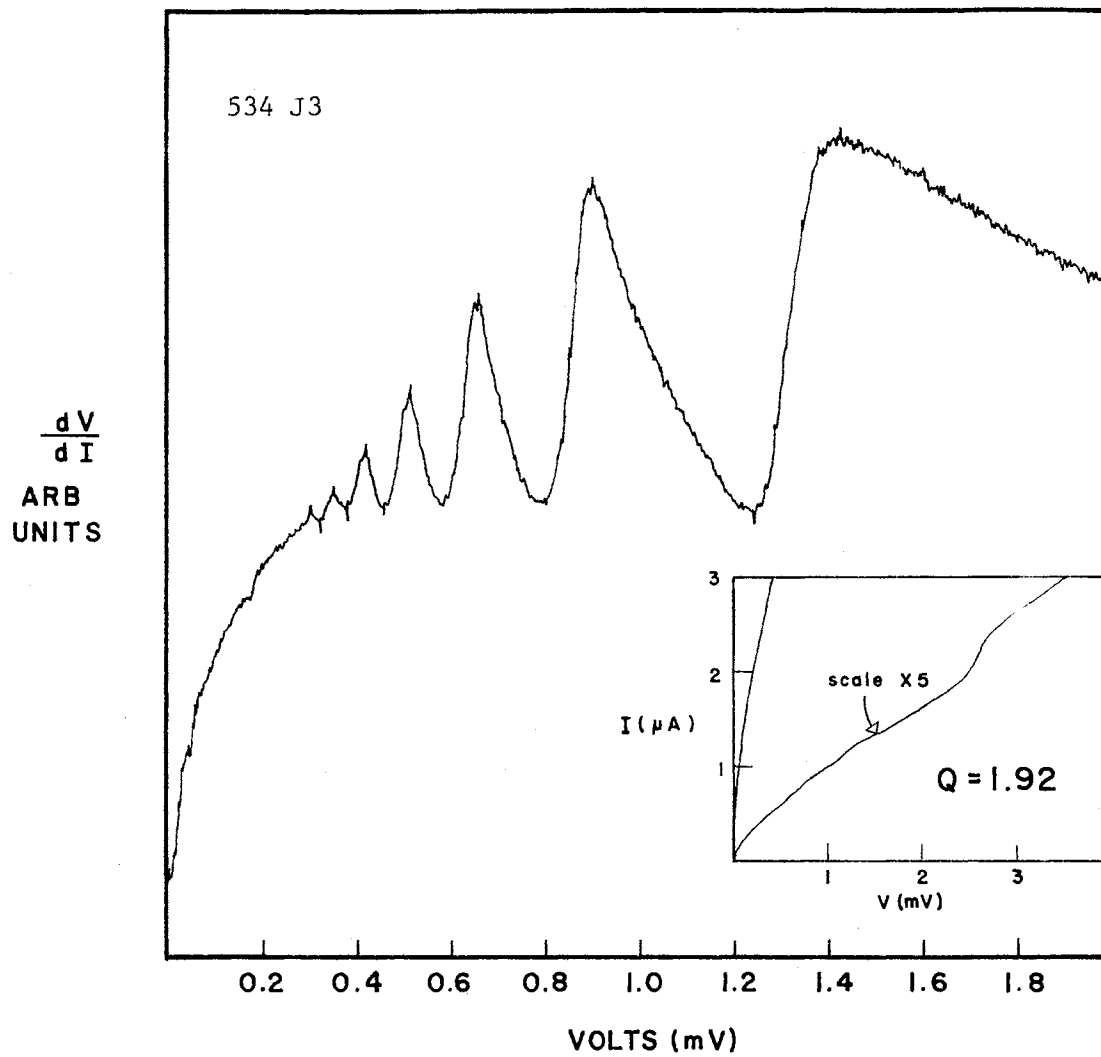


Figure 30. Subharmonic Structure in a Sample Without Zero Bias Current

nonsuperconducting as is indicated by the absence of a finite current at $V = 0$), 2) that the excess current associated with SHS is different from that associated with other tunneling processes (11), i.e., it is independent of temperature except that 2Δ varies with temperature and, 3) that no one particular theory currently models SHS (28).

2. The Creation of Subharmonic Structure

In this study, as in others, it was discovered that SHS occurs only when the Q of the junction is significantly less than 30, i.e., on the order of 2 or less. As far as is known, Yanson and Albegova (25) are the only other investigators which have attained this condition through a systematic aging process. Giaever and Zeller (10) created SHS by using a thin layer of CdS in the insulating region of their junction. As the CdS is exposed to light, the conductivity of the junction changes giving rise to excess current below 2Δ which shows up as SHS on the derivative measurements. It should be pointed out that they saw structure other than pure SHS which depended on the amount of current through the CdS layer and the current through oxide covered spots which are holes in the CdS layer.

The argument has been made in the previous section that during the aging process a filament is formed although the filament is not necessarily pure lead. In Table VII the zero bias current is displayed for the samples listed in Table VI. Again the zero bias current is the current through a junction with 0 volts developed across the junction or, in other words, the I value at $V = 0$ on the I - V curve, such as samples 546, 547, 583, 588 and 589 in Table VII. It was found that the appearance of a zero bias current was independent of the aging method (see

TABLE VII
VALUES OF ZERO BIAS CURRENT

Junction Number	SHS Investigated	Zero Bias Current (Microamps)			SHS With Zero Bias Current
		J1	J2	J3	
534	J3	0	0	0	No
536	J1, J2, J3	0	0	0	No
537	J2	0	0	0	No
546	J2	920	20	30	Yes
547	J2	0	15	34000	Yes
583	J1	394	0	23,900	Yes
588	J1, J3	510	15	138	Yes
589	J2	0	53	0	Yes

547 for example, where all three junctions experienced identical aging but the zero bias current is different for all three). The nature of the filaments will be discussed in the next section.

SHS without a metallic filament has been displayed in Figure 30, and SHS with a zero bias current is displayed in Figure 31. The similarities between the two curves from 0.6 mV to 1.8 mV are obvious. In Figure 31, the derivative for $V < 0.6$ mV reflects the strong effect of the d.c. current through the junction with the a.c. Josephson effect being displayed by the presence of Fiske Modes in this region. The d.c. Josephson current is zero in this particular sample but was not necessarily zero in all samples. The test for this current was to rotate the sample in the earth's field while the d.c. current was flowing through the junction at $V = 0$. If a component of the d.c. current was due to the d.c. Josephson current, a voltage would develop across the junction as the junction was swept through the field. The d.c. Josephson current (29) is given by

$$j = j_1 \sin \phi$$

where j_1 is a constant determined by the size, barrier thickness, geometry, etc., of the junction, and ϕ is the phase difference between the electron pair wave functions on the two sides of the junction. In the presence of a magnetic field, H_0 , j becomes (29)

$$j = j_1 \sin \left(\phi - \frac{2ed}{\hbar c} H_0 z \right)$$

where d is the barrier thickness, and z is the distance along the barrier. It then becomes clear that j depends on H_0 and in fact can vanish for certain values of H_0 . The reduction of the d.c. Josephson current

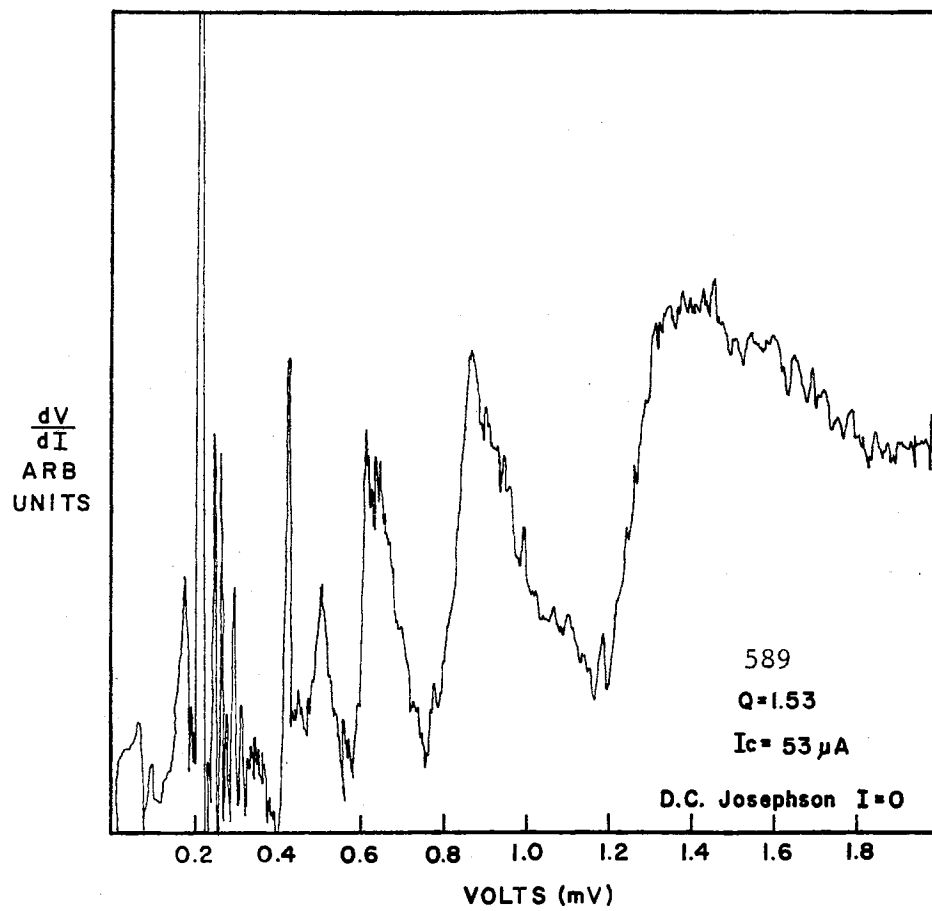


Figure 31. Subharmonic Structure in a Sample With Zero Bias Current

is tantamount to breaking of the pairs, and thus the tunneling process reverts back to quasiparticle tunneling with the development of a voltage across the junction.

The conclusions drawn after investigating a large number of samples are as follows. 1) SHS appears after an aging process in which a filament is formed, 2) the method of filament formation has no effect on the nature of the SHS, 3) the SHS pattern is identical for both metallic and non-metallic filaments, and 4) the SHS pattern is identical both when d.c. Josephson currents are present and not present.

3. Investigations of the Detail of Sub-harmonic Structure

The following question that comes to mind when looking at the SHS data is: does the relative magnitudes of the peaks versus the minimum give any new information? In order to label the structure the peak at ≈ 1.4 mV will be called $N = 2$, the peak at $\approx .85$ mV $N = 3$, the peak at $\approx .65$ mV $N = 4$, etc. In Table VIII the ratio of the first three peak heights to the average minimum is displayed. The average minimum is used for data like Figure 31 where the minima are not the same due to the effect of the large d.c. current. When the d.c. current is zero the minima are approximately equal. In all cases the ratios are in good agreement with the difference between the smallest and the largest being on the order of 50%, even when the d.c. current is on the order of 400 μ A (Sample 583 J1). The conclusion is then drawn that the ratios of the magnitude of the oscillations of the SHS is independent of the means of filament production and is independent of filament size.

If one looks at the conductivity of the junction rather than the

TABLE VIII
RATIO OF PEAK HEIGHT TO AVERAGE MINIMUM

	N = 2	N = 3	N = 4
534 J3	1.81	1.71	1.45
536 J1	1.95	2.0	1.72
536 J2	2.0	2.15	1.76
536 J3	1.96	2.04	1.74
537 J2	1.98	2.0	1.69
547 J2	1.88	1.85	1.51
546 J2	1.94	1.97	1.71
583 J1	1.76	2.19	1.50
588 J1	1.9	1.81	1.38
588 J3	1.74	1.60	1.37
589 J2	2.07	1.83	1.45

resistance, the SHS appears as a small oscillation on the background junction conductance. In Figure 32 the junction conductance is plotted as a function of voltage with the lower curve being the conductance before aging and the upper curve the conductance after aging. Note the lower curve scale is a factor of 100 less than the upper curve. Drawing a dotted line through the conductance minima (i.e., the resistance maxima on the dV/dI curves) gives the two curves a similar shape which is nearly flat from .6 mV to 2 mV, with the conductance of the aged junction being increased by a factor of 200. This type of behavior is identical to the comparison of the conductance of two junctions of different resistance when measured prior to any aging. Table IX shows an order of magnitude difference in the $V < 2\Delta$ conductance for two junctions of different resistance. Thus, the conclusion is drawn that the order of magnitude change in the conductance in Figure 32 is due to the change in conductance of the junction due to the aging process including the formation of the filament. The oscillatory behavior is due to the superconducting properties of the lead films interacting through the filament.

TABLE IX
COMPARISON OF CONDUCTANCE MINIMUM OF TWO JUNCTIONS

Junction	Resistance at 4.2 °K Ohms	$\frac{dV}{dI}$ Max Ohms	σ_{\min} Ohms ⁻¹
539J2	26.9	507	1.97×10^{-3}
537J1	233	4320	1.88×10^{-4}

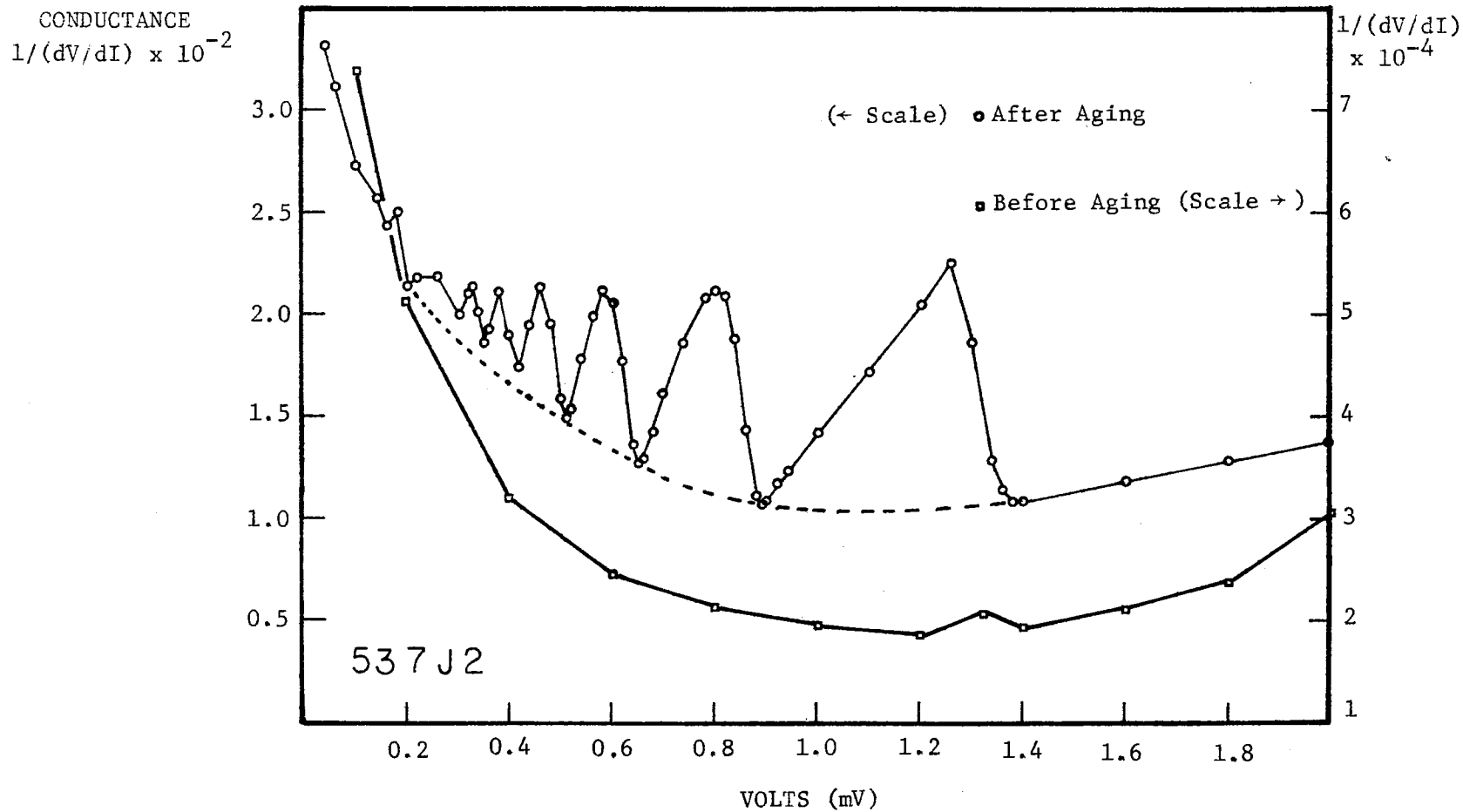


Figure 32. Conductance Versus Voltage for a Junction Before and After Aging

In Table VIII the ratio of the first three resistance maxima to the minima are displayed. Another resistance relationship of interest is displayed in Figure 33 where the maxima are plotted as a function of N number for a typical sample (534). This sample was chosen due to its large number of oscillations displayed, i.e., $N = 7$ whereas the oscillations for order of $N = 5$ or higher cannot be seen in samples with zero bias current. In Figure 33A the maxima are measured assuming the minimum of the dV/dI curve as zero. There is no correlation between the $N = 2$ and $N = 3$ maxima, however, for $N \geq 3$ the maxima of the oscillations behave as an exponential. The change in this region is due to the change in background conductance in this region. In the region where the background conductance is constant ($N = 2, N = 3$), there is not any relationship between the maxima.

A feature of SHS which has been pointed out by other investigators (12,30) is that the peaks of the dV/dI data do not coincide with a perfect subharmonic series. This same observation was made in this work along with the observation that the minima do not follow a perfect SH series, although they are more closely aligned with the SH series than are the maxima. Figure 34 displays the divergence from a $2\Delta/N$ series for both maxima and minima. The ΔV which is plotted in Figure 34 is

$$\Delta V = \frac{2\Delta}{N} (ds) - \frac{2\Delta}{N} (data)$$

where the $2\Delta_{ds}$ is 2.61 mV as measured from the density of states curve (see Section B). The $2\Delta/N (data)$ is the voltage measured directly from the data for each N. For any particular N

$$\Delta V = V_{ds} - V_d .$$

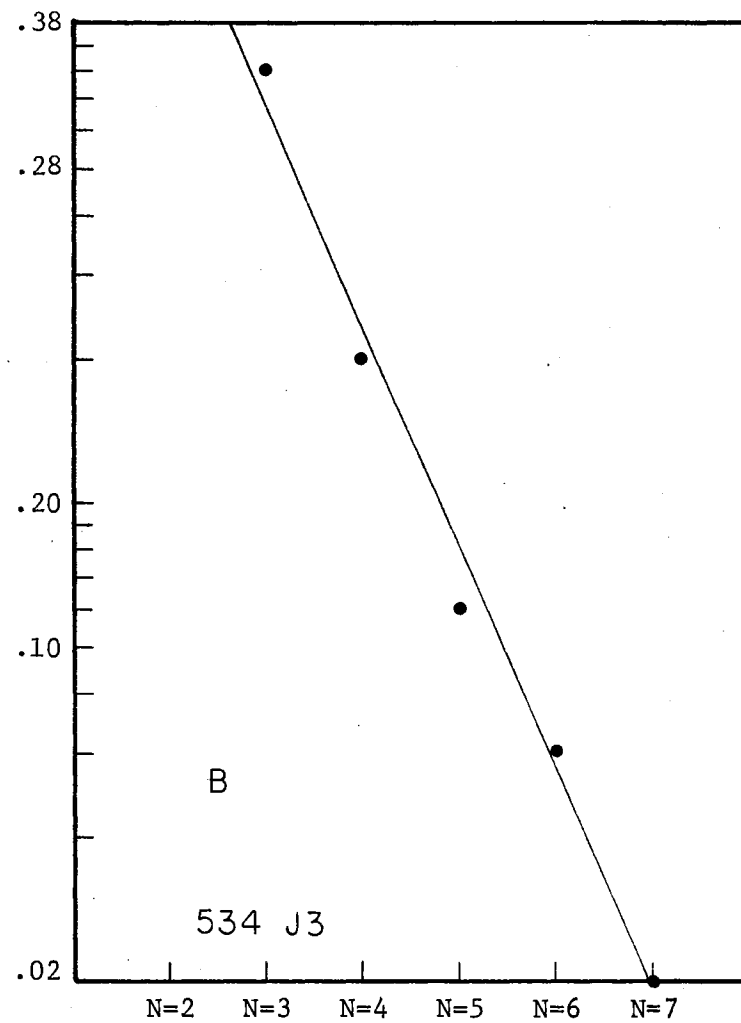
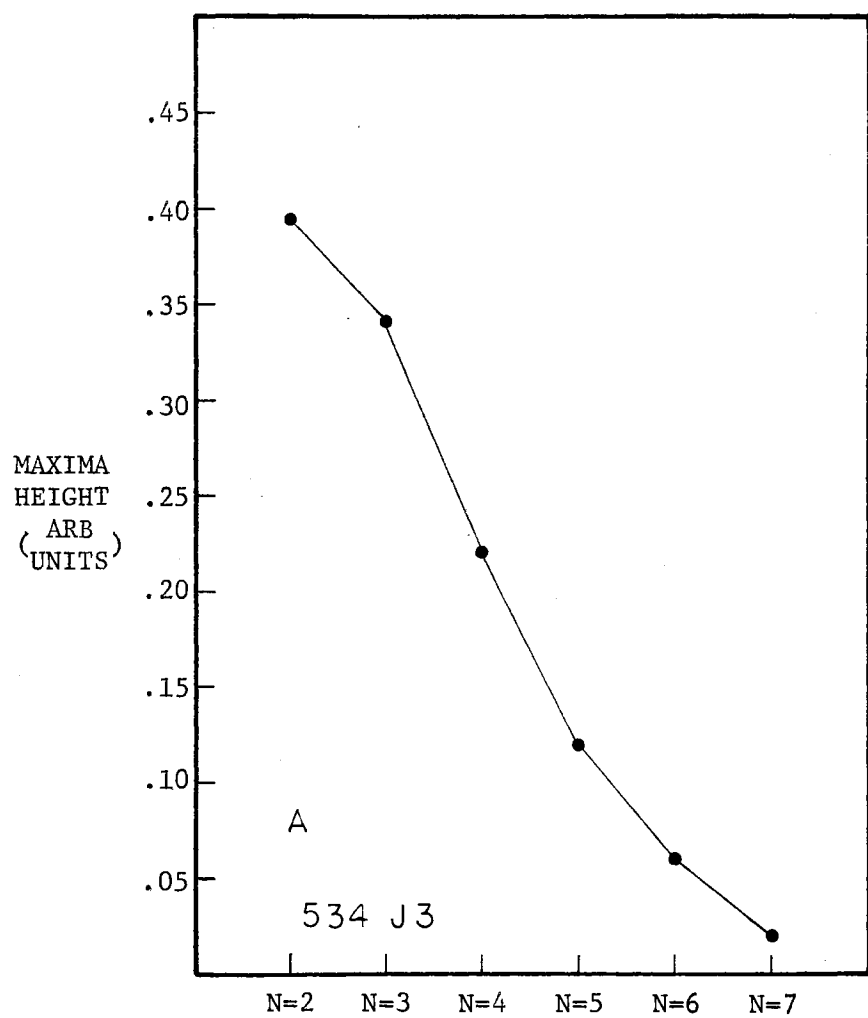


Figure 33. Subharmonic Peak Maxima Versus N

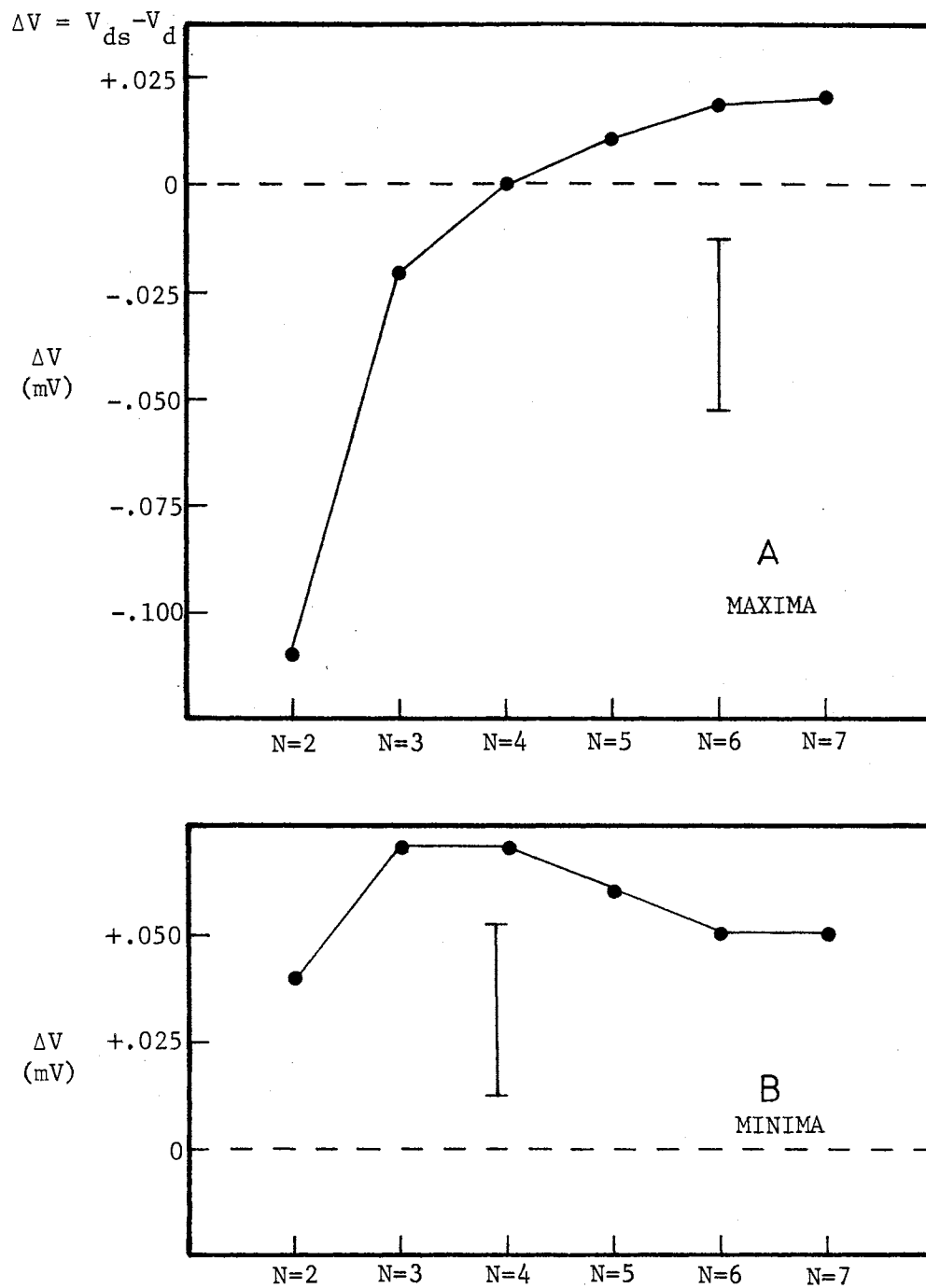


Figure 34. Divergence From Pure Subharmonic Series for Maxima and Minima

If either the maxima or minima were a true subharmonic series, ΔV would be 0 for each N . Figure 34A is a plot of ΔV versus N for the maxima and Figure 34B is the same plot for the minima. The fact that the peaks are not a true series is obvious, however, the minima approach a true series with the zero of Figure 34B shifted by approximately .06 mV. Bright and Merrill (30) believe the structure is not a pure subharmonic due to the sloping background current. This cannot be the case since the SHS is a small oscillation imposed on the basic conductance curve. The shape of the basic conductance curve is the same with and without SHS (See Figure 32).

4. Review of Some Models of Subharmonic Structure

A unified explanation of subharmonic structure has yet to be presented. Many investigators (see references 10,11,12,28,30-36) are cognizant of the problem and have attempted to present plausible theories but all of the theories proposed, including the most recent (28) and the model for Dayem Bridges (12), require the formulation of two models, one for each of the N even and N odd series. A typical model (and most widely accepted) has been proposed by Rowell and Feldmann (11) and will be reviewed here. In addition to the single-particle tunneling current in the junction there is an a.c. Josephson current which gives rise to microwave power of frequency $\nu = 2eV/h$. It is assumed that the shorts will give power to the junction at $N2eV$ where N is an integer 1, 2, 3, etc. This ac field can interact with the junction in two ways. 1) the ac field, when absorbed by the lead films, can break pairs creating quasiparticles in each film when $Nh\nu = N2eV \geq 2e\Delta$. Thus, whenever the

voltage is such that $V = 2\Delta/2N$, pairs are broken and quasiparticles can tunnel. This is the even series. 2) Dayem and Martin observed that when an ac field of frequency ν was applied they observed current steps at $eV = 2\Delta - N h\nu_A$. It was suggested to Rowell that similar interactions should occur for the a.c. Josephson radiation when $Nh\nu = N2eV$. Then $eV = 2e\Delta - N2eV$ or $V = 2\Delta/2N+1$. This is the odd series. 3) A third possibility involves a so called intermediate state. Briefly, the intermediate state is due to the destruction of a pair in film 1, the excitation of one resulting quasiparticle in film 1 and the other in film 2, then quasiparticle 1 tunnels to film 2 where it recombines with quasiparticle 2 to reform a pair. The energy of this state is $(eV + 2\Delta) - 2eV = 2\Delta - eV$. If the a.c. field exists in the junction then the energy is $(eV + 2\Delta) - (2eV + N2eV) = 2\Delta - (eV + N2eV)$. The expression for the amplitude of the pair current has the above energy in the denominator. Hence, the current maxima occur at

$$eV + N2eV = 2\Delta \text{ or } eV = \frac{2\Delta}{2N+1} .$$

This section can be summarized by quoting Rowell and Feldmann (11), "as, experimentally, the shapes of the odd and even structures appear identical and their magnitudes are not appreciably different, it appears that a single explanation of the whole series is yet to be found."

5. Conclusions on Subharmonic Structure

The following conclusions can be drawn from this study on SHS.

- (1) The SHS appears in junctions which have been aged changing their Q from 30 to ≈ 2 .
- (2) The creation of a filament, although not necessarily a metallic

filament, is necessary for SHS.

(3) The SHS pattern is totally independent as to the method of filament creation.

(4) The basic SHS is the same for all junctions independent of initial and final resistance.

(5) The SHS in the dV/dI curve is a perturbation to the normal tunneling dV/dI behavior indicating the current arises from two mechanisms, the tunneling and the filament.

(6) The SHS in tunneling junctions is identical to that in Dayem-Bridges (12).

(7) The SHS pattern is the same for both superconducting and non-superconducting filaments.

Another conclusion which was made by Bright and Merrill (30) but is important to this work is that the SHS has a temperature dependence identical to that of the energy gap throughout the range $T < T_c$. This is consistent with (7) in that the superconducting filaments would show a temperature dependence. This study has developed a means of systematically creating SHS in a good junction which has been characterized at both 4.2°K and room temperature. It is hoped that this work will enhance the theoretical study of the phenomena.

E. The Filaments Formed

1. Introduction

The argument has been made that the filaments formed during aging can be of either superconducting material or of material other than a superconductor at least at $T \geq 4.2^\circ\text{K}$. It should also be pointed out that filaments can and have been formed by methods other than the normal

aging methods heretofore mentioned. These methods include an aging or a diffusion process in which a relatively large current is passed through the junction, a traumatic process in which a spurious electrical signal causes a severe short across the junction, and finally filaments which were formed due to incomplete or inhomogeneous oxidation during the fabrication process. Filaments of all types will be discussed in this section with the appropriate formation method mentioned when known. In some cases a combination of the above methods occur making the true formation pattern unknown.

The conclusions which will be drawn from the data presented in this section are

- 1) during normal aging the oxide at the edge of the junction is a semiconductor which undergoes a change in resistivity changing a region from a semiconductor to a metal, in some cases a superconducting metal,
- 2) the change in the resistivity is enhanced by the presence of water vapor,
- 3) when the filament is a superconducting material, evidence indicates it has a temperature dependence similar to bulk lead, however,
- 4) it displays a critical current density as much as three orders of magnitude larger than that of the lead films used to fabricate the junctions.

2. Nature of the Filament

When the junction is aged extensively or when a traumatic process occurs, the superconducting nature of the filament appears in the form of a zero bias current as is seen in Figure 35.

The reader should recall that the voltage is measured across the

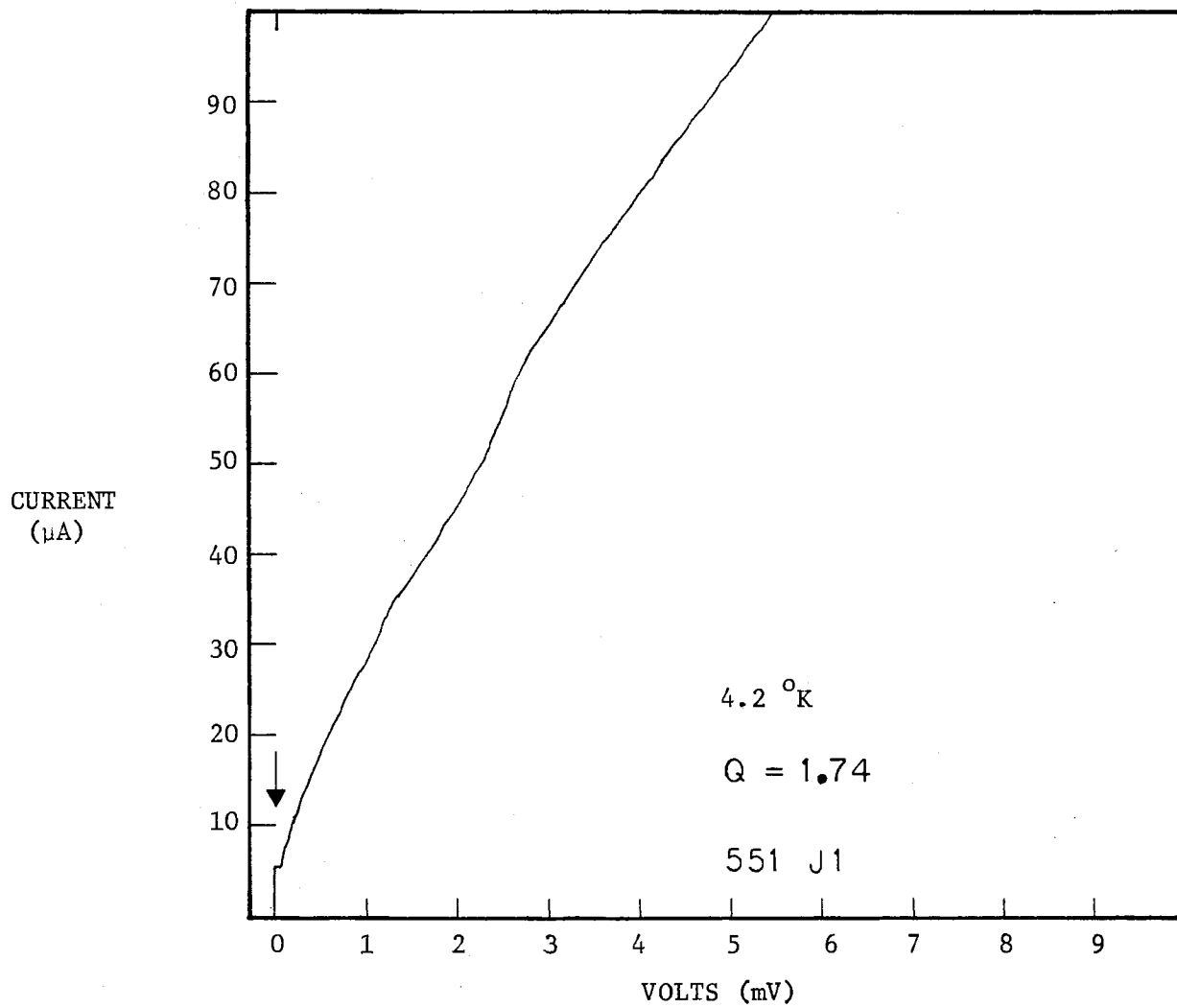


Figure 35. Zero Bias Current in I-V Curve

junction only, so the appearance of a current at $V = 0$ is due to either a superconducting element or a d.c. Josephson current, which in most cases is ruled out by the test discussed in a previous section (rotating the sample in a magnetic field, Chapter III, Section D-2). The zero bias currents range from a few microamps to many milliamps depending on the size of the filaments and, as will be seen below, the temperature behavior of these filaments is similar to that of bulk lead.

During a regular aging process, it is believed that filaments form at the edge of the junction which are not purely metallic, but are of a semiconductor nature. The reason it is believed that the formation is at the edge of the junction rather than in the bulk area is the sudden decrease in the resistance of the junction during aging combined with the dependence of the water vapor, since the water vapor can only attack the edge of the junction. Evidence that some of the filaments are of a semiconductor material rather than metallic can be obtained by looking carefully at Tables VI and VII. Recall that when the junction Q is high, the 4.2°K resistance of the junction is much larger than the room temperature resistance. In a number of cases, after aging the 4.2°K resistance increased over the room temperature resistance even though the Q was significantly decreased. The reader's attention is called to 537 in Table VI and VII. After aging, J3 showed a slight increase in resistance in going from room temperature to 4.2°K despite the fact that the Q is 2.79. The resistance of J2 of 537 decreased only slightly in going from 300°K to 4.2°K even though the Q was 2.11 and the resistance change due to aging was 53%. Neither of these junctions exhibit a zero bias current. This evidence of itself, is not conclusive due to the multiple interactions taking place in the junction. One would be remiss

not to point out the increase in resistance of 546 J3 even though a small zero bias current was observed. However, it should also be pointed out that the small initial resistance of the junction could be on the order of the normal resistance of the filament. In this case, it is much more difficult to predict what varied processes might take place. In the case of 536 the filaments appear to be in an intermediate metallic state. After aging the resistance of the junction decreases in going from 300°K to 4.2°K much like a normal metal. Yet one can assume that the change in resistance due to aging occurred at the junction edge since the resistance was reduced by 2 orders of magnitude in $\approx 1\frac{1}{2}$ hours. The simple model thus generated for the junction after aging is displayed in Figure 36 where the cross hatched region represents the connection area or filament. This model is simple in that it assumes square edges at the lead--lead oxide interface, a condition which probably does not exist.

To gain further insight into the nature of the filaments and to seek a means of permanently protecting the junction, some samples were submitted to the oxidation process after they were fabricated, a process which will be referred to as the overlay process. The pictorial results of such a process are illustrated in Figure 37 which is a cross sectional view of a junction. The results of these overlay processes were different from those of normal junction aging but gave evidence to the semiconductor behavior of the filament. The overlay for sample #549 was fabricated with a O_2 pressure of 140 microns for 100 sec, and the aging data is displayed in Figure 38. In Region A, the sample was in the plastic container used to transfer the samples from the dry box. The characteristic increase in resistance can be seen for junction 1 with a

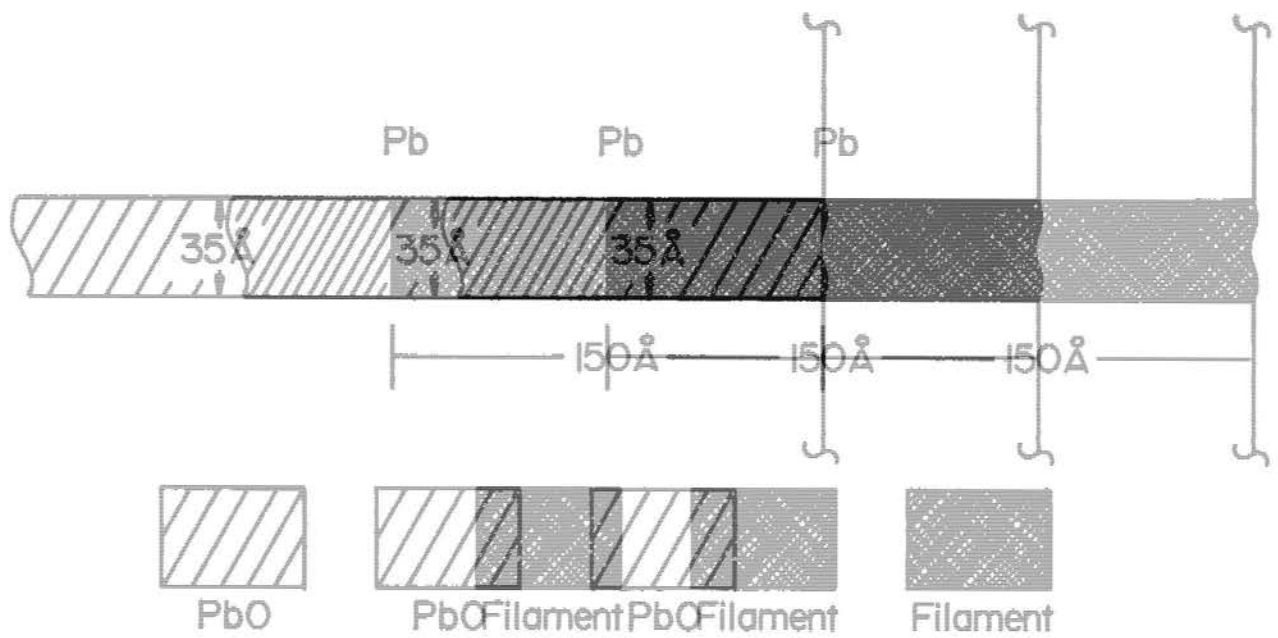
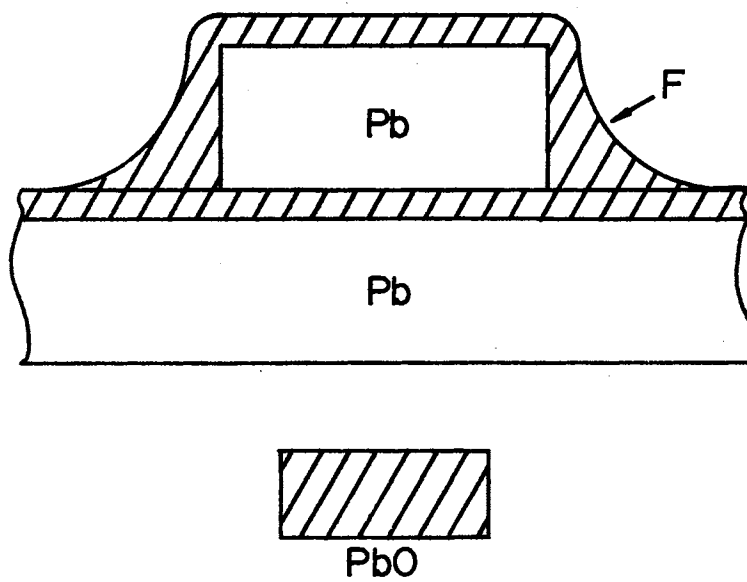


Figure 36. Diagram of Filament Region of Filament Region



Not to Scale

Figure 37. Cross Sectional View of Junction Showing Overlay

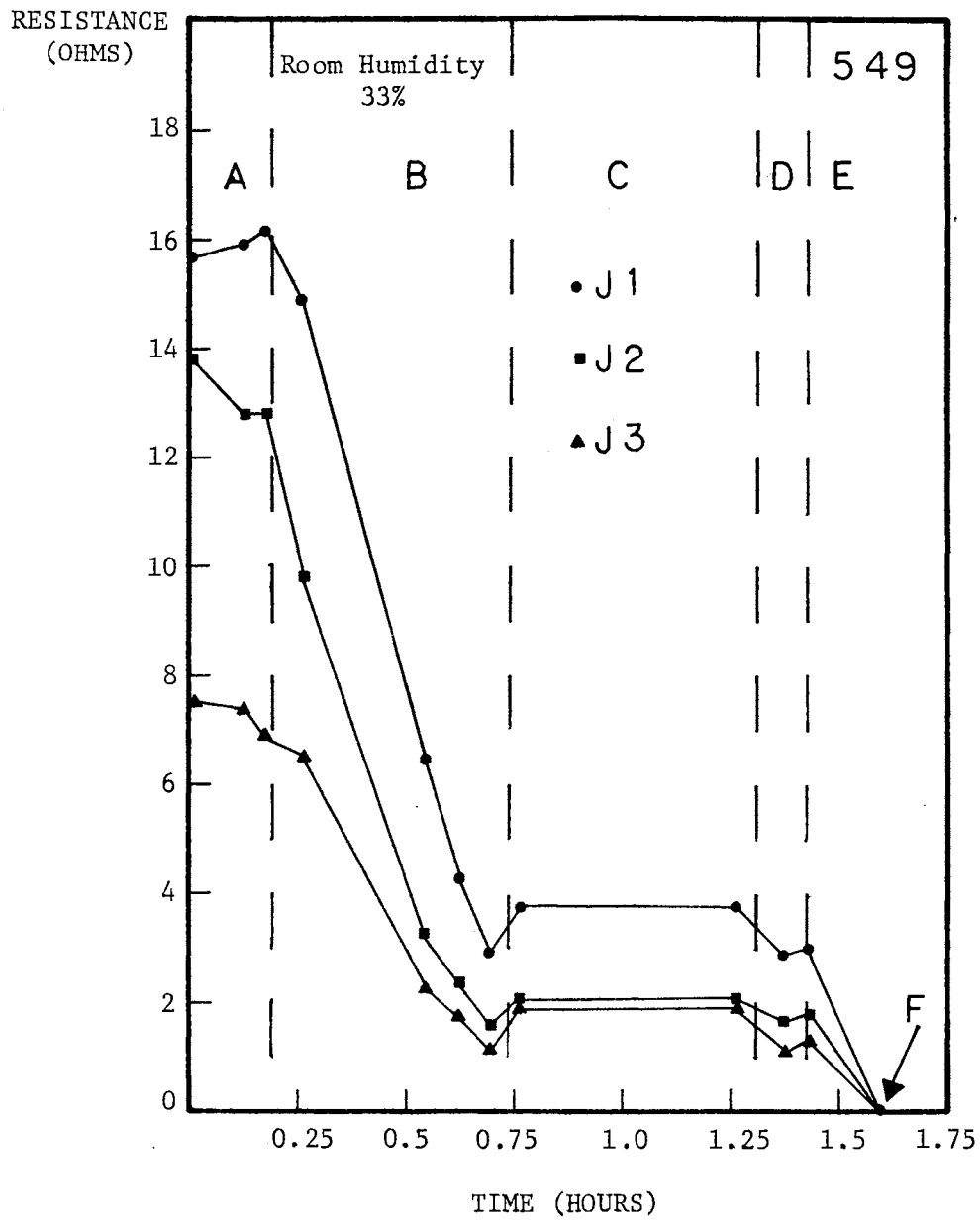


Figure 38. Resistance Versus Time for Sample 549

decrease in resistance in Region B where the junctions were exposed to the room atmosphere. In Region C the samples were immersed in liquid nitrogen causing a slight increase in resistance. It was this increase in resistance at 77°K that again gave evidence to the semiconducting character of the filaments, since it was assumed that the oxide in region F of Figure 37 was the mechanism for conduction. Again this assumption was made due to the rapid decrease in resistance as a function of time. In region D nitrogen gas was being blown over the surface of the junctions, then the samples were immersed in liquid nitrogen again and then removed directly into the room atmosphere in region E, at which time frost appeared on the sample chamber, a process which would have destroyed normal junctions. At point F the junctions were immersed in distilled water and were immediately destroyed. The results of aging sample #551 are displayed in Figures 39, 40 and 41. The original values are listed in Table X.

TABLE X
ORIGINAL RESISTANCE FOR SAMPLE 551

	R Room Ohms	R 4.2°K Ohms	Q
J1	342	741	14.6
J2	280	541	4.93
J3	174	390	30

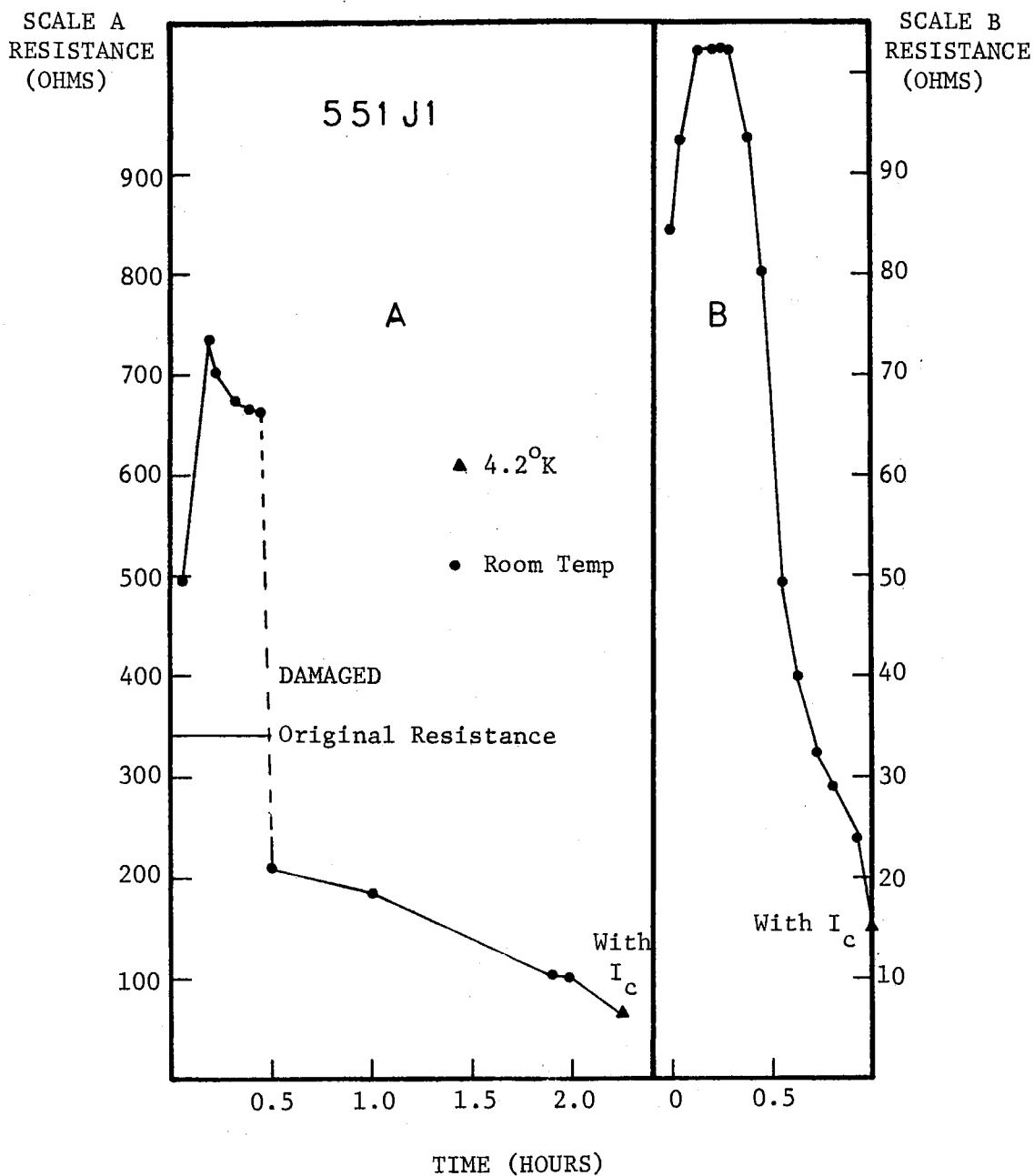


Figure 39. Resistance Versus Time for Sample 551J1

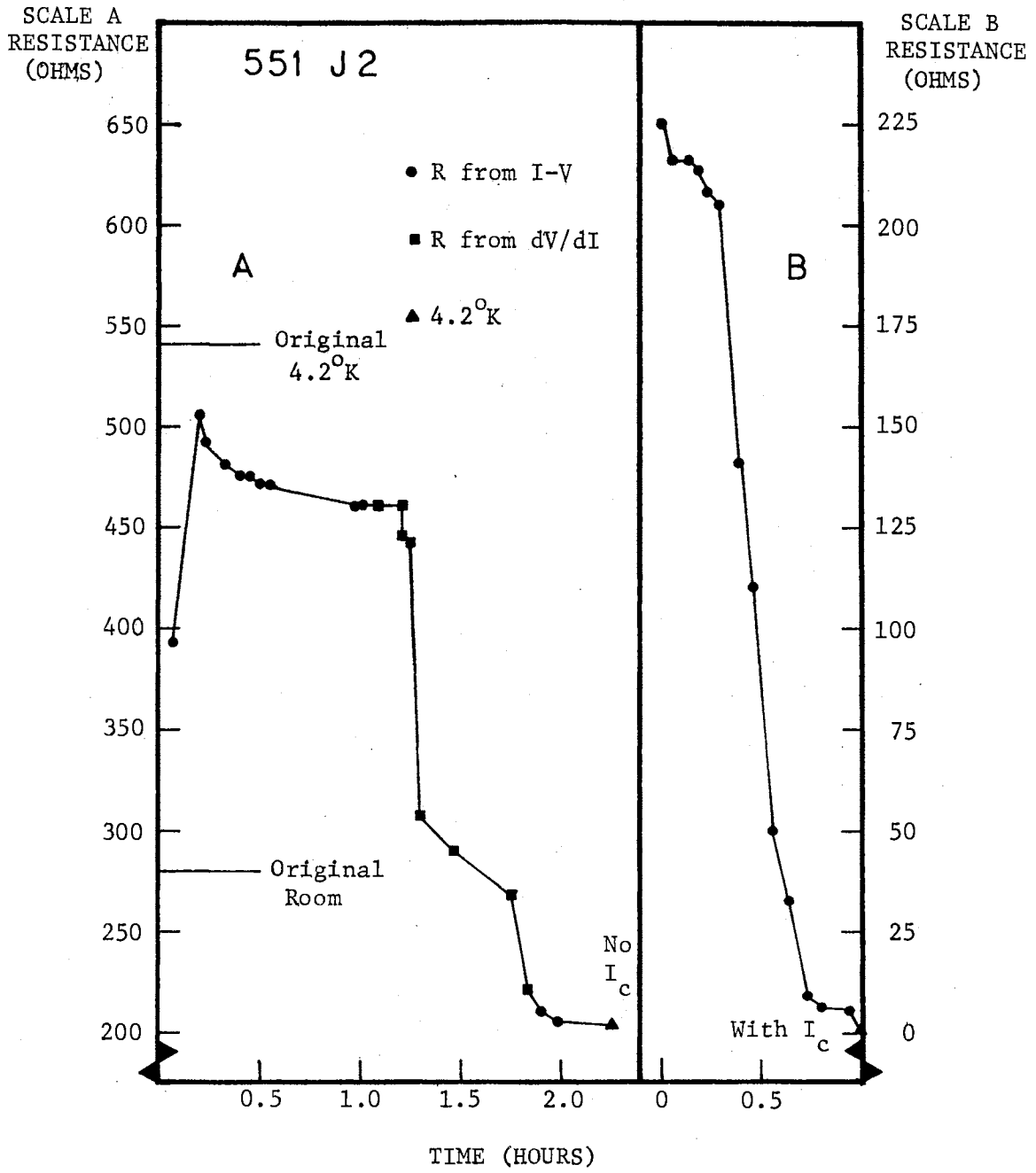


Figure 40. Resistance Versus Time for Sample 551J2

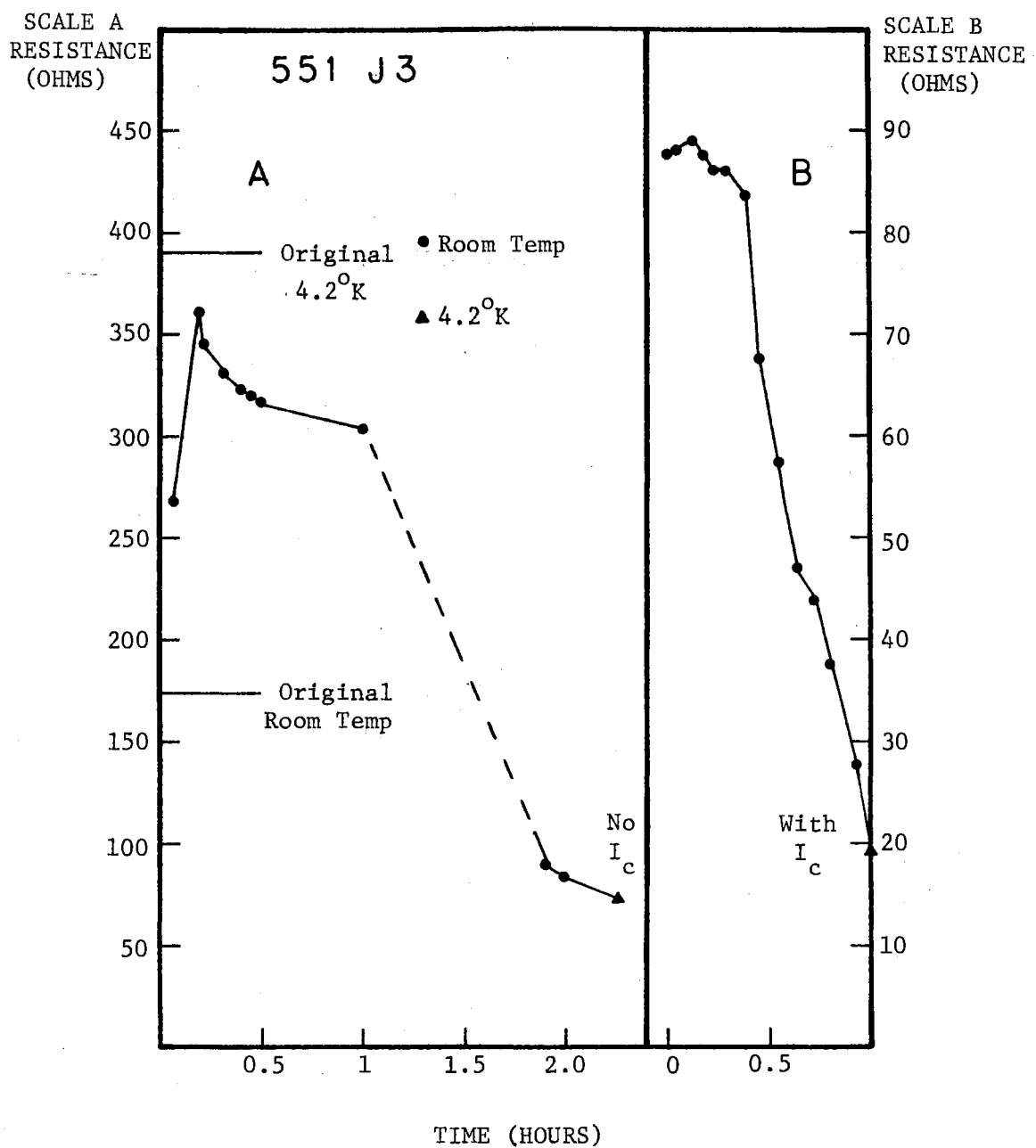


Figure 41. Resistance Versus Time for Sample 551J3

It is interesting to note that the Q value for J1 and J2 are somewhat low yet no SHS or zero bias current was found, indicating the effect of the overlay on the conduction. The sudden decrease in resistance at ≈ 0.5 hours in Figure 39 represents a traumatic process occurring due to the inadvertent switching of a voltage to the junction. This idea is substantiated by the presence of a zero bias current which does not appear in junctions 2 or 3, the data of which is displayed in Figures 40 and 41. The resistance points in Figure 40 were monitored by the dV/dI measurement to obtain a true decay picture. The major difference between this overlay data and normal aging data is twofold. First, there is a sharp rise in resistance followed by an exponential like behavior. The sudden change in conductivity of the overlay region is probably due to a change in the stoichiometry of the oxide in this region. Note that the resistance increases to a value near that of the 4.2°K resistance value. The sudden decrease at ≈ 1.25 hours is like that occurring in a normal decay, with again the 4.2°K resistance showing only a slight decrease. Both J2 and J3 did not exhibit any zero bias current, however, all three junctions displayed SHS of the same pattern as discussed earlier. The second significant difference in the overlay data and normal aging data appears in Section B of all three figures, 39, 40 and 41. Here the junctions were removed from the liquid helium directly into the room atmosphere without warmup in the helium boil off gas. The relative humidity of the room was 34%. Of monumental significance is the fact that the junctions did not immediately become shorted but underwent a normal decay pattern even though the sample was covered with frost. The rapid part of the decay did occur at 0.5 hours as opposed to 1.25 hours for the previous decay. The filaments formed were superconducting as

indicated by a zero bias current and a decrease in resistance in going from room temperature to 4.2°K .

Another very qualitative and naive experiment which proved the effect of water on lead was performed in the following manner. Three identical samples of lead were etched in a 1:1 solution of acetic acid and hydrogen peroxide. One sample was placed in a helium gas atmosphere, a second sample was placed in the room atmosphere, and the third sample was placed in a vial containing some deionized water. After a period of several months the sample in the helium gas was still moderately clean, the sample in air had a surface layer of black, blue, and grey foreign substance, but around the sample in the deionized water atmosphere was a powder like yellow substance which looks similar to the PbO powder purchased commercially. This seems to be a simple but strong indication that the water aided in the growth of a lead oxide-like material.

Another possible mechanism for filament formation may be similar to the reaction in a battery (37). The constituents of a battery are two plates of lead, one of which is coated with a layer of PbO_2 , immersed in a solution of dilute sulfuric acid. It is possible that the water vapor could act as a catalyst for a similar reaction between the lead, lead oxide and impurities in the air or impurities on the surface of the lead.

A question as to the constituents of the filament arises when it is superconducting, i.e., is it pure lead or is it an alloy, or is it lead with some impurities. The results of the measurement of the critical current, I_c , as a function of temperature indicate the superconducting filaments are pure lead. The temperature of the sample was varied as described in Chapter II, Section I, and was measured using the 2Δ of the junction as the thermometer. From BCS (38) theory Δ is approximated by

$$\Delta \approx 3.2 k_B T_c [1 - (T/T_0)]^{1/2}. \quad (\text{III-14})$$

For this work the constant was determined by measuring 2Δ on the dV/dI measurement using the minimum of the resistance spike as 2Δ , and determining the boiling point of the helium by measuring the barometric pressure. Once the constant was determined for a particular junction, the temperature can be determined by measuring 2Δ and solving Equation (III-14) for T . The results for sample 589, displayed in Figure 42, indicate the critical current approaches zero as T approaches T_c of bulk lead, which in turn implies that the filament is lead. In this sample the d.c. Josephson current was zero, and there was no effect due to trapped flux, as is indicated by the data points labeled by a square. A number of measurements on similar samples yielded the same results even though the filaments on some samples were generated by passing a large current through the sample. In other words, when the filaments are superconducting they are lead independent of the process of creation. The results of these measurements are consistent with those of Yeong-du Song and Rochlin (39) who measured the critical current as a function of temperature for microbridges made of tin.

3. Measurement of Filament Size

The method of determining the filament size is a subject worthy of discussion since it bears heavily in the discussion of the results of the critical current density section. Since the very term critical current implies superconductivity in this text, the size is measured only for the filaments which exhibit a zero bias current. The filament area is calculated from the resistance equation

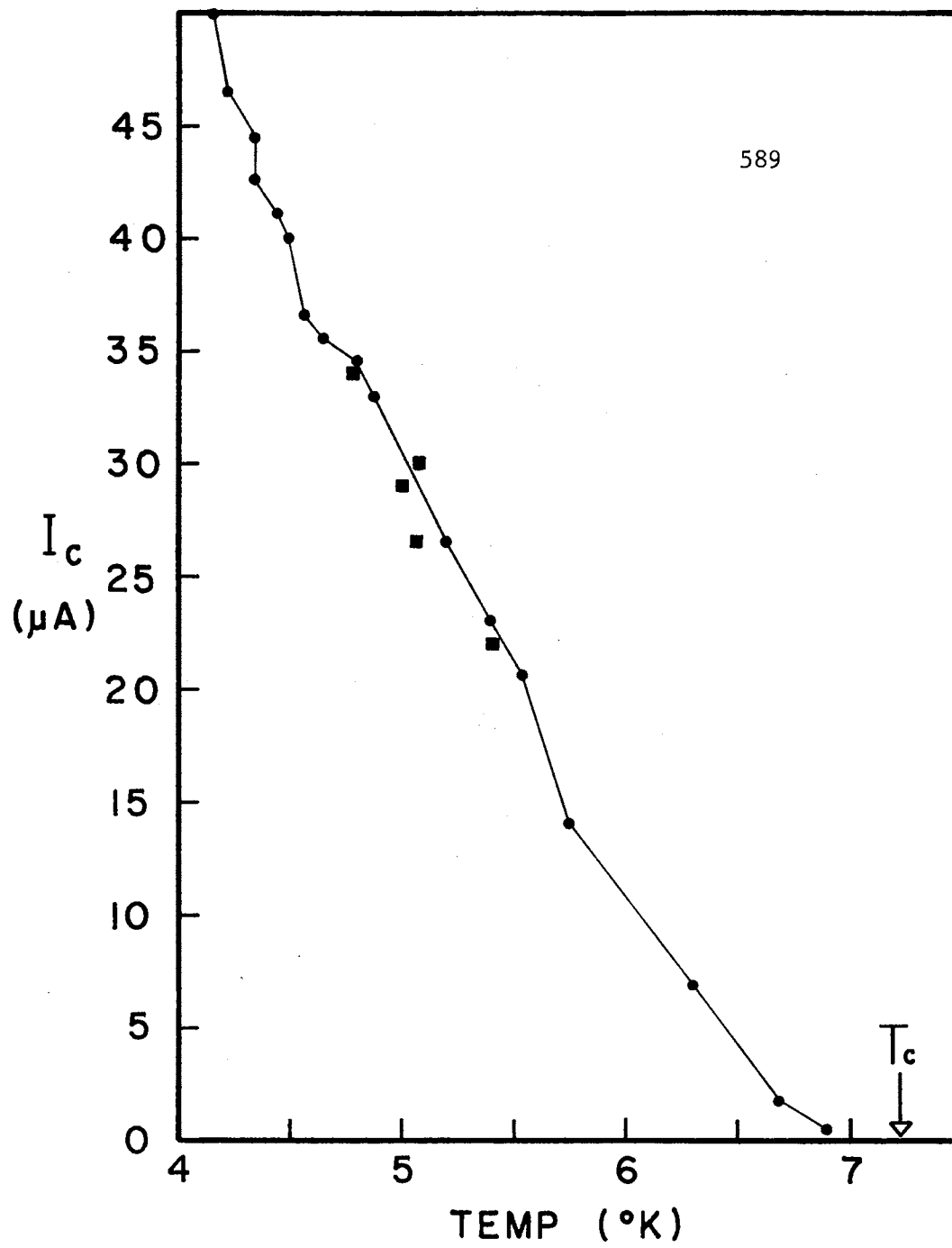


Figure 42. The Temperature Dependence of the Critical Current in a Filament

$$R = \frac{\rho L}{A}, \quad A = \frac{\rho L}{R}, \quad (\text{III-15})$$

assuming ρ is the room temperature resistivity of bulk lead, $L = 40\text{\AA}$, and R is the room temperature resistance of the filament. One can assume that the resistance one measures is due to the resistance of the insulating barrier and the resistance of the filament, the two being in parallel. The total resistance then is

$$\frac{1}{R_T} = \frac{1}{R_F} + \frac{1}{R_O} \quad (\text{III-16})$$

where R_F and R_O are the resistance of the filament and the oxide respectively. The aging experiments indicate that over any short period of time, i.e., < 10 hours, the resistance due to the oxide does not change appreciably. This is also born out by Yanson and Albegova (25). Thus, assuming the oxide contribution to the resistance measurement remains constant, the filament resistance is

$$R_F = \frac{R_T R_O}{R_O - R_T} \quad (\text{III-17})$$

where R_O is the room temperature junction resistance prior to aging and R_T is the junction resistance after the filament formation. If the change in R is on the order of three orders of magnitude, $R_O \gg R_F$ and $R_F \approx R_T$. It has been shown that the critical current of the filament behaves like bulk lead, thus using ρ of bulk lead in Equation (III-15) is a valid assumption. Some results of the filament size measurements are displayed in Table XI.

TABLE XI
CRITICAL CURRENT DENSITY OF FILAMENTS

Sample Number	Critical Current (Amps)	J_c (Amps/m ²)	Filament Diameter (Å)
539-1	2.75×10^{-6}	3×10^{10}	40
547-2	1.5×10^{-5}	2.54×10^{12}	27
546-2	2.2×10^{-5}	5.27×10^{11}	73
546-3	3.0×10^{-5}	7.43×10^{11}	72
546-1	9.20×10^{-4}	1.89×10^{13}	79
532-3	1.15×10^{-3}	1.93×10^{13}	87
534-1	3.63×10^{-3}	2.54×10^{13}	135
539-1*	8.0×10^{-3}	8.1×10^{13}	112
480-3	9.2×10^{-3}	9.9×10^{12}	340
538-1	1.25×10^{-2}	6.43×10^{13}	157
538-3	1.3×10^{-2}	7.67×10^{13}	147
534-3	1.5×10^{-2}	2.65×10^{13}	268
538-2	1.7×10^{-2}	1.07×10^{14}	142
532-2	2.5×10^{-2}	1.92×10^{14}	130
547-3	3.4×10^{-2}	1.9×10^{14}	150
588-3	1.37×10^{-4}	1.61×10^{12}	104
589-2	5.3×10^{-5}	2.99×10^{12}	150

*This data was taken after the junction was submitted to a traumatic electrical discharge.

4. Critical Current Density for Lead Filaments

It has been pointed out by Huebener (40) and others (29) that films of type I superconductors with a thickness less than the coherence length have properties which are similar to those of a type II superconductor. Hence, a determination of the critical current density of the lead films in the junction was made. The critical current in the film was measured by making a junction without the oxide formation process, then the I-V characteristics were measured at 4.2°K. With the 4 probe method being used on the junction area, a current was flowing with $V = 0$ across the junction area. When the stripe went normal, the current level then decreased, so the maximum current was the critical current. The thickness of the films were obtained by measuring the room temperature resistance of the film and calculating t , thickness, from Equation (III-15) where $A = t \times w$. The width, w , and length, L , of the films were measured with a traveling microscope. The results of the measurements, displayed in Table XII, are quite consistent for 6 different films formed on two different substrates. The critical current density, J_c , for the filaments in aged junctions are displayed in Table XI. The critical current for the junction was determined by measuring the current level in the I-V plot corresponding to the appearance of a voltage across the junction. The significant point of this part of the experiment is the inordinately large values for J_c compared to the values of J_c for the films. To get some feeling for the relationship between the J_c for the films and the filaments, one can look at the critical current densities of Dayem Bridges, which are an intermediate step between the two extremes. Chen et al. (41) did not calculate a critical current density for their lead bridges, but one can be inferred from the numbers

TABLE XII
CRITICAL CURRENT DENSITY OF FILMS

Junction #	Stripe Resis. Ohms	Stripe Thickness Å	Deposition Rate A/Sec	$J_c \times 10^{10} \frac{\text{amp}}{\text{m}^2}$
J1-544	59.17 Ω	1338	67	3.85
J2-544	56.82	1288	64.4	3.23
J3-544	52.36	1297	64.85	3.81
J1-543	43.5	1525	50.83	3.39
J2-543	43.75	1574	52.47	3.07
J3-543	43.5	1556	51.87	2.91
				Average
				3.38

they do provide. They report that their films are 1000\AA thick, and the construction of the bridge is 2μ or less, which makes the bridge area $\approx 2 \times 10^{-13} \text{ m}^2$. The maximum d.c. supercurrent for one sample was 570 ma and thus $J_c = 3 \times 10^{12} \text{ A/m}^2$, a value which is consistent with the data in Table XI.

One might make the argument that the filament is not pure lead in the room temperature state but rather a lead core surrounded by a non-superconducting outer layer which is conducting. Then the total area measured would actually be larger than the true lead filament area. However, using a too large area in the calculation of J_c would decrease rather than increase the value of J_c , thus not explaining the orders of magnitude too large critical current density.

In another attempt to explain the critical current density a comparison was made between the critical current observed and the critical currents predicted from Silsbee's current (42), which is

$$I_c = 5rH_c$$

where I_c is critical current, r is the radius of the wire in cm, and H_c is the critical field in oersteds. Realizing that 1 amp turn/cm = 1.257 oersteds, and taking H_c for lead to be 803 oersteds, one can calculate a radius for the filament. For one sample (#480-J3) the calculated Silsbee radius is 576\AA , and the measured radius is 340\AA . For another sample (#546-2) the calculated Silsbee radius is 1.38\AA , and the measured is 73\AA . Using 500 oersted for H_c , the approximate value at $T = 4.2^\circ\text{K}$, does not improve the agreement. Clearly, the filament cannot be thought of as a wire in the sense of Silsbee rule. However, Lynton (29) points out that smaller samples remain superconducting with much higher currents.

than those calculated from Silsbee's rule.

5. Summary

The results indicate that during the aging process filaments are formed at the edge of the junction which are either semiconducting or superconducting in nature. When a junction with a semiconducting filament is aged to a greater degree the filament eventually becomes a superconducting. The chemistry involved in the filament formation is complex and unknown but does require the presence of water or at least water vapor.

The critical current densities of the filaments in this study were in some cases three orders of magnitude greater than the critical current densities of the films themselves. As has been seen in this section, this phenomenon cannot be explained by considering the simple Silsbee current in wire. Lynton (29) points out that small samples remain superconducting at much higher currents than the Silsbee current. Some work has been done to obtain high critical currents in alloys for use in superconducting magnets. However, the temperature dependence of the filaments in this work indicate they are not alloys. It should be further noted that the diameter of the filaments is actually larger than the length, so rather than a filament, the region is a contact area. Obviously, more work needs to be done in this area, but the technological significance of having a connection capable of current densities of this order of magnitude is obvious.

CHAPTER IV

SUMMARY AND SUGGESTIONS FOR FUTURE STUDY

The superconducting tunneling phenomenon has contributed greatly to the basic understanding of superconducting materials by providing an excellent tool to measure the energy gap and other parameters (22) associated with superconductivity. It was the scope of this study to contribute to the understanding of the tunneling phenomenon by determining some of the characteristics of the oxide barrier by measurement and by inducing anomalies in the tunneling process in lead-lead oxide-lead junctions.

One characteristic that was measured directly was the thickness of the oxide barrier. It was found that all junctions regardless of their resistance had an oxide barrier thickness on the order of $35\overset{\circ}{\text{A}}$. Since junctions exhibit resistances varying over three orders of magnitude with all of the barriers being the same thickness, it is concluded that the oxide behaves like a semiconductor. That is during the oxidation procedure a certain cut off thickness is reached after which time the oxide is doped by the addition of more oxygen, changing its stoichiometry and resistivity.

The anomalies in the tunneling process were induced by aging the junctions at room temperature. It was found that after a period of time which depends on the water vapor content of the ambient, a sudden decrease in resistance occurs which corresponds to the formation of a fil-

ament between the two lead films making up the junction. Depending on the extent of the aging process, these filaments ranged from a semiconducting nature to a superconducting (lead) path.

A study of the superconducting filaments found that they exhibit a critical current density two to three orders of magnitude greater than the critical current density of the films composing the junction, yet their diameters were an order of magnitude smaller than the film thickness.

In all cases when a filament was formed, subharmonic structure appeared in the voltage range below the energy gap. This subharmonic structure depends only on the superconducting properties of the films making up the junction, not on the properties of the filament. This study provides an excellent tool for future investigators to use to study subharmonic structure, a problem which needs more theoretical and experimental work.

It is also felt that this work makes a major contribution to the technology of the superconducting tunneling phenomenon in the following way. The Pb/PbO/Pb system is advantageous to use because the transition temperature of lead is 7.2°K and the boiling temperature of helium is 4.2°K . Hence, the lead system can be studied without elaborate apparatus to further cool the helium. However, the lead junctions have proven to be very unstable at room temperatures and in normal room environments due to their destruction in the presence of water vapor. This study then contributes an understanding to this fault and will perhaps lead to a solution which will make the Pb/PbO/Pb junctions much more reliable in technological systems.

This work suggests a number of interesting areas of study which

would enhance the understanding of the tunneling phenomenon. First, it was discovered that when the sample was in a chamber through which helium gas was passing, the sudden decrease in junction resistance occurred in a relatively short period of time. It is known that this helium gas was not pure and certainly not dry in the sense that no water vapor existed. It is suggested then that this experiment be performed by passing the helium through an oxygen Gettering Furnace such as the Centorr Model 2-B to obtain a pure dry inert gas atmosphere in which to age the junction. This will then allow one to see the decay of the junction without the presence of O_2 , N_2 or C impurities or water vapor.

This study now offers a means by which subharmonic structure in tunneling between two different superconductors could be investigated. It is proposed that a Pb/PbO/Sn junction be fabricated and aged in the same manner as was done in this work. The aging of this system would give further insight into the mechanism for aging Pb/PbO/Pb tunneling junctions, and a comparison of the critical current densities of the filaments would be interesting. The question that arises is would the filaments be lead, tin or an alloy?

Finally, now that the behavior of the tunneling junctions in the normal room ambient is better understood, one can attempt to ion implant the lead films with ferromagnetic ions, and then use the tunneling phenomenon to study the effect of this implantation. Prior to this study, the tunneling properties were destroyed while the sample was undergoing the ion implantation process. The effect of the ferromagnetic ions on the superconducting properties of the lead is not well understood, but the tunneling phenomenon is a powerful tool to aid in this understanding.

REFERENCES

- (1) Giaever, I., Phys. Rev. Letters 5, 147 (1960).
- (2) Giaever, I., Phys. Rev. Letters 5, 464 (1960).
- (3) Fiske, M. D. and I. Giaever, Proc. IEEE, 52, 1155 (1964).
- (4) Schwidtal, K. and R. D. Finnegan, Phys. Rev. B, 2, 148 (1970).
- (5) Giaever, I. and K. Megerle, Phys. Rev., 122, 1101 (1961).
- (6) Schroen, Walter, Journal of Applied Physics, 39, 2671 (1968).
- (7) Bardeen, J., L. N. Cooper, and J. R. Schrieffer, Phys. Rev., 108, 1175 (1957).
- (8) Kittel, C., Introduction to Solid State, John Wiley and Sons, New York, 4th edition.
- (9) Giaever, I., In Tunneling Phenomena in Solids, E. Burstein and Stig Lundquist, eds., (Plenum Press, New York, 1969), p. 262.
- (10) Giaever, I. and H. R. Zeller, Phys. Rev. B, 1, 4278 (1970).
- (11) Rowell, J. M. and W. L. Feldmann, Phys. Rev., 172, 393 (1968).
- (12) Gregers-Hansen, P. E., et al., Phys. Rev. Letters 31, 524 (1973).
- (13) Guess, J. F., Unpublished Ph.D. Dissertation, Oklahoma State University, May 1972.
- (14) Schroen, Walter, J. Appl. Phys., 39, 2671 (1968).
- (15) Basavaiah, S., J. M. Eldridge, and J. Matisoo, J. Appl. Phys., 45, 457 (1974).
- (16) McBride, Duncan, Gene Rochlin and Paul Hansma, J. Appl. Phys., 45, 5, 2305 (1974).
- (17) Faraci, G., G. Giaquinta, and N. A. Mancini, Physics Letters 30A, 7, 400 (1969).
- (18) Chou, N. J., J. M. Eldridge, R. Hammer, and D. Dong, Journal of Electronic Materials, 2, 1, 115 (1973).

- (19) Eldridge, J. M. and D. W. Dong, *Surface Science*, 40, 512 (1973).
- (20) Schwidtal, K. and R. D. Finnegan, *Phys. Rev.* 2B, 1, 148 (1970).
- (21) Heijne, L., *J. Phys. Chem. Solids*, 22, 207 (1961).
- (22) Rowell, J. M., W. L. McMillan, and W. L. Feldmann, *Phys. Rev.*, 178, 3, 897, (1969).
- (23) Rowell, J. M., P. W. Anderson, and D. E. Thomas, *Phys. Rev. Letters*, 10, 8, 344 (1963).
- (24) Wyatt, P. W. and A. Yelon, *Phys. Rev.* 2B, 11, 4461 (1970).
- (25) Yanson, I. K. and I. Kh. Albegova, *Soviet Physics JETP*, 28, 5, 826 (1969).
- (26) Coon, D. D. and M. D. Fiske, *Phys. Rev.* 128, 3A, A744 (1965).
- (27) CRC Handbook of Chemistry and Physics, Chemical Rubber Publishing Co., Cleveland, 44 edition, 1963.
- (28) Hasselberg, L. E., M. T. Levinsen, and M. R. Samuelsen, *Phys. Rev.* 9B, 9, 3757 (1974).
- (29) Lynton, E. A., Superconductivity, Chapman and Hall, London, 1969.
- (30) Bright, A. A. and J. R. Merrill, *Phys. Rev.*, 184, 2, 446 (1969).
- (31) Sorensen, O. Hoffman, et al., *Phys. Rev.* 9B, 9, 3746 (1974).
- (32) Strässler, S. and H. R. Zeller, *Phys. Rev.* 3B, 1, 226 (1971).
- (33) Marcus, S. M., *Physics Letters*, 20, 3, 236 (1966).
- (34) Sullivan, D. B., et al., *J. Appl. Phys.*, 41, 12, 4865 (1970).
- (35) Marcus, S. M., *Physics Letters*, 19, 8, 623 (1966).
- (36) Bermon, Stuart and R. M. Mesak, *Solid State Communications*, 9, 23, 2143 (1971).
- (37) Quaglino, James V., Chemistry, Prentice-Hall, Englewood Cliffs, N.J. (1963).
- (38) DeGennes, P. G., Superconductivity of Metals and Alloys, W. A. Benjamin, New York, 124 (1966).
- (39) Song, Yeong du and Gene J. Rochlin, *Physical Review Letters*, 29, 7, 416 (1972).
- (40) Huebener, R. P., et al., Cryogenics, Page 100 (1972).

- (41) Chen, J. T., et al., J. Appl. Phys., 43, 3, 1218 (1972).
- (42) Livingston, J. D. and W. Desorbo, In Superconductivity, edited by R. D. Parks, Marcel Dekker, New York, Page 1236 (1969).
- (43) Langenberg, et al., Proceedings of the IEEE, 54, 4, 560 (1966).

APPENDIX

In Chapter III, Section A-3, a quadratic equation with ρ_o , the lead oxide resistivity, as the variable is developed. Equation III-11 is

$$\frac{1}{\rho_o^2} - \frac{1}{\rho_o \rho_{Pb}} + \left[\left(\frac{t_T}{\rho_{Pb}} - \frac{K}{R_T} \right) \frac{1}{R_J C'} \right] = 0. \quad (A-1)$$

In Equation (A-1)

- ρ_o = lead oxide resistivity,
- ρ_{Pb} = bulk lead resistivity = 19.8×10^{-6} ohm cm,
- t_T = total thickness of lead film before oxidation,
- K = length divided by the width of the film,
- R_T = total resistance of the lead film after oxidation,
- R_J = the room temperature junction resistance,
- C' = the junction area which is the width of 50 times the width of S1, S2 or S3.

Now letting,

$$x = \frac{1}{\rho_o}$$

$$a = 1$$

$$b = -\frac{1}{\rho_{Pb}}$$

$$c = \left[\left(\frac{t_T}{\rho_{Pb}} - \frac{K}{R_T} \right) \frac{1}{R_J C'} \right], \quad (A-2)$$

A-1 has solutions

$$X = \frac{-b \pm b \sqrt{1 - \frac{4ac}{b^2}}}{2a}. \quad (A-3)$$

Letting $y = \frac{-4ac}{b^2}$ one can use the binomial expansion

$$(1 + y)^{\frac{1}{2}} = 1 + \frac{1}{2}y - \frac{1}{8}y^2 \dots$$

if $-1 < y \leq 1$. For a typical sample, i.e., #584J1,

$$t_T = 920 \text{ \AA} = 9.2 \times 10^{-6} \text{ cm}$$

$$R_T = 40 \text{ ohms}$$

$$K = 18$$

$$\rho_{Pb} = 19.8 \times 10^{-6} \text{ ohm cm}$$

$$R_J = 392 \text{ ohms}$$

$$C' = 1.1 \times 10^{-3} \text{ cm}^2$$

Thus,
$$c = .0348 \frac{1}{\text{ohm}^2 \text{ cm}^2},$$

$$b = -\frac{1}{\rho_{Pb}} = \frac{-1}{19.8 \times 10^{-6} \text{ ohm cm}} = -5.05 \times 10^4 \frac{1}{\text{ohm cm}}$$

and $b^2 = 2.55 \times 10^9 \frac{1}{\text{ohm}^2 \text{ cm}^2}$.

Thus, $\frac{-4ac}{b^2}$ becomes

$$\frac{-1.39 \times 10^{-1} \frac{1}{\text{ohm}^2 \text{ cm}^2}}{2.55 \times 10^9 \frac{1}{\text{ohm}^2 \text{ cm}^2}} = -5.45 \times 10^{-11}$$

which is between -1 and +1. Since $\frac{-4ac}{b^2}$ is so small compared to 1 it is a good approximation to replace the radical by

$$1 - \frac{2ac}{b^2}$$

Then, Equation (A-3) becomes

$$X = \frac{-b \pm b \left[1 - \frac{2ac}{b^2}\right]}{2} \quad (\text{A-4})$$

Taking the plus root of Equation (A-4),

$$X = \frac{-b + b - \frac{2ac}{b}}{2}$$

or

$$X = -\frac{c}{b}$$

Thus,

$$\rho_o = \frac{1}{\rho_{pb} c}$$

or

$$\rho_o = \frac{1}{\rho_{Pb} \left[\left(\frac{t_T}{\rho_{Pb}} - \frac{K}{R_T} \right) \frac{1}{R_J C_T} \right]} \quad (A-5)$$

If one assumes the minus root of Equation (A-4)

$$X = \frac{-b - b + \frac{2ac}{b}}{2} \quad \text{or} \quad (A-6)$$

$$X = \frac{-b^2 + c}{b} \quad \text{and} \quad \frac{1}{X} = \frac{b}{-b^2 + c}$$

Replacing $1/X$ by ρ_o and b by $-\frac{1}{\rho_{Pb}}$ equation (A-6) becomes

$$\rho_o = \frac{-\rho_{Pb}}{-1 + c \rho_{Pb}^2} \quad (A-7)$$

However, $\rho_{Pb} \approx 10^{-6}$ and c is < 10 in all cases making $c \rho_{Pb}^2 \ll 1$ which implies that $\rho_o \approx \rho_{Pb}$. This is physically impossible for the junction resistances that are observed. Hence, the plus root of Equation (A-4) is the proper solution.

VITA

Kenneth Dean Duerksen

Candidate for the Degree of

Doctor of Philosophy

Thesis: ANOMALIES IN THE SUPERCONDUCTING LEAD-LEAD OXIDE-LEAD TUNNELING JUNCTION INDUCED BY AGING: INCLUDING SUBHARMONIC STRUCTURE AND OXIDE MODIFICATION

Major Field: Physics

Biographical:

Personal Data: Born in Cordell, Oklahoma, December 13, 1943, the son of Erwin R. and Luella H. Duerksen.

Education: Graduated from Corn High School, Corn, Oklahoma, in May, 1962; received the Bachelor of Science degree in physics from Southwestern Oklahoma State University, Weatherford, Oklahoma, in May, 1966; enrolled in the master's program at the University of Arkansas, 1966 - 1967; received the Master of Science degree at Oklahoma State University in May, 1972; completed requirements for the Doctor of Philosophy degree at Oklahoma State University in December, 1974.

Professional Experience: Undergraduate Laboratory Teaching Assistant, Southwestern State College, 1964 - 1966; Research Technician, Oak Ridge National Laboratory, Summer 1966; Graduate Teaching Assistant, Department of Physics, University of Arkansas, 1966 - 1967; Instructor of Physics, Westark Junior College, Fort Smith, Arkansas, 1967 - 1969; Graduate Teaching Assistant, Department of Physics, Oklahoma State University, 1969 - 1971; Graduate Research Assistant, Department of Physics, Oklahoma State University, 1971 - 1974.

Professional Organizations: Associate Councilor from Zone 10 on the National Council of the Society of Physics Students, the SPS, Sigma Pi Sigma National Physics Honor Society, The American Physical Society.

Publications: "Exploding-Wire Aerosol Generator", Health Physics Division Annual Progress Report, Oak Ridge National Laboratory, Report No. ORNL-4168 (October 1967), p. 296.